ulm university universität
uulm

Fakultät für Mathematik und Wirtschaftswissenschaften
Institut für Numerische Mathematik

Specific Phase Space Structures in Dynamical Systems: Attracting Manifolds in Optimal Control and Separatrix Characterization

Dissertationsschrift zur Erlangung des Doktorgrades Dr. rer. nat.
der Fakultät für Mathematik und Wirtschaftswissenschaften
der Universität Ulm

Vorgelegt von:
Marcus Heitel
geboren in Mutlangen

2020

Amtierender Dekan:	Prof. Dr. Martin Müller
1. Gutachter:	Prof. Dr. Dirk Lebiedz
2. Gutachter:	Prof. Dr. Moritz Diehl
Tag der Promotion:	18. Juni 2020

Fassung: 22. Juli 2020

Satz: LaTeX 2_ε.

Abstract

Simulation and optimal control of multi-scale dynamical systems arising, e.g., in chemical reaction mechanisms is usually very time-consuming despite increasing computing power of modern computers. To reduce both stiffness and complexity of the model, manifold-based model reduction methods compute so-called slow invariant manifolds of the phase space, which contain essential information about the long-term behavior. This work aims to efficiently integrate manifold computation techniques into the optimal control of chemical reactions to make computations less expensive.

The central topic of this work are specific structures in the phase space of dynamical systems. We want to gain a deeper understanding and identify their geometric and topological properties. Besides slow invariant manifolds of multi-scale dynamical systems, we consider phase space structures of holomorphic flows in the complex plane: separatrices. Research has shown that properties of these separatrices at infinity potentially reveal information about the location of the equilibria, e.g., the zeros of Riemann's zeta function. We contribute to this area of research by studying separatrices at infinity and characterizing them topologically. By means of compactification of the complex plane, we show that critical points at infinity in polynomial flows have separatrices. The results of this work show the general importance of phase space structures for the long-term and asymptotic behavior and contribute to a deeper understanding of their role.

Zusammenfassung

Trotz zunehmender Rechenleistung moderner Computer ist die Simulation und Optimalsteuerung von multiskaligen dynamischen Systemen, wie sie zum Beispiel bei chemischen Reaktionsmechanismen auftreten, gewöhnlicherweise sehr zeitaufwendig. Um sowohl die Steifheit als auch die Komplexität des Modells zu reduzieren, berechnen mannigfaltigkeitsbasierte Modellreduktionsmethoden so genannte langsame invariante Mannigfaltigkeiten, die wesentliche Informationen über das Langzeitverhalten enthalten. Ziel dieser Arbeit ist die effiziente Integration von Techniken der Mannigfaltigkeitsberechnung in die optimale Steuerung chemischer Reaktionen, um diese weniger aufwendig zu machen.

Zentrales Thema dieser Arbeit sind spezifische Strukturen im Phasenraum dynamischer Systeme. Wir wollen deren geometrische und topologische Eigenschaften identifizieren und ein tieferes Verständnis gewinnen. Neben langsamen, invarianten Mannigfaltigkeiten in multiskaligen dynamischen Systemen werden auch Phasenraumstrukturen von holomorphen Flüssen in der komplexen Zahlenebene betrachtet: Separatrizen. Die Forschung hat gezeigt, dass Eigenschaften von Separatrizen bei unendlich möglicherweise Informationen über die Lage von Gleichgewichtspunkten, wie zum Beispiel den Nullstellen der Riemannschen Zetafunktion, liefern. Zu diesem Forschungsgebiet tragen wir bei, indem wir Separatrizen bei Unendlich studieren und diese topologisch charakterisieren. Mittels Kompaktifizierung der komplexen Ebene zeigen wir, dass kritische Punkte bei unendlich in polynomiellen Flüssen Separatrizen besitzen. Die Resultate dieser Arbeit zeigen die allgemeine Bedeutung von Phasenraumstrukturen für das Langzeit- und asymptotische Verhalten und tragen zu einem tieferem Verständnis ihrer Rolle bei.

Acknowledgments

Aus Gründen des Datenschutzes entfernt.

Diese Seite wurde aus Gründen des Datenschutzes entfernt.

Contents

List of Figures

List of Tables

1 Introduction

In mathematical modeling, we translate problems arising, e.g., in engineering, biology, physics, and chemistry into the mathematical language. This serves not only to represent reality but also to make predictions, find answers, optimize processes, and to provide us with useful insights. With the rise of computers in the 20th century, the evaluation of such models became more convenient and faster. On the other hand, scientific issues and progress led to more accurate but more complicated mathematical models. Despite ever increasing processing power of modern computers, the complexity of realistic models often prevents the best computers from detailed computations in decent time.

One of such rather complicated models emerges in the optimal control of chemical reaction mechanisms. Chemical kinetics are typically modeled by Ordinary Differential Equations (ODEs). In optimal control, these differential equations are parameterized by some *control variables*. For example, chemical reactions can be controlled by addition of a chemical species, or by heating. For the numerical treatment, differential equations of the model have to be discretized appropriately. Although the numerical model is finite-dimensional, it usually comprises so many variables that it often cannot be solved efficiently.

Model order reduction methods are developed to reduce the complexity and dimension of models. They simplify the model such that it becomes comparatively cheap to evaluate while keeping the precision of the results accurately enough. An overview of model order reduction methods can be found in [ASG01; Kue15; LU16]. We focus on model reduction based on the geometry of the phase space, i.e., the space of all differential equation solution curves (called *trajectories*). For the dynamical systems considered in this work, a bundling of trajectories occurs at specific structures of the phase space. A brief and general motivation for the usage of such structures for model reduction is given in the next paragraph.

Motivation for Specific Phase Space Structures

Imagine a map where all sources of water, creeks, rivers, and seas are charted. It

is observed that many sources of water bundle into a creek. Creeks bundle into rivers and rivers into seas. For the long-term behavior of the water dynamics from dropping down on a mountain through to a sea or ocean, it is intuitive to follow the closest river on the map and neglect the exact path of a simple water drop through a creek to the river. Water falls very quickly from the top of a mountain to a valley where it bundles into a river. Once in a river, the cruising speed is much slower than before and remains slow on the way to the sea.

Translated into mathematical terms, this leads to the idea of model reduction, bundling behavior, and multiple time scales. For the long-term behavior of a water drop, it is sufficient to know which river it enters. All other information can be neglected for this purpose. This is the basic idea of model reduction. To scrutinize the exact location of a hypothetically marked water drop in a mountain creek, a fast time scale is needed in comparison to determine the location of a water drop in the river in the sense that a water drop spends way more time in a river than in a mountain creek. Analogously, in multiple time scale dynamics, e.g., so-called slow-fast systems, usually there are Slow Invariant Manifolds (SIMs) onto which all trajectories (cf. path of a water drop) relax in some neighborhood. Computation of such manifolds reduces the dimension of the mathematical model but still contains all relevant information for the long-term behavior of trajectories.

To answer the question in which sea a river enters, the only needed information is the location of (continental) divides. For example, the location relative to the European watershed between Rhine and Danube decides whether a river flows into the North Sea or the Black Sea. In mathematical terms, divides are named *separatrices* because they separate different attraction regions (in the water analogy the attraction region of a sea). For a specific class of functions called holomorphic functions, it appears evident that there is a connection between the location of separatrices (divides) and equilibria (seas).

The analogy of separatrices to continental divides stems from Prof. Schleich.

In the next paragraph, we focus on the first specific phase space structure considered in this work, namely SIMs and their usage for model reduction of optimal control problems.

Slow Invariant Manifolds

In multi-scale systems, a part of the dynamics evolves much faster than the rest of the dynamics. For instance, in chemical reactions, some partial reactions have

a time scale in the range of nanoseconds while other reactions occur in multiple seconds. If dynamics are modeled by differential equations, this timescale separation leads to so-called stiff differential equations. Explicit numerical methods typically are unstable for such problems. Even modern computers and the usage of sophisticated numerical tools cannot overcome the challenges of numerical stiffness and high-dimensionality.

Model order reduction techniques present a way to avoid these issues. In this work, we focus on a subclass of manifold-based model reduction methods. The first methods were developed at the beginning of the 20th century [Bod07; Bod13; CU13]. Over the past 35 years there has been a significant increase in model reduction techniques (cf. Section 2.4). One reason for this increase is the theory of Fenichel [Fen74; Fen77; Fen79] published in the 70s. He showed the existence of so-called *Slow Invariant Manifolds* (*SIMs*) in singularly perturbed systems. These SIMs contain all relevant information about the long-term behavior of all variables (cf. Tikhonov [Tik52]). Fast variables relax comparatively fast to low-dimensional manifolds. Figure 1.1 shows the phase portrait (i.e., some arbitrarily chosen trajectories) of an 2-D enzyme example by Michaelis, Menten, and Henri [MM13] including the SIM. The corresponding numerical methods aim to compute or

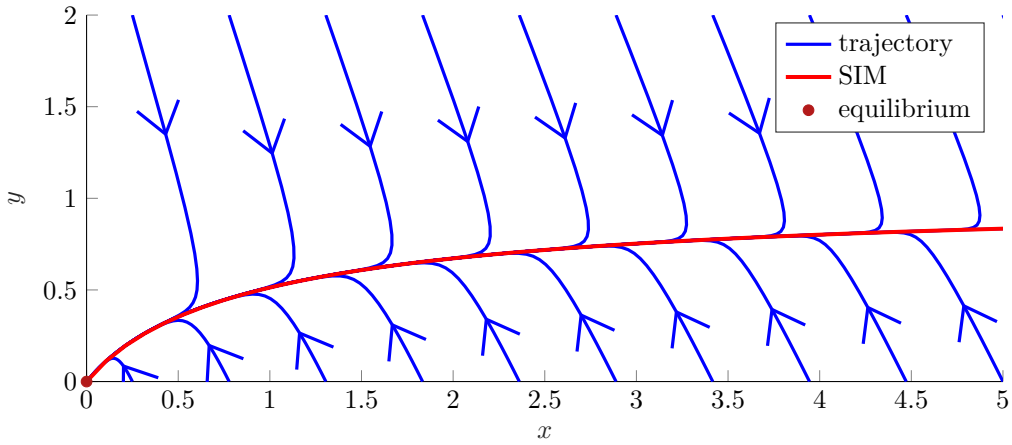

Figure 1.1: Phase portrait of simplified Michaelis-Menten-Henri enzyme reaction [MM13]. Trajectories bundle onto red 1-D SIM curve that is approximately given by $y = x/(1+x)$. All trajectories end in the equilibrium at the origin.

approximate this manifold. We do not intend to survey such methods, but refer to e.g. [LU16] for a compact overview.

In practice, many chemical reactions can be controlled, e.g., by adding a general input to the reactive system. Mathematically, this is modeled by optimal control problems. Central object of optimal control problems are differential equations that can be controlled by some control variables. In optimal control problems, a desired cost function depending on the controls and states is minimized. The problem is constrained by differential equations. Thus, optimal control problems inherit the difficulties of handling differential equations. To this end, it seems natural to investigate whether numerical manifold-based model reduction techniques can be applied to optimal control problems as well. Hellbrück (born Rehberg) [Reh13] has taken a step in this direction. In an offline phase, he approximated a great number of points on the SIM. Afterwards, in the online computation, he interpolated points on the SIM which reduced the dimension of the dynamics to the dimension of the manifold simplifying the optimal control problem. This led to an effective method for low-dimensional problems. Since interpolation and storage cost increases exponentially with the dimension of the problem (known as *curse of dimensionality*), high-dimensional problems cannot be solved efficiently with this ansatz. Consequently, one major aspect in this work is to develop an *online* SIM computation based optimal control method that avoids an offline computation.

Own Contribution. We propose an approach on how to integrate manifold-based model reduction methods into optimal control problems. Adapting the idea of the lifted Newton method [AD10], we introduce an approach that reduces the dimension and stiffness of optimal control problems utilizing the two SIM approximation methods Trajectory-Based Optimization Approach (TBOA) (see Section 2.4.3) and Zero-Derivative-Principle (ZDP) (see Section 2.4.1). Two numerical experiments verify the benefits of the proposed approach. This is joint work with Verschueren, Diehl, and Lebiedz. It can be found in [Hei+17].

Separatrices

The concentrations of chemical species are represented by real numbers. Therefore, if reaction mechanisms are modeled by ODEs, all considered variables were real valued as well. A look at *complex* valued dynamical systems reveals that other phase space structures than SIMs are important and significant for the long-term and asymptotic behavior. So far, we only considered dissipative dynamical systems like chemical reactions, i.e., in which the entropy does not decrease, and SIMs as phase space structures. Since the complex plane and holomorphic functions have a special, non-dissipative, conformal structure, which is expressed by the

Cauchy-Riemann equations, no SIMs in the classical sense can be found. However, other specific phase structures — so-called *separatrices* — with similar geometric properties play a role. Separatrices of 1-D complex dynamical systems and 1-D SIMs of 2-D real dynamical systems both are located in the phase space where the density of trajectories is high. Motivated by this similar local bundling behavior, we examine common features and difference of those two phase space structures. We apply SIM approximation methods to separatrices as well and show their limitations.

Since separatrices divide the phase portrait into regions with distinct dynamical behavior, their name stems from their geometrical property. Figure 1.2 shows the phase portrait of $z' = \cosh(z - 1/2)$. In this example, the separatrices at $y = k\pi$ for $k \in \mathbb{Z}$ divide the phase space into regions that consist of periodic orbits bundling around distinct equilibria.

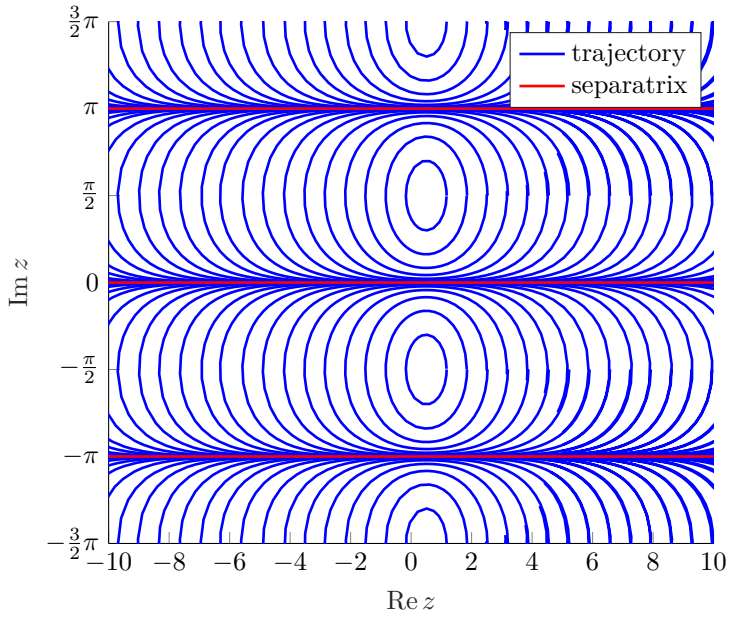

Figure 1.2: Phase portrait of $z' = \cosh(z - 1/2)$. Separatrices (red lines) divide the phase portrait into regions whose trajectories have qualitatively the same (long-term) behavior and stability properties. Modified from [HL19].

Separatrices play a crucial role in other mathematical areas, too. For example, recent research [Bro03a; Bro03b; BB04; Bro05; Neu+14; Neu+15; Sch+18] reveals

the impact of separatrices in holomorphic dynamical systems for analytical number theory. Riemann [Rie59] showed that the Riemann ζ function

$$\zeta(z) \coloneqq \sum_{n=1}^{\infty} \frac{1}{n^z}, \quad z \in \mathbb{C}$$

plays a pivotal role in analytical number theory since the location of its zeros allows locating the prime numbers within the natural numbers. One of the millennium problems is the Riemann hypothesis, which asserts that all non-trivial zeros of the Riemann ζ function are on the critical line $\operatorname{Re} z = 1/2$.

Since equilibria are important structures for dynamical systems, the previously listed research aims to generate information about the zeros of the ζ function by using it as right-hand side of differential equations. It is conjectured that separatrices are in close connection to equilibria. Thus, Broughan [Bro03a; Bro03b; BB04; Bro05] analyzed separatrices for holomorphic flows, in particular for the flow of the Riemann ξ function — a symmetrized version of the ζ function. Schleich et al. [Neu+14; Neu+15; Sch+18] studied the Newton flow of the Riemann ξ and ζ functions. They showed that information of separatrices at infinity might provide insight into the exact location of its zeros. It is evident that a complete separatrix characterization yields significant information about the zeros. In this work, we contribute to this research by studying separatrices "near and at infinity". Topological and geometric aspects of the phase space are investigated aiming at identifying and characterizing separatrices. We want to contribute to a deeper understanding of separatrices and the dynamics at infinity.

Own Contribution. The major contributions of this work are: We apply and compare SIM approximation methods to holomorphic dynamical systems showing that separatrices and SIMs share common geometric features. For 1-D polynomial differential equations, we prove that critical points at infinity have an incoming or outgoing separatrix. We introduce and calculate Lyapunov exponents for holomorphic dynamical systems. For the desingularized Newton flow of $z^2 + 1$, this determines the separatrix exactly. The idea to desingularize the (Newton) flow in this context goes back to Lebiedz. We conclude with a topological characterization of separatrices that divide two centers using the winding number of the corresponding periodic orbits. This work can partially be found in [HL19].

Thesis Outline

To conclude this section, we summarize the aims of this work:

(a) efficiently integrate *online* (manifold-based) model reduction techniques into the optimal control of ODEs in order to speed up computations,

(b) study the behavior of separatrices at infinity,

(c) characterize separatrices by their geometric, analytic or topological properties — ideally such that the resulting criterion is evaluable at infinity,

(d) examine differences and similarities of separatrices and SIMs via application of SIM approximation techniques to separatrices.

In Chapter 2, we briefly review dynamical systems and Fenichel's geometric singular perturbation theory for slow-fast systems. We give a short overview of manifold-based model reduction techniques that are applied in Chapters 3 and 5.

Chapter 3 addresses the issue of efficient integration of manifold-based model reduction methods in optimal control problems where the dynamics have multiple time scales. For this purpose, we develop a new approach and apply it to two example optimal control problems related to chemical kinetics.

Chapter 4 introduces the Riemann ζ and ξ functions. We devote attention to holomorphic and Newton flows and point out some essential properties of separatrices and desingularize the Newton flow.

Chapter 5 is a collection of methods and concepts that reveal key features of separatrices. We study the applicability of SIM approximation methods to holomorphic dynamical systems. Furthermore, we elucidate a direct connection between separatrices and critical points at infinity. We analyze the long-term behavior of separatrices with Lyapunov exponents. Moreover, we prove a topological characterization of separatrices between two centers and highlight complex time holomorphic flows.

We review the topics and results of this work in Chapter 6 and briefly discuss open issues and future research projects.

The following Fig. 1.3 gives a brief graphical overview of the relation between the following chapters.

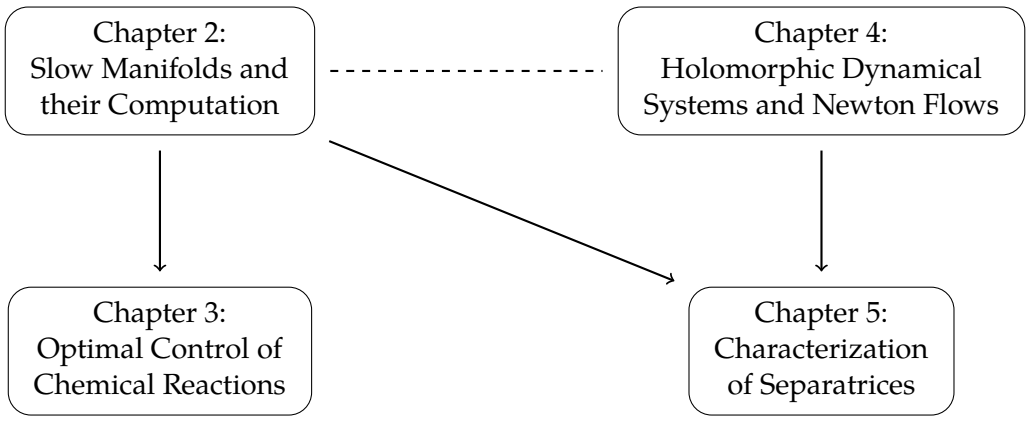

Figure 1.3: Structural relation of chapters in this thesis. An arrow from chapter A to chapter B indicates that B depends on A. The dashed line is a symbol for closely related chapters.

2 Slow Manifolds and Their Computation

This chapter introduces the analytical basics and notations which are used in the rest of this thesis. It is meant to give a quick overview and introduction to slow invariant manifolds, their numerical approximation and differential geometric definition of manifolds. We follow the representations of Kuehn, Hille and Teschl [Kue15; Hil76; Tes04].

Section 2.1 summarizes basic theory about dynamical systems, ordinary differential equations and differential algebraic equations. Section 2.2 captures Fenichel's theory involving slow invariant manifolds for slow-fast systems. We introduce some basic theory of differential geometry in Section 2.3 to define a "manifold". This theory is also used in Section 5.3. Section 2.4 provides some approximation methods for slow invariant manifolds which are relevant for this thesis.

2.1 Dynamical Systems

The Manifold-Based model reduction techniques discussed in this thesis are theoretically based on Fenichel's geometric singular perturbation theory. It involves ordinary differential equations and in general dynamical systems. In the following, we give a short introduction of the basic concepts in dynamical systems that are used in this thesis.

2.1.1 Ordinary Differential Equations

We begin with the following definition of a general dynamical system. Essentially, it is a mapping that describes the evolution of a certain state x with time t.

Definition 2.1 (Dynamical System)**.** Let (M, d) be a metric space. A *dynamical system* (*or flow*) Φ is a mapping $\Phi\colon \mathbb{R} \times M \to M$, $(t, x) \mapsto \Phi(t, x)$ such that

(D1) $\Phi(0, x) = x \quad \forall x \in M$,

(D2) $\Phi(t + s, x) = \Phi\big(t, \Phi(s, x)\big) \quad \forall t, s \in \mathbb{R}, x \in M$,

(D3) Φ is a continuous mapping.

One of the most basic concepts that describes the change of a variable with time, is an ordinary differential equation. Mathematically, it is an equation that involves the derivative of a function. It can be defined by the following definition and is essential in this work.

First, let $C^k(U, V)$ denote the space of all continuously differentiable functions up to order $k \in \mathbb{N}$ that map from the open set U to V. If $V = \mathbb{R}$, we write $C^k(U)$. Let the space of all continuous function from U to V be denoted by $C(U, V)$ resp. $C(U)$ for $V = \mathbb{R}$.

Definition 2.2 (ODE)**.** Let $U \subset \mathbb{R}^{k+2}$ be open, $F \in C(U)$. An *Ordinary Differential Equation* (*ODE*) is a relation of the form

$$F\left(t, z(t), z'(t), \dots, z^{(k)}(t)\right) = F\left(t, z(t), \frac{\mathrm{d}}{\mathrm{d}t} z(t), \dots, \frac{\mathrm{d}^k}{\mathrm{d}t^k} z(t)\right) = 0 \tag{2.1}$$

for an unknown function $z \in C^k(I), I \subset \mathbb{R}$. The highest derivative that appears in F is called the *order* of the differential equation. If F does not explicitly depend on t, the differential equation is called *autonomous*.

A *solution* of (2.1) is a function $z \in C^k(I_0)$ on an interval $I_0 \subset I$ such that

$$\Big(t, z(t), z'(t), \dots, z^{(k)}(t)\Big) \in U \quad \text{and} \quad F\left(t, z(t), z'(t), \dots, z^{(k)}(t)\right) = 0 \quad \forall\, t \in I_0.$$

We focus on ODEs of order k, where the matrix $\frac{\partial F}{\partial z^{(k)}}(\cdot)$ is regular (i.e. $\frac{\partial F}{\partial z^{(k)}}(\cdot) \neq 0$), such that the implicit function theorem is applicable and results at least locally in the *explicit* form of an ODE:

$$z^{(k)}(t) = f(t, z(t), \dots, z^{(k-1)}(t))$$

The definition of ODEs can be extended to vector-valued functions $z \in C^k(I, \mathbb{R}^{n_z})$, $n_z \in \mathbb{N}$. This leads to so-called systems of differential equations.

Definition 2.3 (explicit ODE system)**.** Let $I \coloneqq [t_0, t_\mathrm{f}]$ be an interval with $t_0 < t_\mathrm{f}$. Let $f_1, \dots, f_{n_z} \in C(U)$ for $U = I \times \underbrace{\mathbb{R}^{n_z} \times \cdots \times \mathbb{R}^{n_z}}_{k-\text{times}}$. An *explicit system of ODEs* is a system of the form

$$\begin{pmatrix} z_1^{(k)}(t) \\ \vdots \\ z_{n_z}^{(k)}(t) \end{pmatrix} = \begin{pmatrix} f_1\big(t, z(t), \dots, z^{(k-1)}(t)\big) \\ \vdots \\ f_{n_z}\big(t, z(t), \dots, z^{(k-1)}(t)\big) \end{pmatrix}, \quad \text{for all } t \in I, \tag{2.2}$$

where $z = (z_1, \dots, z_{n_z})^\mathsf{T}$.

By means of the vector-valued function $f = (f_1, \dots, f_{n_z})^\mathsf{T}$, (2.2) can be written as

$$z^{(k)}(t) = f\big(t, z(t), z'(t), \dots, z^{(k-1)}(t)\big).$$

The *order* of such a system of ODEs is defined analogously to Definition 2.2.

A special class of an explicit ODE of order 1 combined with a fixed value for a fixed point of time t_0 is the so-called initial value problem.

Definition 2.4 (IVP)**.** An *Initial Value Problem* (*IVP*) is a relation of the form

$$\begin{aligned} z'(t) &= f(t, z(t)) \quad \text{for all } t \in I \coloneqq [t_0, t_\mathrm{f}] \\ z(t_0) &= z_0, \end{aligned} \tag{2.3}$$

where $f \in C(U, \mathbb{R}^{n_z})$ and U is an open subset of $\mathbb{R}^{n_z+1}$ containing (t_0, z_0).

If we denote by $z(\cdot; z_0)$ the solution $z\colon I \to \mathbb{R}^{n_z}$ of the IVP (2.3) with initial value $z(0) = z_0 \in \mathbb{R}^{n_z}$, then $\Phi(t, z_0) \coloneqq z(t; z_0)$ is a dynamical system. For this reason, ordinary differential equations are special forms of dynamical systems.

So far, we did not show any results concerning the well-posedness of ordinary differential equations, i.e., we did not mention if such a problem has a solution. If there is a solution of an initial value problem, it should be unique. The following Theorem 2.5 shows that this is the case.

Theorem 2.5 (Picard-Lindelöf [Tes04, Theorem 2.3])**.** *Suppose $f \in C(U, \mathbb{R}^n)$, where U is an open subset of $\mathbb{R}^{n+1}$, and $(t_0, x_0) \in U$. If f is locally Lipschitz continuous in the second argument, then there exists a unique local solution $z(t)$ of the IVP* (2.3)*.*

Proof. A proof can be found, e.g, in [Tes04, Theorem 2.3]. □

Terminology, notation and basic definitions in dynamical systems
In this section, we shortly present notations and terms that are frequently used in dynamical systems. We follow the terminology used in the literature, e.g., see Broughan [Bro05, Section 2]. Let f be a differentiable function. The unique solution of an IVP with $z(0) = z_0$ is denoted by $z(t; z_0)$ and the corresponding mapping $t \mapsto z(t; z_0)$ is called *orbit or trajectory*. In the following, we will loosely speak of "the flow of f" sometimes even though not all solution trajectories exist globally. The flow of f can be seen as ensemble of orbits. Its graphical representation for (finitely many) trajectories is called a *phase portrait*.

For the sake of brevity, we will omit the arguments of functions whenever needed and context is clear. For instance, we write $z' = f(z)$ for the autonomous differential equation $z'(t) = f\big(z(t)\big)$.

The zeros of the right-hand side f are of particular interest for the global behavior of ODEs. They are called *equilibria, critical points or zeros* and yield constant trajectories $z(t; z_0) = z_0$. In the following, we define the type of such a critical point in the plane $\mathbb{R}^2$ (cf. [Per00] and [Bro05]). The phase portrait of a non-linear ODE is close to equilibria locally given by its linearization (see e.g. [Per00]).

- A *stable* (*resp. unstable*) *node* is a zero z^* for which there is a $\delta > 0$ such that each trajectory in a deleted neighborhood $\dot{U}_\delta(z^*) = U_\delta(z^*) \setminus \{z^*\}$ of z^* approaches z^* along a well-defined tangent line as $t \to \infty$ (resp. $t \to -\infty$).
- A *center* is a zero z^* for which there is a $\delta > 0$ such that every solution curve in the deleted neighborhood $\dot{U}_\delta(z^*)$ is a closed curve with z^* in its interior.
- A *saddle* (*point*) is a zero z^* for which there are trajectories which tend to z^* in both positive and negative time.
- A *stable* (*resp. unstable*) *focus* is a zero z^* for which there is a $\delta > 0$ such that every trajectory in a deleted neighborhood $\dot{U}_\delta(z^*)$ spirals toward (away from) z^*, i.e., when the ODE is transformed to polar coordinates (r, θ) it satisfies $r(t) \to 0$ and $|\theta(t)| \to \infty$ as $t \to \infty$ (resp. $t \to -\infty$).

2.1.2 Holomorphic Ordinary Differential Equations

For isothermal chemical reactions the underlying ODE based on the law of mass action has a right-hand side f that is real-analytic. So far, we did not make use of this additional information. In this work, we also consider dynamical systems

in the complex plane (see Chapter 4). A (right-hand side) function which is (complex) differentiable in an open set $U \subset \mathbb{C}$, is always infinitely many times differentiable. We call such functions *holomorphic*. The next section briefly presents dynamical systems involving holomorphic functions.

Definition 2.6 (Holomorphic IVP)**.** A *holomorphic IVP* is a relation of the form

$$\begin{aligned} z'(t) &= f(t, z(t)) \quad \text{for all } (t, z) \in U \\ z(t_0) &= z_0, \end{aligned} \tag{2.4}$$

where $f : U \to \mathbb{C}^n$ is holomorphic in an open subset $U \subset \mathbb{C}^{n+1}$ containing (t_0, z_0).

The solution of (2.4) is a parametrized holomorphic curve $z : V \to \mathbb{C}^n$, defined in an open subset $V \subset \mathbb{C}$ such that $\big(t, z(t)\big) \in U$ for all $t \in V$. Existence and uniqueness of a solution for this holomorphic IVP is similar to the real case as the following theorem shows. Furthermore, it shows that the solution $z(t)$ depends holomorphically on its initial value.

Theorem 2.7. (*Existence and Uniqueness* [*Ily07, Theorem 1.1*]) *For any holomorphic differential equation $z'(t) = f\big(t, z(t)\big)$ and every point $(t_0, z_0) \in U$ there is a $\varepsilon > 0$ such that the polydisk*

$$D_\varepsilon = \big\{|t - t_0| < \varepsilon, \big|z_j - z_{0,j}\big| < \varepsilon, j = 1, \ldots, n\big\} \subset U,$$

is included in U. Further, a solution of the initial value problem (2.6) *exists and is unique in this polydisk D_ε. This solution depends holomorphically on the initial value $z_0 \in \mathbb{C}^n$ and on any additional parameters, provided that the vector function f depends holomorphically on these parameters.*

Proof. see e.g. [Ily07, Theorem 1.1]. □

2.1.3 Boundary Value Problems

For IVPs, the state vector $z(\cdot)$ at the beginning of the considered time interval $I = [t_0, t_\mathrm{f}]$ is fixed. In many applications, we do not require all initial values to be fixed but have restrictions for a subset of the variables at the end of the time interval. In particular, for optimal control problems we might want some variables

to satisfy additional constraints, e.g., at the end of a chemical reaction a species should be depleted. The next definition introduces such problems in a general setting. Later, we will see that problems of this type naturally arise as necessary optimality conditions for optimal control problems.

Definition 2.8 (BVP)**.** Let $f\colon I \times \mathbb{R}^{n_z} \to \mathbb{R}^{n_z}$ and $r\colon \mathbb{R}^{n_z} \times \mathbb{R}^{n_z} \to \mathbb{R}^{n_z}$ be a sufficiently smooth function with an interval $I = [t_0, t_\mathrm{f}]$. A *two-point Boundary Value Problem* (*BVP*) is a problem of the form

$$\begin{aligned} z'(t) &= f\big(t, z(t)\big), && \text{for all } t \in I \\ 0 &= r\big(z(t_0), z(t_\mathrm{f})\big). \end{aligned}$$

The existence and uniqueness of solutions of BVP (2.8) is more complicated than for IVPs. For more details see, e.g., [AMR87].

2.1.4 Differential Algebraic Equations

Many dynamical systems are not in the form of an ODE (2.1) but rather depend on additional parameters or even variables. Imagine again a chemical reaction mechanism, where we can "manipulate" the reaction by addition of a certain reactant. A special class of such problems is introduced in this subsection. The following introduction is based on [Ger12] and [Bie10].

Definition 2.9 (DAE)**.** Let $I \coloneqq [t_0, t_\mathrm{f}] \subset \mathbb{R}$, with $t_0 < t_\mathrm{f}$ be a compact interval, $F : I \times \mathbb{R}^{n_z} \times \mathbb{R}^{n_z} \times \mathbb{R}^{n_u} \to \mathbb{R}^{n_z}$ a sufficiently smooth function. The function $u\colon I \to \mathbb{R}^{n_u}$ is an external input and referred to as *control* (*function*/*variable*). The implicit equation

$$F\big(t, z(t), z'(t), u(t)\big) = 0 \quad \text{for all } t \in I, \tag{2.6}$$

is called *Differential-Algebraic Equation* (*DAE*). We call the function $z(\cdot)$ *state* (*function*/*variable*).

By "sufficiently smooth" function, we mean that this function is at least continuous. If derivatives up to order $k \in \mathbb{N}$ of this function are present, then it is a function in $C^k(\cdot)$.

We consider a special class of DAEs, where the derivative of some of the state variables is given explicitly. This form is a more structured DAE and has still a wide variety of applications.

Definition 2.10 (Semi-Explicit DAE)**.** Let $I \coloneqq [t_0, t_\mathrm{f}] \subset \mathbb{R}$ with $t_0 < t_\mathrm{f}$ be a compact interval, the state $z = (x, y)^\mathsf{T} \in \mathbb{R}^{n_z}$ be decomposed into components $x : I \to \mathbb{R}^{n_x}$ and $y : I \to \mathbb{R}^{n_y}$. Let $u : I \to \mathbb{R}^{n_u}$ be a given control function. Let $f : I \times \mathbb{R}^{n_x} \times \mathbb{R}^{n_y} \times \mathbb{R}^{n_u} \to \mathbb{R}^{n_x}$ and $g : I \times \mathbb{R}^{n_x} \times \mathbb{R}^{n_y} \times \mathbb{R}^{n_u} \to \mathbb{R}^{n_y}$ be sufficiently smooth functions. A DAE of the form

$$x'(t) = f\big(t, x(t), y(t), u(t)\big) \quad \text{for all } t \in I, \tag{2.7a}$$

$$0 = g\big(t, x(t), y(t), u(t)\big) \quad \text{for all } t \in I, \tag{2.7b}$$

is called *semi-explicit DAE*. The function $x(\cdot)$ is called *differential variable* and $y(\cdot)$ *algebraic variable*. Correspondingly, Eq. (2.7a) is called *differential equation* of Eq. (2.7) and Eq. (2.7b) *algebraic equation*.

The fully-implicit DAE (2.6) can be transformed to semi-explicit form by adding a new algebraic variable y:

$$\begin{aligned} z'(t) &= y(t), \\ 0 &= F\big(t, z(t), y(t), u(t)\big). \end{aligned}$$

Thus, the class of semi-explicit DAEs still contains fully-implicit DAEs. However, the introduction of new algebraic variables can lead to discontinuities in the differential state (cf. [Ger12, Example 1.1.6]).

Consider the time derivative of the algebraic equation (2.7b)

$$0 = D_t g(\cdot) + D_x g(\cdot) x'(t) + D_y g(\cdot) y'(t) + D_u g(\cdot) u'(t), \tag{2.8}$$

where the arguments $\big(t, x(t), y(t), u(t)\big)$ were omitted. If the matrix $D_y g(\cdot)$ is invertible, then (2.8) can be used to derive an underlying ODE:

$$\begin{aligned} x'(t) &= f\big(t, x(t), y(t), u(t)\big) \quad \text{for all } t \in I, \\ y'(t) &= -D_y^{-1} g(\cdot) \left(D_t g(\cdot) + D_x g(\cdot) x'(t) + D_u g(\cdot) u'(t)\right), \quad \text{for all } t \in I. \end{aligned}$$

This consideration can be generalized and leads to the concept of the index of a DAE.

Definition 2.11 (Index of a DAE)**.** Consider the DAEs of the form (2.6) or (2.7) with a given control function $u(\cdot)$. The *index of a DAE* is the minimum integer $k \in \mathbb{N}_0$ such that the system of the first k differentiations of the DAE system (w.r.t. time t) determine an ODE. For an implicit DAE, the set of differential equations

$$0 = \frac{\mathrm{d}^i}{\mathrm{d}t^i} F\big(t, z(t), z'(t), u(t)\big) \quad i = 0, 1, \ldots, k$$

yields an ODE. For a semi-explicit DAE, the index can be determined through iterative differentiations of the algebraic equation w.r.t. time t:

$$\begin{aligned} x'(t) &= f\big(t, x(t), y(t), u(t)\big) \\ 0 &= \frac{\mathrm{d}^i}{\mathrm{d}t^i} g\big(t, x(t), y(t), u(t)\big) \quad i = 0, 1, \ldots, k. \end{aligned}$$

Numerically, DAEs of higher index are in general more difficult to solve than those of lower index.

Having introduced the basic concepts of dynamical systems, we will now move to Fenichel's theory. This theory is essential for the existence of manifolds which we use to reduce the ODE models and optimal control problems.

2.2 Slow Manifolds and Singular Perturbation Theory

For instance in ordinary differential equations arising in chemistry and biology, the velocity of change of the variables differs from slow to fast. This leads to slow invariant manifolds in the phase space. The theory of slow (invariant) manifolds was first introduced for singular perturbed systems. Hence, we consider so-called slow-fast systems where an explicit separation of the variables $z = (x, y)^{\mathsf{T}}$ is given:

Definition 2.12 (Slow-Fast System)**.** Let $m, n \in \mathbb{N}$. An (m,n)*-slow-fast system* is a system of ordinary differential equations in the form

$$\begin{array}{rcll} \frac{\mathrm{d}}{\mathrm{d}\tau} x(\tau) & = & \dot{x}(\tau) & = f(x(\tau), y(\tau), \varepsilon), \\ \varepsilon \frac{\mathrm{d}}{\mathrm{d}\tau} y(\tau) & = & \varepsilon \dot{y}(\tau) & = g(x(\tau), y(\tau), \varepsilon), \end{array} \tag{2.10}$$

where $f\colon \mathbb{R}^m \times \mathbb{R}^n \times \mathbb{R} \to \mathbb{R}^m$, $g\colon \mathbb{R}^m \times \mathbb{R}^n \times \mathbb{R} \to \mathbb{R}^n$ are smooth functions and $0 < \varepsilon \ll 1$. The quantity τ is called *slow time*, the variables $x = (x_1, \ldots, x_m)$ are

called *slow variables* and $y = (y_1, \ldots, y_n)$ are called *fast variables*. If the *slow time* τ is transformed to the *fast time* $t := \tau/\varepsilon$, this equivalent form is obtained

$$\begin{aligned} \tfrac{\mathrm{d}}{\mathrm{d}t}x(t) &= x'(t) &&= \varepsilon f(x(t), y(t), \varepsilon), \\ \tfrac{\mathrm{d}}{\mathrm{d}t}y(t) &= y'(t) &&= g(x(t), y(t), \varepsilon), \end{aligned} \tag{2.11}$$

Remark 2.13. The parameter ε in Eq. (2.10) measures the time scale separation between the slow variables x and the fast variables y. Thus, ε is called *time-scale parameter*. The notation $0 < \varepsilon \ll 1$ indicates that ε is small and positive.

Remark 2.14. The functions f and g in Eq. (2.11) can still depend on ε. They have to be in $\mathcal{O}(1)$, where $v(x_0, y_0, \varepsilon) \in \mathcal{O}\left(w(x_0, y_0, \varepsilon)\right)$ holds by definition if for $\varepsilon \to 0$, there exist positive functions $k(x, y)$ and $\varepsilon(x, y)$ such that

$$\left|v(x_0, y_0, \varepsilon)\right| \leq k(x_0, y_0) \left|w(x_0, y_0, \varepsilon)\right| \quad \forall\, 0 < \varepsilon < \varepsilon(x_0, y_0) < \varepsilon_0.$$

Example 2.15. Consider the following example.

$$\begin{aligned} x'(t) &= \varepsilon(-x(t) + \varepsilon), \\ y'(t) &= x(t) - y(t). \end{aligned}$$

It is a (1,1)-slow-fast system with $f(x, y, \varepsilon) = -x + \varepsilon$ and $g(x, y, \varepsilon) = x - y$. $f \in \mathcal{O}(1)$, because

$$\left|f(x_0, y_0, \varepsilon)\right| = |-x_0 + \varepsilon| \leq \left(|x_0| + \varepsilon_0\right) \cdot 1 \quad \forall\, 0 < \varepsilon < \varepsilon_0$$

and $g \in \mathcal{O}(1)$, which can be shown analogously.

Since ε is a small positive number, it is natural to consider the limit $\varepsilon \to 0$, where the time scale separation is infinitely high.

Definition 2.16 (Slow and Fast Subsystems)**.** In the special case $\varepsilon = 0$ (that is called *singular limit*), Eq. (2.10) turns into the semi-explicit DAE

$$\begin{aligned} \dot{x}(\tau) &= f(x(\tau), y(\tau), 0), \\ 0 &= g(x(\tau), y(\tau), 0). \end{aligned} \tag{2.12}$$

This DAE is called *slow subsystem*. The system obtained by setting $\varepsilon = 0$ in (2.11)

is called the *fast subsystem*.

$$\begin{aligned} x'(t) &= 0, \\ y'(t) &= g(x(t), y(t), 0). \end{aligned} \tag{2.13}$$

The slow variables x are constant in the fast subsystem (2.13) and can be inserted directly in the ODE for the fast variables y. The slow subsystem can be interpreted as an ODE w.r.t. x on the set

$$0 = g(x(\tau), y(\tau), 0).$$

If this set describes a manifold it is called *critical manifold*.

Definition 2.17 (Critical manifold)**.** The set

$$C_0 \coloneqq \left\{(x, y) \in \mathbb{R}^m \times \mathbb{R}^n \colon g(x, y, 0) = 0\right\}$$

is called *critical set*. If C_0 is a submanifold of $\mathbb{R}^m \times \mathbb{R}^n$, we refer to C_0 as the *critical manifold*.

Example 2.18. Consider again Example 2.15:

$$\begin{aligned} x'(t) &= \varepsilon(-x(t) + \varepsilon), \\ y'(t) &= x(t) - y(t). \end{aligned}$$

The critical manifold is given by the identity line $y = x$, i.e.,

$$C_0 = \left\{(x, y) \in \mathbb{R} \times \mathbb{R} \colon x = y\right\}.$$

Fenichel's geometric singular perturbation theory [Fen71; Fen74; Fen77; Fen79] extends the invariant manifold theory to slow-fast systems and tackles the question whether a manifold exists for $\varepsilon > 0$ as well.

Definition 2.19 (Normally Hyperbolic)**.** A set $S \subset C_0$ is called *normally hyperbolic* if the $n \times n$ matrix of the partial derivatives of g w.r.t. y, denoted as $(D_y g)(p, 0)$, has no eigenvalues with zero real part for all $p \in S$.

For a normally hyperbolic critical manifold C_0, the slow subsystem (2.12) is a semi-explicit DAE of index 1.

Definition 2.20 (Attracting, Repelling, Saddle Type)**.** A normally hyperbolic subset $S \subset C_0$ of the critical manifold is called *attracting* if all eigenvalues of $(D_y g)(p, 0)$ have negative real part for all $p \in S$. It is called *repelling* if all eigenvalues of $(D_y g)(p, 0)$ have positive real part for all $p \in S$. If S is normally hyperbolic and neither attracting nor repelling, it is of *saddle type*.

The following definition is used to define a meaningful distance between two different sets.

Definition 2.21 (Hausdorff Distance)**.** Let $d \in \mathbb{N}$. The *Hausdorff distance* between two nonempty sets $V, W \subset \mathbb{R}^d$ is defined by

$$d_H(V, W) \coloneqq \max \left\{ \sup_{v \in V} \inf_{w \in W} \|v - w\| \, , \sup_{w \in W} \inf_{v \in V} \|v - w\| \right\}.$$

Finally, we are able to state Fenichel's theorem.

Theorem 2.22 (Fenichel's theorem [Kue15, Theorem 3.1.4])**.** *Suppose $S_0 \subset C_0$ is a compact normally hyperbolic submanifold (possibly with boundary) of the critical manifold of (2.10) and that $f, g \in C^r$ with $r < \infty$. Then for $\varepsilon > 0$ sufficiently small, the following holds:*

(*F1*) *There exists a locally invariant manifold S_ε diffeomorphic to S_0. Locally invariant means that trajectories can enter or leave S_ε only through its boundary.*

(*F2*) *S_ε has Hausdorff distance $\mathcal{O}(\varepsilon)$ from S_0, i.e., $d_H(S_\varepsilon, S_0) = \mathcal{O}(\varepsilon)$.*

(*F3*) *The flow on S_ε converges to the slow flow of (2.12) as $\varepsilon \to 0$.*

(*F4*) *S_ε is C^r-smooth.*

(*F5*) *S_ε is normally hyperbolic and has the same stability properties (attracting, repelling or of saddle type) w.r.t. the fast variables as S_0.*

(*F6*) *S_ε is usually not unique. In regions with fixed distance from ∂S_ε, all manifolds satisfying (F1)–(F5) lie at a Hausdorff distance $\mathcal{O}(e^{-K/\varepsilon})$ from each other for some $0 < K = \mathcal{O}(1)$.*

Definition 2.23. A manifold S_ε, as obtained in Theorem 2.22, is called *Slow Invariant Manifold (SIM)*.

Furthermore, Fenichel proves a representation of a SIM as regular asymptotic expanion in the time scale parameter ε.

Theorem 2.24 ([Kue15, Theorem 11.1.1])**.** *Under the same assumptions as for Theorem 2.22, a locally invariant manifold S_ε exists according to Theorem 2.22. Further, S_ε can be represented locally as a graph*

$$S_\varepsilon = \{(x, y) \in \mathbb{R}^{m+n} \colon y = h_\varepsilon(x)\},$$

where the map $h_\varepsilon \colon \mathbb{R}^m \to \mathbb{R}^n$ has a regular asymptotic expansion

$$h_\varepsilon(x) = h_0(x) + \varepsilon h_1(x) + \varepsilon^2 h_2(x) + \varepsilon^3 h_3(x) + \cdots .$$

The dynamics on S_ε are given by $\frac{\mathrm{d}}{\mathrm{d}\tau} x(\tau) = f(x(\tau), h_\varepsilon(x(\tau)), \varepsilon)$ using the slow time $\tau = \varepsilon t$.

Fenichel's Theorem 2.22 states that S_ε is not unique. Therefore, it is formally not correct to call S_ε "the" slow manifold. However, all manifolds satisfying Fenichel's Theorem 2.22 lie at Hausdorff distance $\mathcal{O}(e^{K/\varepsilon})$ from each other. These $\mathcal{O}(e^{K/\varepsilon})$-terms do not affect the regular asymptotic expansion of $h_\varepsilon(x)$ because $e^{K/\varepsilon} = \mathcal{O}(\varepsilon^k)$ for all $k \in N$ as $\varepsilon \to 0$. Thus, the choice of a slow manifold satisfying (F1)–(F5) is arbitrary in most analytical and numerical treatments.

Theorem 2.24 can be used to compute S_ε analytically as the following Remark 2.25 illustrates.

Remark 2.25 (Invariance Equation). Derivation of the graph representation $y = h_\varepsilon(x)$ of S_ε w.r.t. t yields

$$g(x, h_\varepsilon(x), \varepsilon) = \varepsilon D h_\varepsilon(x) f(x, h_\varepsilon(x), \varepsilon), \tag{2.14}$$

where we used (2.11) and omitted the dependence on t in all arguments for the sake of brevity.

Taylor expansion of f and g about $\varepsilon = 0$ and plugging in the series expansion for $h_\varepsilon(x)$ allows us to compare the coefficients of ε^k. This leads iteratively to the coefficient functions $h_i(x)$ of $h_\varepsilon(x)$ for $i = 0, 1, \ldots$. It is easy to see that the coefficient $h_0(x)$ coincides with the critical manifold.

We demonstrate Remark 2.25 with the following example:

Example 2.26. Consider once again Example 2.15.

$$\begin{aligned} x'(t) &= \varepsilon(-x(t)+\varepsilon), \\ y'(t) &= x(t)-y(t). \end{aligned} \tag{2.15}$$

Applying the invariance equation (2.14) to this example results in

$$x - h_\varepsilon(x) = g(x, h_\varepsilon(x), \varepsilon) = \varepsilon Dh_\varepsilon(x) f(x, h_\varepsilon(x), \varepsilon) = \varepsilon Dh_\varepsilon(x)(-x+\varepsilon).$$

This can be rewritten and ordered in terms of the powers of ε to:

$$\begin{aligned} &x - h_0(x) - \varepsilon h_1(x) - \varepsilon^2 h_2(x) - \varepsilon^3 h_3(x) + \mathcal{O}(\varepsilon^4) \\ =&\varepsilon(-xh_0'(x)) + \varepsilon^2(-xh_1'(x) + h_0'(x)) + \varepsilon^3(-xh_2'(x) + h_1'(x)) + \mathcal{O}(\varepsilon^4). \end{aligned} \tag{2.16}$$

For the calculation of the slow invariant manifold, we compare the term of the powers of ε starting with ε^0: The coefficient of ε^0 of the left-hand side in Eq. (2.16) is $x - h_0(x)$. Thus, it holds $h_0(x) = x$. Comparison of the coefficients of ε^1 yields the equation

$$-h_1(x) = -xh_0'(x) = -x \quad \Leftrightarrow \quad h_1(x) = x.$$

The ε^2 terms in Eq. (2.16) show that

$$-h_2(x) = -xh_1'(x) + h_0'(x) = -x + 1 \quad \Leftrightarrow \quad h_2(x) = x - 1.$$

It easily follows by induction that the solution of the equation for coefficient ε^k

$$-h_k(x) = -xh_{k-1}'(x) + h_{k-2}'(x)$$

is $h_k(x) = x - 1$ for all $k \geq 2$. The asymptotic expansion is thus given by

$$y = h_\varepsilon(x) = x + \varepsilon x + (x-1)\sum_{k=2}^{\infty} \varepsilon^k = x + \varepsilon x + (x-1)\frac{\varepsilon^2}{1-\varepsilon} = \frac{x-\varepsilon^2}{1-\varepsilon}, \tag{2.17}$$

which leads directly to

$$S_\varepsilon = \left\{ (x,y) \in \mathbb{R}^2 \colon y = h_\varepsilon(x) = \frac{x-\varepsilon^2}{1-\varepsilon} \right\}.$$

For this example, the slow invariant manifold S_ε does not coincide with the critical manifold C_0 which was shown in Example 2.18 to be the identity line $y = x$.

The following functions solve the ordinary differential equations (2.15):

$$\big(x(t), y(t)\big) = \left(\varepsilon + c_1 e^{-\varepsilon t},\, \varepsilon + \frac{c_1 e^{-\varepsilon t}}{1-\varepsilon} + c_2 e^{-t}\right),$$

where the constants $c_1, c_2 \in \mathbb{R}$ are given implicitly by the initial values for $x(0)$ and $y(0)$. Eliminating the time t, the solution in the phase plane is

$$y(x) = \varepsilon + \frac{x-\varepsilon}{1-\varepsilon} + c_2\left(\frac{x-\varepsilon}{c_1}\right)^{\frac{1}{\varepsilon}} = \frac{x-\varepsilon^2}{1-\varepsilon} + c_2\left(\frac{x-\varepsilon}{c_1}\right)^{\frac{1}{\varepsilon}}.$$

On the slow flow for (2.26) the constant c_2 has to vanish, because otherwise the dynamics of y would include a term in $\mathcal{O}(e^{-t})$, which converges faster to zero than terms in $\mathcal{O}(e^{-\varepsilon t})$. But then, we obtain the same representation for the SIM as in Eq. (2.17).

The next example demonstrates the effectiveness of the invariance equation (2.14). A general solution of the ODE need not be known (like in Example 2.26) to calculate the slow invariant manifold (approximately).

Example 2.27 (Michaelis-Menten-Henri enyzme mechanism)**.** A simple chemical reaction mechanism with enzymes is given by the Michaelis-Menten-Henri mechanism [MM13]

$$S + E \underset{k_{-1}}{\overset{k_1}{\rightleftharpoons}} C \overset{k_2}{\to} P + E,$$

where S is a substrate, E is an enzyme, C the corresponding substrate-enzyme-complex and P a product. k_1, k_{-1} and k_2 are the reaction rates and usually determined by the Arrhenius equation with empirical data. Since enzymatic reactions are usually isothermal, we assume these parameters to be constant.

Chemical kinetics translate this mechanism into an ODE in the concentrations $c_{\mathrm{X}}(t)$ of each chemical species X:

$$\begin{aligned}
\dot{c_{\mathrm{S}}}(t) &= -k_1 c_{\mathrm{S}}(t) c_{\mathrm{E}}(t) + k_{-1} c_{\mathrm{C}}(t) \\
\dot{c_{\mathrm{E}}}(t) &= -k_1 c_{\mathrm{S}}(t) c_{\mathrm{E}}(t) + (k_{-1} + k_2) c_{\mathrm{C}}(t) \\
\dot{c_{\mathrm{C}}}(t) &= k_1 c_{\mathrm{S}}(t) c_{\mathrm{S}}(t) - (k_{-1} + k_2) c_{\mathrm{C}}(t) \\
\dot{c_{\mathrm{P}}}(t) &= k_2 c_{\mathrm{C}}(t)
\end{aligned} \tag{2.18}$$

with initial value $(c_{\mathrm{S}}(0), c_{\mathrm{E}}(0), c_{\mathrm{C}}(0), c_{\mathrm{P}}(0)) = (c_{\mathrm{S}}^0, c_{\mathrm{E}}^0, c_{\mathrm{C}}^0, c_{\mathrm{P}}^0)$.

We simplify these 4 equations following [Mur93]. In (2.18), the concentration of the product P only depends on C. Furthermore, $c_{\mathrm{E}}(t) + c_{\mathrm{C}}(t)$ is an invariant quantity. Suppose, at the beginning of the reaction no substrate-enzyme-complex C is present. Then $c_{\mathrm{E}}(t) + c_{\mathrm{C}}(t) \equiv c_{\mathrm{E}}^0 + c_{\mathrm{C}}^0 = c_{\mathrm{E}}^0$.

A subsequent transformation with

$$\begin{aligned} \tau &= k_1 c_{\mathrm{E}}^0 t, \quad x(t) = \tfrac{c_{\mathrm{S}}(t)}{c_{\mathrm{S}}^0}, \quad y(t) = \tfrac{c_{\mathrm{C}}(t)}{c_{\mathrm{C}}^0} \\ \beta &= \tfrac{k_2}{k_1 c_{\mathrm{S}}^0}, \qquad \kappa = \tfrac{k_{-1}+k_2}{k_1 c_{\mathrm{S}}^0}, \quad \varepsilon = \tfrac{c_{\mathrm{E}}^0}{c_{\mathrm{S}}^0}. \end{aligned}$$

gives rise to the following two-dimensional system of ODEs:

$$\begin{aligned} \dot{x}(t) &= -x(t) + \big(x(t) + \kappa - \beta\big)\, y(t) \\ \varepsilon \dot{y}(t) &= x(t) - \big(x(t) + \kappa\big)\, y(t), \end{aligned}$$

which is already in singularly perturbed form. The time scale separation parameter ε has a concrete interpretation. It is the initial concentration of the enzyme E divided by the initial concentration of the substrate S.

The invariance equation (Remark 2.25) is evaluated with the help of Maple and shows that the regular asymptotic expansion is

$$h_\varepsilon(x) = \frac{x}{x+\kappa} + \frac{\kappa\beta x}{(x+\kappa)^4}\varepsilon - \frac{\kappa\beta x(\kappa^2 - 2\kappa\beta + \kappa x + 3\beta x)}{(x+\kappa)^7}\varepsilon^2 + \mathcal{O}(\varepsilon^3).$$

Thus, the critical manifold C_0 does not coincide with the slow invariant manifold. Since the coefficients $h_i(x)$ of the powers ε^i become very complicated, an explicit formula for $h_\varepsilon(x)$ is unknown. To conclude this section, the invariance equation (2.14) is a useful tool to calculate invariant manifolds.

2.3 Introduction to Smooth Manifolds

In Fenichel's theory (see Section 2.2) a very import mathematical term is the manifold. Until now, we handled the dynamics and manifolds in the surrounding space $\mathbb{R}^n$. However, it is possible to regard manifolds as objects without surrounding space. In this section, we give a brief introduction into differential geometry.

2.3.1 Smooth Manifolds

To be able to define smooth manifolds in an abstract setting, we define topologies first.

Definition 2.28 (Topology)**.** Let X be a set. A subset $\mathcal{T}$ of the power set of X is a *topology*, if it satisfies the following statements:

(T1) $\emptyset, X \in \mathcal{T}$,

(T2) If $U, V \in \mathcal{T}$, then $U \cap V \in \mathcal{T}$,

(T3) If $U_i \in \mathcal{T}$, $i \in I$ for an arbitrary index set I, then $\bigcup_{i \in I} U_i \in \mathcal{T}$.

We call the elements of a topology *open sets* and its complements *closed sets*. A topology $\mathcal{T}$ is *Hausdorff* if for arbitrary $p, q \in X, p \neq q$ there are $U, V \in \mathcal{T}$ such that

$$p \in U, q \in V \text{ and } U \cap V = \emptyset.$$

$\mathcal{T}$ satisfies the *second axiom of countability* if there is a countable subset $\mathcal{B}$ of $\mathcal{T}$ such that for all $p \in X$ and $U \in \mathcal{T}$ there is $V \in \mathcal{B} \subset \mathcal{T}$ such that $p \in V \subset U$.

With this, manifolds in the context of differential geometry can be defined in the following way.

Definition 2.29 (Smooth Manifold)**.** Let $n \in \mathbb{N}$. A *smooth manifold of dimension* n is a set M with a topology $\mathcal{T}$ and a set $\mathcal{A} = \left\{(U_\alpha, \phi_\alpha)\right\}_{\alpha \in A}$ for an index set A such that

(M1) $U_\alpha \in \mathcal{T}$ for all $\alpha \in A$ and $\mathcal{T}$ is Haussdorff and satisfies the second axiom of countability,

(M2) $\bigcup_{\alpha \in A} U_\alpha = M$,

(M3) for all $\alpha \in A$ the mapping $\phi_\alpha \colon U_\alpha \to \phi_\alpha(U_\alpha) \subset \mathbb{R}^n$ is a homeomorphism (thus, the image $\phi_\alpha(U_\alpha) \subset \mathbb{R}^n$ is open). The mappings ϕ_α are called *charts* (see Fig. 2.1).

(M4) for all $\alpha_1, \alpha_2 \in A$ with $U_{\alpha_1} \cap U_{\alpha_2} \neq \emptyset$ the mapping

$$\phi_{\alpha_2} \circ \phi_{\alpha_1}^{-1} \colon \phi_{\alpha_1}(U_{\alpha_1} \cap U_{\alpha_2}) \to \phi_{\alpha_2}(U_{\alpha_1} \cap U_{\alpha_2})$$

is a smooth diffeomorphism. We call those charts *compatible*.

(M5) $\mathcal{A}$ is a maximal family satisfying (M1)–(M4), i.e., there is no other chart that is compatible with all other charts of $\mathcal{A}$.

A set $\mathcal{A}$ satisfying (M2)–(M4) is called *atlas*.

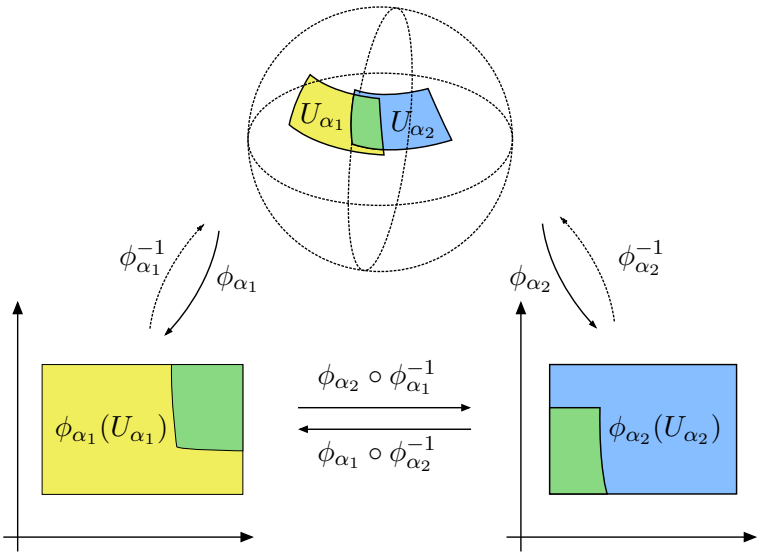

Figure 2.1: Illustration of a smooth manifold of dimension 2 (sphere) and compatible charts.

In order to define the concept of derivatives for smooth manifolds, it is necessary to define the so-called tangent space. The tangent space can be seen as a vector space that linearly approximates a smooth manifold at a given point p of this manifold.

Definition 2.30 (Tangent Space)**.** Let M be a smooth manifold and $p \in M$. The *tangent space* in p of M is the linear space

$$T_pM \coloneqq \{\omega \colon C^\infty(M) \to \mathbb{R} \mid \omega \text{ is linear and satisfies the product rule } \omega(fg) = \omega(f)g(p) + f(p)\omega(g) \quad \forall\, f, g \in C^\infty(M)\}$$

with $(\omega_1 + \omega_2)(f) \coloneqq \omega_1(f) + \omega_2(f)$ and $(\lambda\omega)(f) \coloneqq \lambda\omega(f)$ for $\lambda \in \mathbb{R}$. The elements of T_pM are called *tangential vectors*.

If $M = \mathbb{R}^n$ and consequently $T_pM = \mathbb{R}^n$, it can be shown that there is a one-to-one relation between the differentiations $\omega \in T_pM$ and directional derivatives in direction $v \in \mathbb{R}^n = T_pM$.

The union of tangent spaces for all points of a manifolds form the tangent bundle.

Definition 2.31 (Tangent Bundle)**.** Let M be a smooth manifold. The *tangent bundle* of M is given by

$$TM \coloneqq \left\{(p, v) \colon p \in M, v \in T_pM\right\}.$$

We will use the definition of the tangent space and bundle for the definition of Lyapunov exponents in Section 5.3. There, we need a set of a all possible directions in which one can tangentially pass through a point of a smooth manifold.

2.4 Manifold-Based Model Reduction Techniques

In Section 2.2, we introduced the slow invariant manifold. The regular asymptotic expansion is a way of computing this slow manifold. However for more than just one slow variable, this is not very practical because partial derivatives increase the number of computations.

In the context of combustion mechanisms, many model reduction methods were developed to calculate or approximate SIMs. A concise overview is given in [LU16]. Among those methods are in chronological order Quasi-Steady State Approximation (QSSA) [Bod07; Bod13; CU13], Partial Equillibrium Assumption (PEA) [MM13], Computational Singular Perturbation (CSP) [Lam85; LG88; LG94], Intrinsic Low-Dimensional Manifold (ILDM) [MP92], TBOAs [Leb04; RWL08; Leb10; LRS10; LSU11; LU16; HL18], ZDP [Gea+05; Zag+09; Ben+15], Flow Curvature Method (FCM) [GR06; GR08; Gin13], methods based on heteroclinic orbits and saddle points [DS99; Al-+09; Pow+15] and a method based on Finite-Time Lyapunov Exponents (FTLEs) [Mea+16].

Most of the above mentioned methods aim at calculating the SIM pointwise. A general pointwise SIM approximation method is summarized in the following Algorithm 1. We call it a general *species reconstruction method*. It should be mentioned that it is an open problem how to choose the reaction progress variables in Line 1 in a reasonable way. For practical purposes in chemical reaction mechanisms, the species H_20 and O_2 are used for Reaction Progress Variables (RPVs). Even the number of chosen RPVs is an issue.

Algorithm 1 General species reconstruction method.

Input Dynamical system $z' = f(z)$

1: Choose some of the state variables $z(\cdot)$ — RPVs — to parameterize the SIM.
2: Divide z into $z(t) = (z_{\text{RPV}}(t), z_{\text{nRPV}}(t))$.
3: Choose fixed values z^*_{RPV} for $z_{\text{RPV}}(t^*)$.
4: Use any strategy to calculate values $\tilde{z}^*_{\text{nRPV}}$ for the non-reaction progress variables such that the composite vector is near the SIM.
5: **return** Approximation $\tilde{z}^* = (z^*_{\text{RPV}}, \tilde{z}^*_{\text{nRPV}})$ ▷ should be near unknown value $z^* = (z^*_{\text{RPV}}, z^*_{\text{nRPV}}) \in S_\varepsilon$.

In the following the most important model reduction methods used in this work are briefly introduced.

2.4.1 Zero-Derivative-Principle

The Zero-Derivative-Principle (ZDP) was first presented by Gear et al. [Gea+05; Zag+09]. They propose to solve

$$\frac{\mathrm{d}^m}{\mathrm{d}t^m} z_{\text{nRPV}}(t) = 0 \tag{2.19}$$

for a fixed $m \in \mathbb{N}$ as approximation method in Line 4 of the above mentioned algorithm.

Intuition of this approach is that the process of differentiation with respect to time t amplifies fast varying components of z more than the slow ones. Thus, solutions of the local criterion (2.19) have in some sense no or at least small fast varying components.

Gear et al. [Gea+05] show that for singularly perturbed systems, the asymptotic expansion in ε of the solution of (2.19) is locally up to order $m - 1$ identical with the regular asymptotic expansion of the slow invariant manifold S_ε, i.e., the error is in $\mathcal{O}(\varepsilon^m)$. Thus, we refer to (2.19) as the ZDP of order m.

Benoît et al. [Ben+15] extend the zero-derivative-principle. They prove that for a fixed $m \in \mathbb{N}$, the equation

$$\frac{\mathrm{d}^m}{\mathrm{d}t^m} z_{\text{RPV}}(t) = 0$$

yields in the same manner a solution which has the exact regular asymptotic expansion in ε up to the terms in $\mathcal{O}(\varepsilon^{m-2})$. Therefore, the order of the error decreases by 1 such that the error is in $\mathcal{O}(\varepsilon^{m-1})$.

The choice of reaction progress variables in Line 1 is crucial and for high-dimensional systems linked with combinatorial complexity. However, for the ZDP and its extension the choice of RPVs determines the error in the asymptotic expansion of S_ε and even a linear combination of slow and fast variables leads to the same order of error (cf. [Ben+15, Theorem 6]).

From a geometric point of view, the SIM as a manifold in the phase space is independent from the choice of RPVs. In Fenichel's theory the manifold is parametrized by the slow variables. Therefore, the ZDP encourages a geometric perspective on slow manifolds.

2.4.2 Flow Curvature Method

Another SIM approximation method is the Flow Curvature Method (FCM) by Ginoux [GR06; GR08; Gin13]. It is designed to compute a $(n-1)$-dimensional submanifold of n-dimensional systems of autonomous ODEs $z'(t) = f\big(z(t)\big)$ by solving the following equation:

$$\Phi_{\text{FCM}}(z) \coloneqq \det\Big(z'(t), z''(t), \ldots, z^{(n)}(t)\Big) = 0.$$

For a two-dimensional system of ODEs the function $\Phi_{\text{FCM}}(z)$ vanishes if and only if the curvature

$$\kappa = \frac{\Phi_{\text{FCM}}(z)}{\big\|z'(t)\big\|^{\frac{3}{2}}}$$

of a solution trajectory of $z'(t) = f\big(z(t)\big)$ vanishes. This explains the name of the method.

For singularly perturbed systems with exactly one fast variable y, i.e. $(m, 1)$-slow-fast systems, the FCM yields a smooth function that coincides with the Fenichel manifold graph h_ε up to $\mathcal{O}(\varepsilon)$ — assuming some non-degeneracy condition. For more details, we refer to [Ben+15].

By means of the Darboux invariance theorem (see [GR08, Proposition 2.2]), the flow curvature manifold is shown to be invariant if the Jacobian of the right-hand side f does not depend on time, i.e., the total differential $\frac{\mathrm{d}J_f(z(t))}{\mathrm{d}t}$ vanishes on

trajectories $z(\cdot)$. Especially for linear systems, the FCM computes an invariant manifold.

Benoît et al. [Ben+15] reveal the close relationship between the FCM and the Intrinsic Low-Dimensional Manifold (ILDM). The ILDM is another model reduction technique by Maas and Pope [MP92], first proposed 1992. It approximates the SIM by a manifold such that the vector field of the flow is included in the linear subspace of all slow modes. For $(m, 1)$-slow-fast-systems, the ILDM is included in the zero curvature set $\Phi_{\text{FCM}}(z) = 0$. The difference between those two methods is for this case that the FCM includes so-called "ghost" or spurious solutions which can be interpreted in the context of the ILDM as incorrectly identified fast eigendirections.

2.4.3 Trajectory-Based Optimization Approach

Lebiedz proposes a species reconstruction method in [Leb04] which is refined in a couple of succeeding articles [LRK06; RWL08; Leb10; LRS10; LSU11; LU16; HL18]. To reconstruct non-reaction progress variables for fixed values z^*_{RPV}, the Trajectory-Based Optimization Approach (TBOA) consists in solving the following variational problem:

$$\begin{aligned} \min_{z(\cdot)} \quad & \int_{t_0}^{t_\text{f}} \Phi\big(z(t)\big)\,\mathrm{d}t \\ \text{s.t.} \quad & z'(t) = f\big(z(t)\big), \qquad \text{for } t \in [t_0, t_\text{f}], \\ & 0 = g\big(z(t)\big), \qquad \text{for } t \in [t_0, t_\text{f}], \\ & z_{\text{RPV}}(t^*) = z^*_{\text{RPV}}, \end{aligned} \tag{2.20}$$

where the point of time t^* is either chosen to be t_0 (forward mode) or t_f (backward mode). The solution $z(\cdot)$ evaluated at time t^* is assumed to approximate the SIM S_ε well — in the sense that the point $\tilde{z}^* = \big(z^*_{\text{RPV}}, z_{\text{nRPV}}(t^*)\big)$ is near S_ε.

In contrast to the root-finding problems in the ZDP and FCM, variational problem (2.20) searches conceptually a trajectory of $z'(t) = f\big(z(t)\big)$ that minimizes the objective functional Φ. The set of considered trajectories is constrained by some equality conditions $g\big(z(t)\big) = 0$ (usually given by linear mass conservation restrictions) and partially determined by initial resp. final conditions $z_{\text{RPV}}(t^*) = z^*_{\text{RPV}}$ for a subset of all species z.

This method was first considered for chemical reaction mechanisms, where the underlying ODE stems from the law of mass action for each reaction step of the mechanism.

The success of the TBOA thus depends on the choice of the objective functional Φ. In the first approach of Lebiedz [Leb04; LRK06], Φ is chosen to represent the square deviation from zero entropy productions. Thus, for this choice of Φ, the solution trajectory of (2.20) is called *Minimal Entropy Production Trajectory* (*MEPT*). The idea behind this method is that thermodynamic driving forces of the chemical reactions are supposed to be maximally relaxed on the slow manifold.

This species reconstruction method is refined in [RWL08; Leb10; LRS10; LSU11]. It turns out that the choice

$$\Phi(z) = \left\|z''(t)\right\|_2^2 = \left\|J_f\big(z(t)\big) \cdot f\big(z(t)\big)\right\|_2^2$$

leads to slightly better results than for the MEPT. It is motivated geometrically as well as physically. Trajectories on which the optimization is based on, are considered in the phase space. Examples suggest the slow attractive invariant manifold to have smaller curvature than other manifolds. Moreover, curvature is closely related to chemical forces that pull trajectories onto attractive manifolds. The existence of a solution of (2.20) is shown in [LSU11].

Further investigation by Lebiedz and Unger [LU16] show that the following optimization problem (2.21) improves the before-mentioned approaches.

$$\begin{aligned}
\min_{z(\cdot)} \quad & \left\| \frac{\mathrm{d}^m}{\mathrm{d}t^m} z(t)\Big|_{t=t_0} \right\|_2^2 && && \text{(2.21a)}\\
\text{s.t.} \quad & z'(t) = f\big(z(t)\big), && \text{for } t \in [t_0, t_\mathrm{f}], && \text{(2.21b)}\\
& 0 = g\big(z(t_\mathrm{f})\big), && && \text{(2.21c)}\\
& z_\mathrm{RPV}(t_\mathrm{f}) = z_\mathrm{RPV}^{t_\mathrm{f}}, && && \text{(2.21d)}
\end{aligned}$$

where the precision of this approach increases with ascending $m \in \mathbb{N}$ (see [LSU11; LU16]). Often, $m = 2$ is chosen for numerical computations as trade-off between accuracy and computational effort.

For this method, the integral objective function is replaced by a (higher) derivative of the state variables. This objective function is reminiscent of the ZDP but (2.21)

has a form that is closely related to a two-point BVPs. Investigations revealed that this criterion benefits from choosing the interval time $t_f - t_0$ as large as possible. The local case $t_f = t_0$ is computationally cheap to evaluate but less accurate. Henceforth, we refer to (2.21) as the Trajectory-Based Optimization Approach (TBOA).

2.4.4 Canonical Invariant Manifolds

In [DS99], Davis and Skodje introduce a new one-dimensional manifold reduction method based on equilibria. They calculate heteroclinic orbits between a saddle point with exactly one unstable mode and a sink. Only one of these equilibria is physically feasible.

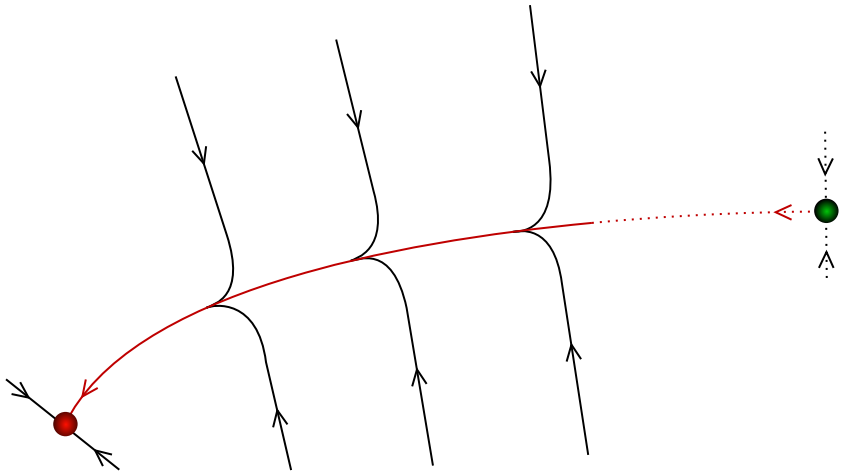

Figure 2.2: Sketch of a one-dimensional SIM (red line) that is a heteroclinic orbit between a saddle (green ball) and a sink (red ball).

The resulting heteroclinic orbit is an invariant manifold because it is a trajectory. The (only) unstable mode of the saddle and the stable modes of the sink ensure the attraction of trajectories near those two equilibria. Further, this method is often applicable even to systems where there is no finite saddle point with one unstable mode. A mapping of the system to a general Poincaré sphere, i.e., also for an arbitrary but finite number of variables, allows to calculate equilibria at infinity. A brief introduction to the Poincaré sphere and equilibria at infinity is given in Section 5.2.

Powers et al. [Al-+09; Pow+15] seized this idea of connecting two equilibria and extend it to their theory of Canonical Invariant Manifolds (CIMs). A Canonical

Invariant Manifold (CIM) is defined to be a heteroclinic clinic starting at an equilibrium with exactly one unstable eigenvector. It is conjectured that CIMs are the only candidates for 1D SIMs. In [Pow+15] it is analyzed whether the slowness or attractivity of a CIM can be determined.

Disadvantage of this method is the restriction to 1D SIMs. However, the power of such heteroclinic orbits is that they can represent the slow invariant manifold exactly and do not rely on any asymptotic expansion in ε.

3 Optimal Control of Chemical Reactions

The previous chapter introduced the analytical basics and Fenichel's theory. Let us now turn to optimal control problems arising in chemical reaction mechanisms. Due to the highly nonlinear and stiff ordinary differential equations, these problems are numerically hard to tackle. Even modern computers cannot solve them in decent time. Thus, the question arises whether model reduction techniques can be applied in order to simplify these optimal control problems. We make use of the theory presented in Chapter 2 and show a possibility to integrate the model reduction techniques ZDP and TBOA in the context of optimal control theory. In the last section, two rather academic examples demonstrate the practicability of the developed simplification. The contents and figures in Sections 3.3 and 3.4 can be found in [Hei+17].

3.1 Optimal Control Problems

The purpose of this section is to introduce Optimal Control Problems (OCPs) as well as their mathematical setting. Furthermore, we state necessary conditions for the optimal solution of such problems. We follow the introduction of Gerdts [Ger12] into this topic.

Optimal control problems arise when dynamical systems can be influenced by some control parameters or functions. The problem is to minimize or maximize some objective functional for given restrictions on the parameters and functions. A simple example is to minimize the transportation costs to bring a car from point A to point B. Essentially, optimal control problems can be seen as infinite-dimensional optimization problems.

In order to provide a mathematical setting where OCPs are well defined, we start with the definition of absolutely continuous functions as well as L^p- and

$W^{k,p}$-spaces.

Definition 3.1 (Absolutely Continuous Function [Ger12, Definition 2.1.19])**.** Let $I \coloneqq [t_0, t_\mathrm{f}]$ be a compact interval with $t_0 < t_\mathrm{f}$. A function $f : I \to \mathbb{R}$ is *absolutely continuous*, if for every $\varepsilon > 0$ there exists $\delta = \delta(\varepsilon) > 0$ such that

$$\sum_{\ell=1}^{m} |b_\ell - a_\ell| < \delta \Rightarrow \sum_{\ell=1}^{m} |f(b_\ell) - f(a_\ell)| < \varepsilon,$$

for all $m \in \mathbb{N}$ and $(a_\ell, b_\ell) \subset I$ for all $\ell = 1, \ldots, m$

Similarly to the space of continuous functions $C(I, \mathbb{R})$ and k-times continuously differentiable functions $C^k(I, \mathbb{R})$, one can define the space of higher derivatives of absolutely continuous functions by the following definition.

Definition 3.2 ($W^{k,p}$-spaces [Ger12, Definition 2.1.21])**.** Let $I \coloneqq [t_0, t_\mathrm{f}] \subset \mathbb{R}$ be a compact interval with $t_0 < t_\mathrm{f}$ and $1 \leq k, p \leq \infty$.

(a) The space $W^{k,p}(I) \coloneqq W^{k,p}(I, \mathbb{R})$ consists of all continuous functions $f : I \to \mathbb{R}$ with absolutely continuous derivatives up to order $k-1$ and $\|f\|_{k,p} < \infty$, where the norm is given by

$$\|f\|_{k,p} \coloneqq \left(\sum_{\ell=0}^{k} \|f^{(\ell)}\|_p^p \right)^{1/p}, \qquad 1 \leq p \leq \infty$$
$$\|f\|_{k,\infty} \coloneqq \max_{0 \leq \ell \leq k} \|f^{(\ell)}\|_\infty.$$

(b) For $1 \leq k, p \leq \infty$ the space $W^{k,p}(I, \mathbb{R}^n)$ is defined as the product space

$$W^{k,p}(I, \mathbb{R}^n) \coloneqq \underbrace{W^{k,p}(I) \times \cdots \times W^{k,p}(I)}_{n\text{-times}},$$

where each element $f \in W^{k,p}(I, \mathbb{R}^n)$ is a mapping from I into $\mathbb{R}^n$.

For the state variable satisfying the ODE constraint of an OCP, we will require that this state is a function in $W^{1,\infty}$. The controls, however, are required to be essentially bounded. A definition of L^p-spaces is thus given below.

Definition 3.3 (L^p-spaces [Ger12, Defintion 2.1.17])**.** Let $I \coloneqq [t_0, t_\mathrm{f}] \subset \mathbb{R}$ be a compact interval with $t_0 < t_\mathrm{f}$.

(a) The space $L^p(I)$ for $1 \leq p < \infty$ consists of all measurable functions $f : I \to \mathbb{R}$ with finite Lebesgue integral

$$\int_{t_0}^{t_\mathrm{f}} |f(t)|^p \,\mathrm{d}t < \infty.$$

Endowed with the norm $\|f\|_p \coloneqq \left(\int_{t_0}^{t_\mathrm{f}} |f(t)|^p \,\mathrm{d}t \right)^{1/p}$, $L^p(I)$ is a Banach space.

(b) The space $L^\infty(I)$ consists of all measurable functions $f : I \to \mathbb{R}$ which are essentially bounded, i.e.,

$$\|f\|_\infty \coloneqq \operatorname*{ess\,sup}_{t \in I} |f(t)| \coloneqq \inf_{\substack{N \subset I \\ N \text{ is set of measure zero}}} \sup_{t \in I \setminus N} |f(t)| < \infty.$$

Endowed with the norm $\|f\|_\infty$, $L^\infty(I)$ is a Banach space.

(c) For $1 \leq p \leq \infty$ the space $L^p(I, \mathbb{R}^n)$ is the product space

$$L^p(I, \mathbb{R}^n) \coloneqq \underbrace{L^p(I) \times \cdots \times L^p(I)}_{n\text{-times}},$$

where each element $f \in L^p(I, \mathbb{R}^n)$ is a mapping from I into $\mathbb{R}^n$.

We finally define the standard form of an OCP:

Definition 3.4 (OCP in Standard Form [Ger12, Problem 3.4.1])**.** Let $I = [t_0, t_\mathrm{f}] \subset \mathbb{R}$ be a non-empty compact time interval. Let

$$\begin{aligned}
\varphi &: \ \mathbb{R}^{n_x} \times \mathbb{R}^{n_x} \to \mathbb{R}, \\
f_0 &: \ I \times \mathbb{R}^{n_x} \times \mathbb{R}^{n_y} \times \mathbb{R}^{n_u} \to \mathbb{R}, \\
f &: \ I \times \mathbb{R}^{n_x} \times \mathbb{R}^{n_y} \times \mathbb{R}^{n_u} \to \mathbb{R}^{n_x}, \\
g &: \ I \times \mathbb{R}^{n_x} \times \mathbb{R}^{n_y} \times \mathbb{R}^{n_u} \to \mathbb{R}^{n_y}, \\
c &: \ I \times \mathbb{R}^{n_x} \times \mathbb{R}^{n_y} \times \mathbb{R}^{n_u} \to \mathbb{R}^{n_c}, \\
s &: \ I \times \mathbb{R}^{n_x} \to \mathbb{R}^{n_s}, \\
\psi &: \ \mathbb{R}^{n_x} \times \mathbb{R}^{n_x} \to \mathbb{R}^{n_\psi}
\end{aligned}$$

be sufficiently smooth functions and $\mathcal{U} \subset \mathbb{R}^{n_u}$ a set. An OCP is a problem of the form

$$\begin{aligned}
\min_{x(\cdot), y(\cdot), u(\cdot)} \quad & \varphi\big(x(t_0), x(t_\mathrm{f})\big) + \int_{t_0}^{t_\mathrm{f}} f_0\big(t, x(t), y(t), u(t)\big)\,\mathrm{d}t && \text{(3.1a)}\\
\text{s.t.} \quad & x'(t) = f\big(t, x(t), y(t), u(t)\big), \text{ for } t \in I, && \text{(3.1b)}\\
& 0 = g\big(t, x(t), y(t), u(t)\big), \text{ for } t \in I, && \text{(3.1c)}\\
& 0 \geq c\big(t, x(t), y(t), u(t)\big), \text{ for } t \in I, && \text{(3.1d)}\\
& 0 \geq s\big(t, x(t)\big), \qquad \text{for } t \in I, && \text{(3.1e)}\\
& 0 = \psi\big(x(t_0), x(t_\mathrm{f})\big), && \text{(3.1f)}\\
& u(t) \in \mathcal{U}, \qquad \text{for } t \in I, && \text{(3.1g)}
\end{aligned}$$

where $x \in W^{1,\infty}(I, \mathbb{R}^{n_x}), y \in L^\infty(I, \mathbb{R}^{n_y}), u \in L^\infty(I, \mathbb{R}^{n_u})$.

Equations (3.1b) and (3.1c) represent the DAE constraints, (3.1a) is called *objective function*, (3.1d) is called *mixed control-state constraint*, (3.1e) is called *pure state constraint*, (3.1f) is called *boundary constraint*, and (3.1g) is called *set constraint*.

The next subsection presents necessary optimality conditions for OCPs. They require the definition of a so-called *Hamiltonian* function. It is defined as

$$\mathcal{H}(t, x, y, u, \lambda_f, \lambda_g, \ell_0) \coloneqq \ell_0 f_0\big(t, x, y, u\big) + \lambda_f^\mathsf{T} f\big(t, x, y, u\big) + \lambda_g^\mathsf{T} g\big(t, x, y, u\big).$$

Similar to the Hamiltonian in classical mechanics, the value of this function is conserved in a special setting justifying the name of this function.

3.1.1 Necessary Optimality Conditions

Necessary conditions for optimal control problems were first proved by Pontryagin [Pon+62] and independently by Hestenes [Hes64] in the 1950s and 60s. These optimality conditions lead to a BVP.

In the following, we only consider optimal control problems without mixed control-state and pure state constraints because our research does not need them. However, the following results can be extended to the case where mixed control-state or pure state constraints are present.

Theorem 3.5 (Pontryagin's Minimum Principle [Ger12, Theorem 3.4.3])**.** *Let the following assumptions be satisfied for OCP* (3.1) (*without mixed-control-state constraints* (3.1d) *and pure state constraints* (3.1e))*:*

(*i*) $(x^*, y^*, u^*) \in W^{1,\infty}(I, \mathbb{R}^{n_x}) \times L^\infty(I, \mathbb{R}^{n_y}) \times L^\infty(I, \mathbb{R}^{n_u})$ *is a local minimum of OCP* (3.1)*.*

(*ii*) φ *and* ψ *are continuously differentiable w.r.t. all arguments.* f_0, f *and* g *are continuous functions and continuously differentiable w.r.t.* x, y *and* u *in* M *uniformly for* $t \in I = [t_0, t_\mathrm{f}]$*, where* M *is a sufficiently large convex compact neighborhood of*

$$\big\{(x^*(t), y^*(t), u^*(t)) \in \mathbb{R}^{n_x} \times \mathbb{R}^{n_y} \times \mathbb{R}^{n_u} : t \in I\big\}.$$

g is twice differentiable w.r.t all arguments. The partial derivatives of f_0, f and g with respect to t are bounded in $I \times M$.

(*iii*) *The matrix*

$$M(t) \coloneqq D_y g\big(t, x^*(t), y^*(t), u^*(t)\big)$$

is non-singular almost everywhere in I and its inverse M^{-1} is essentially bounded in I.

(*iv*) *The control set $\mathcal{U} \subset \mathbb{R}^{n_u}$ is a closed and convex set with non-empty interior.*

Then there exists multipliers

$$\ell_0 \in \mathbb{R}_0^+, \quad \lambda_f \in W^{1,\infty}(I, \mathbb{R}^{n_x}), \quad \lambda_g \in L^\infty(I, \mathbb{R}^{n_y}), \quad \sigma \in \mathbb{R}^{n_\psi}$$

such that

(*a*) $(\ell_0, \sigma, \lambda_f, \lambda_g) \neq 0$*.*

(*b*) *the* adjoint equations *hold almost everywhere in I:*

$$\begin{aligned} \lambda_f'(t) &= -D_x \mathcal{H}\big(t, x^*(t), y^*(t), u^*(t), \lambda_f(t), \lambda_g(t), \ell_0\big)^\mathsf{T}, \\ 0 &= D_y \mathcal{H}\big(t, x^*(t), y^*(t), u^*(t), \lambda_f(t), \lambda_g(t), \ell_0\big)^\mathsf{T}. \end{aligned}$$

(*c*) *the* transversality conditions *hold:*

$$\begin{aligned} \lambda_f(t_0)^\mathsf{T} &= -\ell_0 D_{x_0} \varphi\big(x^*(t_0), x^*(t_\mathrm{f})\big) - \sigma^\mathsf{T} D_{x_0} \psi\big(x^*(t_0), x^*(t_\mathrm{f})\big), \\ \lambda_f(t_\mathrm{f})^\mathsf{T} &= \ell_0 D_{x_\mathrm{f}} \varphi\big(x^*(t_0), x^*(t_\mathrm{f})\big) + \sigma^\mathsf{T} D_{x_\mathrm{f}} \psi\big(x^*(t_0), x^*(t_\mathrm{f})\big). \end{aligned}$$

(*d*) *the* variational inequality *for the Hamiltonian holds:*

$$D_u \mathcal{H}\big(t, x^*(t), y^*(t), u^*(t), \lambda_f(t), \lambda_g(t), \ell_0\big) \cdot \big(u - u^*(t)\big) \geq 0$$

for all $u \in \mathcal{U}$.

Proof. See [Ger12]. □

Remark 3.6. The non-singularity condition of $M(t)$ ensures the DAE constraints to be an index-one DAE. For index-two DAEs further versions of the minimum principle can be shown. An overview on such principles is given in [Ger12].

If $\ell_0 > 0$ w.l.o.g. ℓ_0 can be set to $\ell_0 = 1$ because Pontryagin's minimum principle is then satisfied for $\tilde{\lambda} = \frac{\lambda}{\ell_0}$ as well. Thus we state a second version of the minimum principle (without proof) assuming some regularity conditions to ensure $\ell_0 = 1$.

Theorem 3.7 (cf. [Ger12, Theorem 3.4.6])**.** *Let the assumptions of Theorem 3.5 hold and let*

$$\operatorname{rank}\Big(D_{x_0}\psi\big(x^*(t_0), x^*(t_\mathrm{f})\big)\Phi(t_0) + D_{x_\mathrm{f}}\psi\big(x^*(t_0), x^*(t_\mathrm{f})\big)\Phi(t_\mathrm{f})\Big) = n_\psi,$$

where Φ *is the fundamental system of the homogeneous linear differential equation*

$$\Phi'(t) = \tilde{A}(t)\Phi(t), \quad \Phi(t_0) = I, \quad t \in I,$$

with

$$\tilde{A}(t) \coloneqq D_x f[t] - D_y f[t]\big(D_y g[t]\big)^{-1} D_x g[t].$$

$[t]$ *is the short notation for all arguments of the corresponding function evaluated at time* t *in the optimal solution* (x^*, y^*, u^*)*. Moreover, let there exist* $x \in W^{1,\infty}(I, \mathbb{R}^{n_x})$, $y \in L^\infty(I, \mathbb{R}^{n_y})$ *and* $u \in \operatorname{int}(\mathcal{U} \setminus \{u^*\})$ *such that the following equations are fulfilled*

$$\begin{aligned} D_x f[t]x(t) + D_y f[t]y(t) + D_u f[t]u(t) - x'(t) &= 0 \qquad \text{a.e. in } I, \\ D_x g[t]x(t) + D_y g[t]y(t) + D_u g[t]u(t) &= 0 \qquad \text{a.e. in } I, \\ D_{x_0}\psi\big(x^*(t_0), x^*(t_\mathrm{f})\big)x(t_0) + D_{x_\mathrm{f}}\psi\big(x^*(t_0), x^*(t_\mathrm{f})\big)x(t_\mathrm{f}) &= 0. \end{aligned}$$

Then the statements of Theorem 3.5 hold with $\ell_0 = 1$.

Theorem 3.5 and Theorem 3.7 provide an opportunity to solve OCPs numerically.

The resulting BVP in the case $\mathcal{U} = \mathbb{R}^{n_u}$ can be summarized as

$$\begin{aligned}
x'(t) &= f\big(t, x(t), y(t), u(t)\big),\\
\lambda_f'(t) &= -D_x\mathcal{H}\big(t, x(t), y(t), u(t), \lambda_f(t), \lambda_g(t), \ell_0\big)^\mathsf{T},\\
0 &= g\big(t, x(t), y(t), u(t)\big),\\
0 &= D_y\mathcal{H}\big(t, x(t), y(t), u(t), \lambda_f(t), \lambda_g(t), \ell_0\big)^\mathsf{T},\\
0 &= D_u\mathcal{H}\big(t, x(t), y(t), u(t), \lambda_f(t), \lambda_g(t), \ell_0\big)^\mathsf{T},\\
\lambda_f(t_0)^\mathsf{T} &= -\ell_0 D_{x_0}\varphi\big(x(t_0), x(t_\mathrm{f})\big) - \sigma^\mathsf{T} D_{x_0}\psi\big(x(t_0), x(t_\mathrm{f})\big),\\
\lambda_f(t_\mathrm{f})^\mathsf{T} &= \ell_0 D_{x_\mathrm{f}}\varphi\big(x(t_0), x(t_\mathrm{f})\big) + \sigma^\mathsf{T} D_{x_\mathrm{f}}\psi\big(x(t_0), x(t_\mathrm{f})\big).
\end{aligned}$$

It can be transformed to a nonlinear root-finding problem using the single and multiple shooting method. We refer to [Ger12] for more information about this topic.

3.2 Direct Methods for Optimal Control

Numerical solution strategies for OCPs can be divided into three classes: dynamic programming (including Hamilton-Jacobi-Bellman), direct and indirect methods. While indirect methods aim at solving necessary optimality conditions for the OCP (see Section 3.1.1), direct methods are based on discretization of the OCP with all of its constraints. Typically, direct methods have to handle an optimization problem with more (discretized) variables than indirect methods. However, the resulting optimization problems are finite-dimensional. A further drawback of indirect methods is that convergence of the method often depends on a very good initial guess. Especially in high-dimensional problems, sophisticated knowledge is needed to find a good initial guess as well as to calculate the optimality system.

In contrast to indirect methods, direct methods first discretize the OCP and then optimize it. The result of a discretization is a Nonlinear Program (NLP) which is typically solved by either Sequential Quadratic Programming (SQP) or an Interior Point (IP) method. The advantages of direct optimal control methods are robustness, accuracy and easy applicability (not too much theory or further knowledge are needed to understand these methods). They are suited for large dimensional problems as well — even if the resulting NLP has many optimization variables.

Another class of methods is based on dynamic programming or on the Hamilton-Jacobi-Bellman equation and relies on the principle of optimality: If an optimal control $u(t)$ is known on the interval $I \subset \mathbb{R}$, it has to be optimal for every subset $I_0 \subset I$ as well. This principle can be used to calculate the optimal control u backwards from the end of the interval t_f to the start of the interval t_0.

In the following we only focus on direct optimal control methods. They are widely spread in practice due to their simplicity and robustness.

3.2.1 Direct Multiple Shooting

The multiple shooting method was first introduced to solve two-point boundary value problems and is thus applicable as indirect method to solve the BVP resulting from Pontryagin's minimum principle (Theorem 3.5). Bock and Plitt [BP84] adopted the essential idea of the method to apply it directly to the OCP (3.1) in order to get a finite-dimensional NLP. What follows is an introduction into the steps needed to discretize an OCP.

Discretization of the Time First, the interval $I = [t_0, t_\mathrm{f}]$ is replaced by a grid

$$t_0 < t_1 < \ldots < t_{N-1} < t_N = t_\mathrm{f}$$

for a given natural number $N \in \mathbb{N}$. The subintervals $[t_i, t_{i+1}]$ for $i = 0, \ldots, N-1$ are called *shooting intervals*. For the sake of simplicity, we only consider equidistant intervals of step size $h \coloneqq t_{i+1} - t_i$ for all $i = 0, \ldots, N-1$.

Discretization of the Control Since the interval I is replaced by a finite grid, the control $u(t)$ is replaced by a function that is uniquely represented by a finite number of parameters. Usually, a polynomial approximation of $u(t)$ is used in each shooting interval $[t_i, t_{i+1}]$. B-Splines are quite often used for the approximation because their evaluation is of computationally low costs and well conditioned. Local support of the basis functions prevents numerical instabilities in a shooting interval from spreading and affecting other intervals. See [DH08] and [Ger12] for more information. In the simplest case, $u(t)$ is piecewise constant, i.e.

$$u(t) = u_i \quad \text{for } t \in [t_i, t_{i+1}), \quad i = 0, \ldots, N-1.$$

Discretization of the States Next, we solve the DAEs

$$\begin{aligned} x'(t) &= f\big(t, x(t), y(t), u_i\big), \quad && \text{for } t \in [t_i, t_{i+1}], \\ 0 &= g\big(t, x(t), y(t), u_i\big), && \text{for } t \in [t_i, t_{i+1}], \\ x(t_i) &= x_i, \quad y(t_i) = y_i, \end{aligned}$$

on each shooting interval with artificial initial values $x_i \in \mathbb{R}^{n_x}$,$y_i \in \mathbb{R}^{n_y}$. We denote the differential state solution of such an DAE as $\hat{x}_i(t; x_i, y_i, u_i)$. In the following Fig. 3.1 the state trajectories of the multiple shooting method are illustrated.

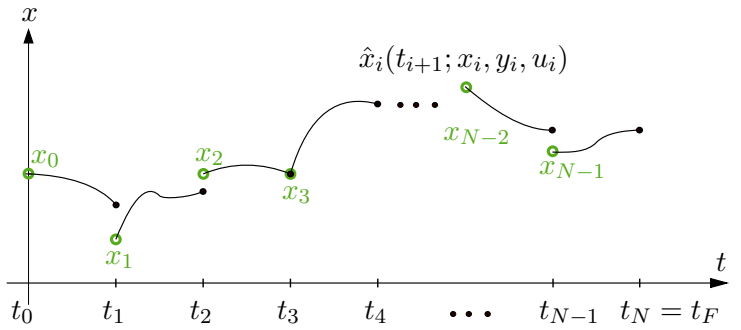

Figure 3.1: Schematic drawing of the multiple shooting method: state trajectories in each shooting interval.

In order to get continuous states x, additionally *continuity constraints* have to be claimed:

$$x_{i+1} = \hat{x}_i(t_{i+1}; x_i, y_i, u_i) \quad \text{for } i = 0, 1, \ldots, N-1.$$

For numerical computations, the analytical solution $\hat{x}_i(t; x_i, y_i, u_i)$ is approximated by a numerical integration method, e.g., a one-step method. We denote the numerical solution in the shooting interval $[t_i, t_{i+1})$ at time t_{i+1} by $\vartheta(x_i, y_i, u_i)$ such that the continuity conditions become

$$x_{i+1} = \vartheta(x_i, y_i, u_i).$$

Discretization of Other Constraints The remaining (infinite-dimensional) constraints are $g\big(t, x(t), y(t), u(t)\big) = 0$ and $0 \geq c\big(t, x(t), y(t), u(t)\big)$ for all $t \in I = [t_0, t_\mathrm{f}]$ and $\psi\big(x(t_0), x(t_\mathrm{f})\big) = 0$. Numerically, semi-infinite problems can be hard to

solve. Thus, it is convenient to require those constraints to be only satisfied at the previously defined time grid, i.e.,

$$\begin{aligned} 0 &= g\big(t_i, x_i, y_i, u_i\big) = 0 \quad \text{for all } i = 0, \dots, N-1, \\ 0 &\geq c\big(t_i, x_i, y_i, u_i\big) = 0 \quad \text{for all } i = 0, \dots, N-1. \end{aligned}$$

At best, these finite conditions force the optimal solution of the NLP to fulfill the continuous constraints $g\big(t, x(t), y(t), u(t)\big) = 0$ on the whole interval I. The boundary constraint $\psi\big(x(t_0), x(t_\mathrm{f})\big) = 0$ can be written with the help of the previously defined variables and functions as

$$\psi\big(x_0, x_N\big).$$

Approximation of the Objective Function Numerical integration is used to approximate the integral part of the objective function in each shooting interval. Hence, we write $F_i(x_i, y_i, u_i)$ for the approximation

$$F_i(x_i, y_i, u_i) \approx \int_{t_i}^{t_{i+1}} f_0\big(t, x(t), y(t), u(t)\big)\, \mathrm{d}t.$$

To conclude this section, the multiple shooting method discretizes OCP (3.1) into the NLP w.r.t. $x = (x_0, x_1, \dots, x_N), y = (y_0, y_1, \dots, y_N), u = (u_0, u_1, \dots, u_{N-1})$:

$$\begin{aligned} \min_{x,\,y,\,u} \quad & \varphi\big(x_0, x_N\big) + \sum_{i=0}^{N-1} F_i(x_i, y_i, u_i) \\ \text{s.t.} \quad & x_{i+1} = \vartheta(x_i, y_i, u_i), \text{ for } i = 0, 1, \dots, N-1, \\ & 0 = g\big(t_i, x_i, y_i, u_i\big), \text{ for } i = 0, 1, \dots, N-1, \\ & 0 \geq c\big(t_i, x_i, y_i, u_i\big), \text{ for } i = 0, 1, \dots, N-1, \\ & 0 = \psi\big(x_0, x_N\big), \\ & u_i \in \mathcal{U}, \text{ for } i = 0, 1, \dots, N-1. \end{aligned}$$

3.2.2 Direct Collocation

The direct collocation is another approach to come from an OCP to a NLP. While the direct multiple shooting solves a nested numerical integration scheme inside

the NLP with possibly additional intermediate variables, the direct collocation *lifts* that nested problem on the integrator level with all of its variables such that they become part of the NLP. Therefore, the direct collocation is a full discretization method.

Discretizaton of Time and Numerical Integration Like for the multiple shooting discretization, the interval $I = [t_0, t_\mathrm{f}]$ is replaced by a grid

$$t_0 < t_1 < \ldots < t_{N-1} < t_N = t_\mathrm{f}$$

for a given natural number $N \in \mathbb{N}$.

As the name of the method suggests, direct collocation uses a collocation method for numerical integration of the embedded DAE or ODE. The idea of a collocation integrator is to approximate the state variables $x(t)$ by polynomial approximation $p_i(t)$ in the interval $[t_i, t_{i+1}]$. For the interpolating nodes in the interval $[t_i, t_{i+1}]$ we set

$$t_{i,j} \coloneqq t_i + \tau_j(t_{j+1} - t_j), \quad \text{for } j = 1, \ldots, d,$$

where $\tau = (\tau_1, \ldots, \tau_d)$ is a fixed set of *collocation points* (i.e. interpolating nodes) that specifies the interpolating polynomial of maximum degree $d - 1$. For a discussion on the choices for the collocation points we refer to [Bie10]. Common choices are the Legendre points and Radau points because the provide exact integration, if f is a polynomial of degree smaller than $2d$ respectively $2d - 1$ for the Radau points.

Thus, in the interval $[t_i, t_{i+1}]$ the collocation integration of the DAE can be written in the form

$$\begin{aligned} p_i'(t_{i,j}) &= f\big(t_{i,j}, x_{i,j}, y_{i,j}, u_i\big), \quad \text{for } j = 1, \ldots, d \\ 0 &= g\big(t_{i,j}, x_{i,j}, y_{i,j}, u_i\big), \quad \text{for } j = 1, \ldots, d \\ p_i(t_{i+1}) &= x_{i+1}, \end{aligned}$$

where $x_{i,j} \coloneqq x(t_{i,j})$ and $y_{i,j} \coloneqq x(t_{i,j})$. These conditions (in particular the values $x_{i,j}$ and $y_{i,j}$) determine the polynomial $p_i(t)$ uniquely.

Approximation of the Objective Function The objective function in the interval $[t_i, t_{i+1}]$ is approximated again by some numerical integration method like for the multiple shooting discretization. The approximation may depend on some of the

introduced intermediate variables $x_{i,j}$ and $y_{i,j}$ for $j = 1, \dots, d$. For brevity, we introduce the notations $x_{i,0} \coloneqq x_i$, $y_{i,0} \coloneqq y_i$,

$$x^{(i)} \coloneqq (x_{i,j})_{j=1,\dots,d} \quad \text{and} \quad y^{(i)} \coloneqq (y_{i,j})_{j=1,\dots,d}$$

We denote the numerical approximation of the integral

$$\int_{t_i}^{t_{i+1}} f_0\big(t, x(t), y(t), u(t)\big)\,\mathrm{d}t$$

as $F_i(x^{(i)}, y^{(i)}, u_i)$.

Finally, we obtain the collocation based NLP w.r.t. $X = \big(x^{(0)}, \dots, x^{(N-1)}, x_N\big)$, $Y = \big(y^{(0)}, \dots, y^{(N-1)}\big)$, and $u = (u_0, u_1, \dots u_{N-1})$:

$$\begin{aligned}
\min_{X,Y,u} \quad & \varphi\big(x_0, x_N\big) + \sum_{i=0}^{N-1} F_i(x^{(i)}, y^{(i)}, u_i) \\
\text{s.t.} \quad & 0 = x_{i+1} - p_i(t_{i+1}), \quad i = 0, \dots, N-1, \\
& 0 = f\big(t_{i,j}, x_{i,j}, y_{i,j}, u_i\big) - p_i'(t_{i,j}), \;\; i = 0, \dots, N-1, \; j = 1, \dots, d, \\
& 0 = g\big(t_{i,j}, x_{i,j}, y_{i,j}, u_i\big), \;\; i = 0, \dots, N-1, \; j = 1, \dots, d, \\
& 0 \geq c\big(t_{i,j}, x_{i,j}, y_{i,j}, u_i\big), \;\; i = 0, \dots, N-1, \; j = 1, \dots, d, \\
& 0 = \psi\big(x_0, x_N\big), \\
& u_i \in \mathcal{U}, \quad i = 0, \dots, N-1.
\end{aligned}$$

3.2.3 Nonlinear Programming

A brief introduction to nonlinear programming is given in this section. The last sections about direct multiple shooting and collocation end up with a NLP, i.e., with a problem of the form

$$\begin{aligned}
\min_{x} \quad & f(x) \\
\text{s.t.} \quad & g(x) \leq 0, \\
& h(x) = 0,
\end{aligned} \tag{3.2}$$

for sufficiently smooth functions $f\colon \mathbb{R}^n \to \mathbb{R}$, $g\colon \mathbb{R}^n \to \mathbb{R}^m$ and $h\colon \mathbb{R}^n \to \mathbb{R}^k$.

The most applied methods to such constrained optimization problems are Sequential Quadratic Programming (SQP), Interior Point (IP) and penalty methods.

Especially the first two methods are very popular. Not only a good overview but also a deeper insight into these families of methods is given in [NW06]. From a mathematical point of view, in general none of these methods is better than the others. However, for all methods there are certain classes of NLPs on which they perform usually more efficient.

In the following, we shortly present the ideas of the SQP and IP method. Both of them rely on first-order necessary conditions for a local minimum of (3.2) which are stated in the following. They are called *KKT conditions* named after the researchers Karush, Kuhn and Tucker.

Theorem 3.8 (KKT Theorem, cf. [Ger12, Theorem 2.3.33])**.** *Let x^* be a local minimum of* (3.2) *and suppose if satisfies some regularity condition. Then there exist some Lagrangian multipliers $(\lambda^*, \mu^*) \in \mathbb{R}^k \times \mathbb{R}^m_+$ such that the following KKT conditions are fulfilled*

$$\begin{aligned} \nabla_x \mathcal{L}(x^*, \lambda^*, \mu^*) &= 0, && (\textit{dual feasibility}) \\ g(x^*) \leq 0, \quad h(x^*) &= 0, && (\textit{primal feasibility}) \\ \mu_i^* g_i(x^*) &= 0 \quad \textit{for all } i = 1, \dots, m, && (\textit{complementarity conditions}) \end{aligned} \tag{3.3}$$

where the Lagrangian functions $\mathcal{L}$ is defined as

$$\mathcal{L}(x, \lambda, \mu) \coloneqq f(x) + \lambda^\mathsf{T} g(x) + \mu^\mathsf{T} h(x).$$

Proof. See [Ger12, Theorem 2.3.33]. □

Remark 3.9. The regularity condition mentioned in Theorem 3.8 is some additional constraint qualification regarding the problem itself (i.e., it involves the functions f, g or h) in the neighborhood of the local optimum x^*. For instance, the Linear Independence Constraint Qualifications (LICQ) is such a regularity condition that ensures the Lagrangian multipliers λ^* and μ^* to be unique. LICQ is satisfied, if the set of active gradients — consisting of all gradients $\nabla h_j(x^*)$ and $\nabla g_i(x^*)$ if $g_i(x^*) = 0$ — is linear independent. A survey on other constraint qualifications is given in [NW06].

Sequential Quadratic Programming The mathematical basis for the SQP are the KKT conditions of Theorem 3.8. It is an iterative method starting in some

(feasible) initial vector $x^{(0)} \in \mathbb{R}^n$ with $g\big(x^{(0)}\big) \leq 0$ and $h\big(x^{(0)}\big) = 0$. The idea is now to approximate the nonlinear KKT conditions locally in the current iterate by a quadratic subproblem which can be solved efficiently. The solution of this subproblems is used for an update of the current iterate and gives a new iterate. Afterwards, a new quadratic subproblem is solved and so on until the iterates converge to a KKT point satisfying Theorem 3.8.

Interior Point Methods Interior point methods are iterative methods as well but different in their nature. They handle the bottleneck of the KKT conditions — the nonlinear complementarity conditions (3.3) — by introducing them as additional costs in the objective function f multiplied by a penalty parameter τ. The prime-dual interior point method is now a combination of solving the KKT conditions for this problem with the penalty term in the objective function and a homotopy approach which sets the penalizing parameter τ piece by piece to zero. In the case of convergence, one can show that the solution satisfies the KKT conditions of the original problem (3.2).

3.3 Manifold-Based Model Reduction of OCPs

So far, this chapter focuses on general DAE-constrained OCPs. Turning now to optimal control problems involving ODEs based on chemical reactions, it seems evident to replace general DAE constraints by singularly perturbed ODEs discussed in Chapter 2. Chemical reaction mechanisms often involve multiple time scales because the rates of various reactions differ strongly. This section can be found in [Hei+17].

We consider the following optimal control problem:

$$\min_{x(\cdot),\, y(\cdot),\, u(\cdot)} \quad \int_{t_0}^{t_\mathrm{f}} f_0\big(x(\tau), y(\tau), u(\tau)\big)\, \mathrm{d}\tau \tag{3.4a}$$

$$\text{s.t.} \quad \dot{x}(\tau) = f\big(x(\tau), y(\tau), u(\tau), \varepsilon\big), \qquad \text{for } \tau \in [t_0, t_\mathrm{f}], \tag{3.4b}$$

$$\varepsilon \dot{y}(\tau) = g\big(x(\tau), y(\tau), u(\tau), \varepsilon\big), \qquad \text{for } \tau \in [t_0, t_\mathrm{f}], \tag{3.4c}$$

$$0 \geq c\big(x(\tau), y(\tau)\big), \qquad \text{for } \tau \in [t_0, t_\mathrm{f}], \tag{3.4d}$$

$$x(t_0) = x^{(0)},\ y(t_0) = y^{(0)}, \tag{3.4e}$$

where $x(\tau) \in \mathbb{R}^{n_x}, y(\tau) \in \mathbb{R}^{n_y}$ are state variables and $u(\tau) \in \mathbb{R}^{n_u}$ are control variables for $\tau \in [t_0, t_\mathrm{f}]$. In the following, we will refer to (3.4) as the original or full problem. We will use it as reference problem for the comparisons in Section 3.4.

3.3.1 OCP on Slow Subsystem

In realistic chemical reaction mechanisms, the full OCP often cannot be solved in real-time because either the total number of optimization variables or the stiffness of ODE (3.4b) and (3.4c) prevents numerical algorithms from calculating local optima of (3.4) efficiently. Thus, either model or stiffness reduction is required.

Since (3.4) comprises a slow-fast system, singular perturbation theory of Section 2.2 can be applied in order to reduce the dimension of the model. Insertion of the manifold mapping h_ε in (3.4) (cf. [Reh13]) and thus solving the ODE constraint on the slow subsystem reduces the number of variables by the dimension of the fast variables. We obtain the following dimension reduced OCP:

$$\min_{x(\cdot),\,u(\cdot)} \quad \int_0^T f_0\big(x(\tau), h_\varepsilon\big(x(\tau), u(\tau)\big), u(\tau)\big)\,\mathrm{d}t \tag{3.5a}$$

$$\text{s.t.} \quad \dot{x}(\tau) = f\big(x(\tau), h_\varepsilon\left(x(\tau), u(\tau)\right), u(\tau), \varepsilon\big), \qquad \text{for } \tau \in [t_0, t_\mathrm{f}], \tag{3.5b}$$

$$0 \geq c\big(x(\tau), h_\varepsilon\left(x(\tau), u(\tau)\right)\big), \qquad \text{for } \tau \in [t_0, t_\mathrm{f}], \tag{3.5c}$$

$$x(t_0) = x^{(0)}. \tag{3.5d}$$

In general $h_\varepsilon(\cdot)$ is unknown or computationally hard to calculate. It can be approximated by one of the model reduction techniques presented in Section 2.4. Numerically, the ZDP and local version of the TBOA turned out in tests to be the computationally cheapest (and still robust) approaches presented in this section. An advantage of the ZDP method is that the order can be chosen arbitrarily in terms of approximation of the SIM. The non-local TBOA benefits from the information in the neighborhood of a trajectory. This leads to a robust method but needs more computational efforts to solve.

Further, note that the controls $u(\tau)$ are regarded as "slow" variables because of several reasons. In chemical reactions, the fast time scale is often too fast for precise control of input species. In the next section, we discretize $u(\tau)$ and the other states in time and use piecewise constant values to approximate $u(\tau)$. This prevents the optimal control from chattering with a huge number of switches and constant values are directly related to slow variables.

The dynamics of (3.5b) are less stiff than those of (3.4) and (3.5) has just $n_x + n_u$ instead of $n_x + n_y + n_u$ optimization variables. However, $h_\varepsilon(\cdot)$ in problem (3.5) will be approximated numerically by a root finding respectively optimization problem, which has to be solved (possibly several times) in each iteration of any algorithm for optimization problem (3.5) and thus represents a nested optimization problem.

3.3.2 Lifted OCP

Having seen that the dimension reduced OCP (3.5) involves a nested optimization problem for handling the SIM computation or approximation, the idea of this section is to avoid such nested Newton schemes. A new approach we propose is based on the idea of *lifting*, as presented in Albersmeyer and Diehl [AD10]. To prevent numerical solvers from calculating $h_\varepsilon(x, u)$ exactly (or an approximation of it) several times in each iteration of a NLP solver for (3.5), the equation $y = h_\varepsilon(x, u)$ is handled as a constraint of the OCP. The converged numerical solution has to satisfy this equation, but it is not necessary to require that all iterates are on the manifold $y = h_\varepsilon(x, u)$. So there is potential to cut computational costs. In our dynamical model, this algorithmic feature can be realized through replacing the dynamics (3.4b) and (3.4c) of the original OCP (3.4) by the following DAE (3.6):

$$\begin{aligned} \dot{x} &= f(x, y, u, \varepsilon) \\ 0 &= y - h_\varepsilon(x, u). \end{aligned} \tag{3.6}$$

Since the manifold mapping $h_\varepsilon(x, u)$ is in general analytically unknown and difficult to calculate, the equation $0 = y - h_\varepsilon(x, u)$ is replaced by another root-finding problem that ensures its solution to be near the slow manifold (see Section 2.4). It turned out in numerical tests that the methods TBOA and ZDP are most promising. Using these for the approximation of h_ε (both can be written in the form of root finding problems $\psi = 0$), we get the following OCP (3.7):

$$\min_{x,\,y,\,u} \quad \int_{t_0}^{t_\mathrm{f}} f_0(x, y, u)\,\mathrm{d}\tau \tag{3.7a}$$

$$\text{s.t.} \qquad \dot{x} = f(x, y, u, \varepsilon), \tag{3.7b}$$

$$0 = \psi(x, y, u, \varepsilon), \tag{3.7c}$$

$$x(t_0) = x^{(0)},\ y(t_0) = y^{(0)}. \tag{3.7d}$$

Henceforth, we will refer to (3.5) as the reduced OCP and to (3.7) as the lifted OCP. It has the same number of optimization variables as the full OCP (3.4). However, its dynamics (3.7b) are less stiff, so the usage of an explicit integrator is often justified. This clearly reduces the effort for solving.

Root Finding Problem for ZDP To get a feeling for the structure of the SIM approximation problem $\psi(x, y, u, \varepsilon) = 0$, the root finding problem is demonstrated for the ZDP of order $m = 2$. The ZDP states that

$$\begin{aligned}
0 = \psi(x, y, u, \varepsilon) &= \frac{\mathrm{d}^2}{\mathrm{d}\tau} y = \frac{1}{\varepsilon}\frac{\mathrm{d}}{\mathrm{d}\tau} g(x, y, u, \varepsilon) \\
&= \frac{1}{\varepsilon}\left(D_x g(x, y, u, \varepsilon)x' + D_y g(x, y, u, \varepsilon)y' + D_u g(x, y, u, \varepsilon)u'\right) \\
&= \frac{1}{\varepsilon}\Bigg(g(x, y, u, \varepsilon) f(x, y, u, \varepsilon) + \frac{1}{\varepsilon} D_y g(x, y, u, \varepsilon) g(x, y, u, \varepsilon) \\
&\quad + D_u g(x, y, u, \varepsilon)u'\Bigg)
\end{aligned}$$

where the term $D_u g(x, y, u, \varepsilon)u'$ vanishes within each open control interval (t_i, t_{i+1}) if piecewise constant control discretization is used. So, derivatives of the right-hand side f have to be computed to use ZDP of order 2. In the case of a higher order ZDP, higher order derivatives have to be calculated and make the evaluation of the ZDP more complicated and expensive. Therefore, the applied order of the ZDP has to be a good compromise between approximation order and numerical efficiency and availability of higher derivatives.

Root Finding Problem for TBOA The deduction of a root finding problem from the TBOA is at first sight not obvious since it is an optimization problem. Thus we consider the local version of the TBOA:

$$\begin{aligned}
\min_{z\,=\,(x,\,y)} \quad & \left\| \frac{\mathrm{d}^m}{\mathrm{d}\tau^m} z(\tau)\Big|_{\tau=t_0} \right\|_2^2 \\
\text{s.t.} \quad & 0 = c\big(x(t_0), y(t_0)\big), \\
& x(t_0) = x^*
\end{aligned} \tag{3.8}$$

Recall that the function c may describe mass conservation laws etc.

If $m = 2$ then (3.8) can be rewritten as

$$\begin{aligned} \min_{y} \quad & \left\| G(x^*, y, u) \right\|_2^2 \\ \text{s.t.} \quad & 0 = c(x^*, y), \end{aligned} \tag{3.9}$$

where $G(x, y, u) := F'(x, y, u)F(x, y, u)$ with the right-hand side $F(x, y, u) = \big(f(x, y, u), \frac{1}{\varepsilon} g(x, y, u)\big)$ of the ODE constraint. The KKT conditions for (3.9) in a local minimum y^* for given u are thus the existence of a Lagrangian parameter λ^* such that

$$\begin{aligned} 0 &= 2D_y G(x^*, y^*, u)^\mathsf{T} G(x^*, y^*, u) + D_y c(x^*, y^*)^\mathsf{T} \lambda^* \\ 0 &= c(x^*, y^*). \end{aligned} \tag{3.10}$$

Since the parameter λ^* is unknown, it may be reasonable to use the implicit function theorem to resolve a part of the variables y^* via the equation $0 = c(x^*, y^*)$, if the theorem is applicable.

Equation (3.10) is the root finding problem related to the local TBOA with $m = 2$ that can be used for the SIM approximation function $\psi(x^*, y^*, u)$ of (3.7c).

3.4 Results

In this section, the previously presented methods are illustrated and tested with two low-dimensional examples of chemical reaction mechanisms as ODE constraints. Both examples involve multiple time scales but only one example is in singularly perturbed form. However, it is demonstrated that for both examples the proposed lifted OCP approach (3.7) is applicable and useful for manifold-based model reduction of OCPs. This section can be found in [Hei+17].

3.4.1 Numerical Solution

The choice of numerical solution method for ODEs (3.4), (3.5), (3.7) is an important decision to make in order to target real-time applications.

We will solve our OCPs with a direct approach. We choose a multiple shooting discretization [BP84], which has been proven to work well and efficiently in practice [Die+02]. We take $N \in \mathbb{N}$ shooting intervals, on which we simulate the slow

dynamics using an explicit Runge-Kutta integrator of order 4, where we take one integration step per shooting interval. Note that the explicit integration method is only suited for the reduced and lifted problem formulations. For the full problem, we use an implicit integration scheme, namely a stiffly accurate Radau II-A method. For all methods discussed, we model the controls as piecewise constant in each shooting interval.

We noted before that the new efficient method for solving manifold-based OCPs is compatible with either the TBOA (2.21) or with the ZDP. In the latter case, we are free to pick any m, such that the m-th time derivative should be equal to zero (see Section 2.4.1). We chose $m = 2$, as it is a good trade-off between accuracy (recall that the error is $\mathcal{O}(\varepsilon^m)$) and computational cost of forming and evaluating the derivatives.

Carrying out the discretization yields a finite-dimensional NLP, which we then solve with a Newton-type optimization method. More specifically, we use the interior point solver IPOPT [WB06], which we call from within the CasADi [And13] framework for dynamic optimization. CasADi implements the necessary algorithmic differentiation routines for the higher-order derivatives of the functions present in the OCP such that we are able to use exact Hessians in our solution method.

Since the used manifold approximation methods yield additional equality constraints for the NLPs, we are free to give more or less weight to these constraints. This if of particular interest if the corresponding functions of these constraints become very large outside the slow manifold. For this purpose, we introduce a weight factor which is multiplied with all corresponding constraints. Initially, we set this factor to 1. But experimental tests for the two tested examples show that smaller factors may lead to faster runtimes (see [Hei20]).

We remark that different choices for discretization of the problem exist. The multiple shooting method is chosen, because it is widely spread for optimal control problems with PDE and ODE constraints. Its advantages are numerical stability (e.g., in contrast with the single shooting) and the usage of a moderate number of optimization variables. Therefore, it is often used for high-dimensional optimal control problems. For instance direct collocation can be used for discretization of chemical reaction mechanism as well (cf. [Hei17]). However, collocation based NLPs involve a lot of more optimization variables than direct multiple shooting based NLPs but with a sparser structure of the corresponding matrices. Having

the ambitious target in mind that the presented method should be applied to high-dimensional problems, we mainly focus on the multiple shooting as benchmark for the new presented lifted OCP. For the sake of completeness, we also apply the collocation based approach to compare it with the other methods.

For readers that are familiar with CasADi, it should be mentioned that in the implementation of the different approaches `SX` variables are used whenever it is possible and `MX` variables are only used for implicit integrators. Symbolic `SX` expressions are typically longer, but faster to evaluate in comparison with `MX` expressions. However, `MX` expressions are more flexible with a larger range of applications, e.g., for root-finding problems based on Newton's method.

For all numerical experiments an Ubuntu 18.04 machine with an Intel® Core™ i7-2600 CPU (8 cores with 3.40 GHz) and 16 GB RAM is used. The software version R2018a of MATLAB and version 3.4.5 of CasADi are installed.

The following examples serve as first benchmark problems and do not have a deeper meaning or specific aim in mind. The objective functions are artificial but motivated by maximizing a specific variable and regularization of the controls.

All implementations can be found and downloaded at [Hei20]. The core element of this Software is the MATLAB function `performReduction.m` which solves the lifted approach (3.7). All efforts has been put into this file to make it easily customizable to applications.

3.4.2 Enzyme Example

The following OCP is based on the Michaelis-Menten-Henri mechanism introduced in Example 2.27. Its chemical mechanism can be written as:

$$S + E \rightleftharpoons C \to P + E,$$

where S is a substrate, E is an enzyme, C the corresponding substrate-enzyme-complex and P a product. As seen before, the simplified underlying ODE of the system is

$$\begin{aligned} \dot{x}(\tau) &= -x(\tau) + \big(x(\tau) + \kappa - \beta\big)\, y(\tau) \\ \varepsilon \dot{y}(\tau) &= x(\tau) - \big(x(\tau) + \kappa\big)\, y(\tau). \end{aligned}$$

We modify this ODE system by adding the possibility to influence the concentration $x(\tau)$ with a control function $u(\tau)$. Introducing an artificial objective function yields the following optimal control problem (3.11) where we denote $\big(x(\tau), y(\tau)\big)$ as $\big(z_\mathrm{s}(\tau), z_\mathrm{f}(\tau)\big)$ to clarify that this ODE was modified. The indices "s" and "f" stand for **s**low and **f**ast. Furthermore, we chose arbitrarily $\kappa = 1$ and $\beta = 0.5$.

$$\begin{aligned} \min_{z(\cdot),u(\cdot)} \quad & \int_0^5 -50\, z_\mathrm{f}(\tau) + u^2(\tau)\, \mathrm{d}\tau \\ \text{s.t.} \quad & \dot{z_\mathrm{s}}(\tau) = -z_\mathrm{s}(\tau) + \big(z_\mathrm{s}(\tau) + 0.5\big)\, z_\mathrm{f}(\tau) + u(\tau), \quad \text{for } \tau \in [0,5], \\ & \varepsilon \dot{z_\mathrm{f}}(\tau) = z_\mathrm{s}(\tau) - \big(z_\mathrm{s}(\tau) + 1\big)\, z_\mathrm{f}(\tau), \qquad\quad \text{for } \tau \in [0,5], \\ & 1 = z_\mathrm{s}(0), \end{aligned} \tag{3.11}$$

where $z(\cdot) = \big(z_\mathrm{s}(\cdot), z_\mathrm{f}(\cdot)\big) \in \mathbb{R}_+ \times \mathbb{R}_+$ and control $u(\tau) \in [0, 10]$ represents the possibility to add some substrate (corresponds to variable z_s) to the system.

The numerical results for this example discretized in $N = 40$ subintervals and with $\varepsilon = 10^{-6}$ can be seen in Fig. 3.2. The solutions of the original system (3.4) in Fig. 3.2a and lifted system (3.7) in Fig. 3.2b are almost equal. It holds

$$\begin{aligned} &\max\Big\{||z_\mathrm{s}^{\text{orig}} - z_\mathrm{s}^{\text{app}}||_\infty, ||z_\mathrm{f}^{\text{orig}} - z_\mathrm{f}^{\text{app}}||_\infty, ||u^{\text{orig}} - u^{\text{app}}||_\infty\Big\} \;= ||z_\mathrm{s}^{\text{orig}} - z_\mathrm{s}^{\text{app}}||_\infty \\ &\approx 0.047, \end{aligned}$$

which gives a relative error smaller than 1.16 % (except of the last control u_N that is almost zero). The objective function values produce a relative error of 0.21 % (the objective function value is about -187.85).

For brevity, we do not list the errors of the direct collocation method here. However, they are in the same range as those of the multiple shooting method. The errors between the multiple shooting and the collocation solution are comparable to the errors between the multiple shooting of the full OCP and the lifted OCP. Just the difference in the numerical values for z_s is a little bit bigger. In total, there is no big difference in the quality of the solutions.

However, there is a big difference in the runtimes which are listed in Table 3.1. Whereas the NLP resulting from the original system (using the multiple shooting) can be solved with CasADi and Ipopt in 0.19233 seconds on average, our proposed approach using ZDP of order $m = 2$ only needs 0.01743 seconds. This gives a significant speed up of factor 11. The order reduced OCP (3.5) takes 0.58269 seconds. It has the smallest number of optimization variables, but the nested root

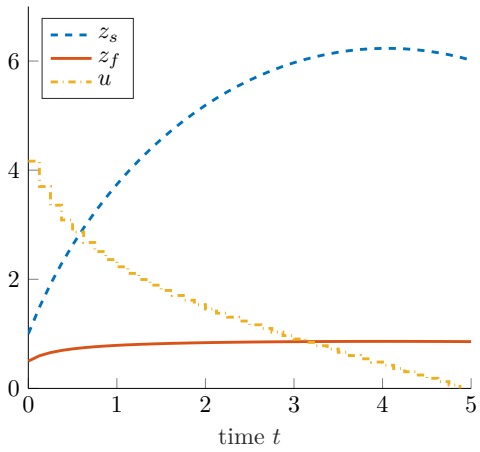

(a) Numerical solution of (3.4) with multiple shooting.

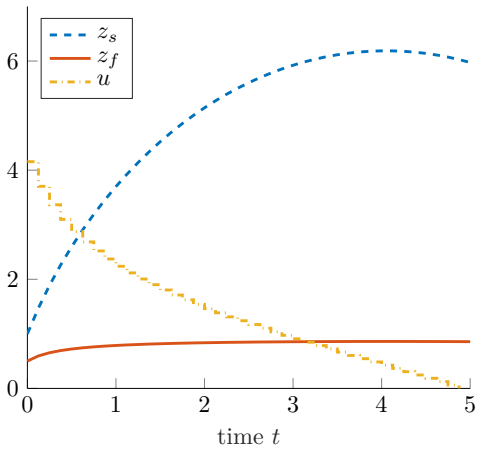

(b) Numerical solution of (3.7) using the ZDP with $m = 2$.

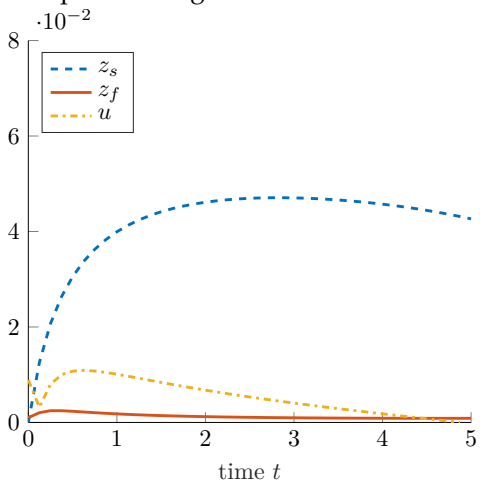

(c) Absolute error between full (3.4) and lifted solution (3.7).

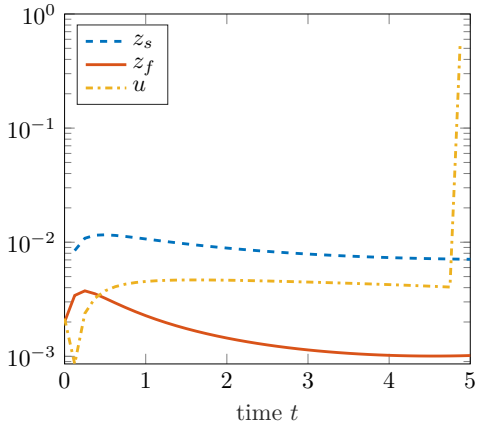

(d) Relative error between full (3.4) and lifted solution (3.7).

Figure 3.2: Numerical solution for the OCP of the enzyme example. Modified from [Hei+17].

finding problem for $h_\varepsilon(\cdot)$ in each interval causes this longer runtime. As already mentioned in [Reh13], the order reduced OCP (3.5) does not need to improve the runtime, although less optimization variables are present. The ZDP-based manifold computation outperforms the TBOA-based computation in the lifted OCP (3.7). Although the focus of comparison is on the multiple shooting discretization of the full OCP (3.4), we consider the collocation as well. In this example, the

collocation based approach is the fastest method. It is slightly faster than the lifted ZDP approach. However, the resulting NLP involves more variables and constraints. Thus, we expect that for higher-dimensional ODEs, the new presented ansatz is more efficient in comparison with the collocation.

Table 3.1: Runtimes for the enzyme example in seconds for $N = 40$ and the number of variables and constraints for the underlying NLP. Used order for ZDP in reduced methods is $m = 2$. We call each method 10 times and compute the mean runtimes.

	full OCP (Mul. S.)	**full OCP (Colloc.)**	**red. OCP (ZDP)**	**lifted OCP (TBOA)**	**lifted OCP (ZDP)**
mean runtime	0.19233	0.01554	0.58269	0.02751	0.01743
std deviation	$1.1 \cdot 10^{-5}$	$6.8 \cdot 10^{-7}$	$4.8 \cdot 10^{-5}$	$1.0 \cdot 10^{-6}$	$1.6 \cdot 10^{-7}$
max runtime	0.19651	0.01745	0.59545	0.02994	0.01849
min runtime	0.18854	0.01443	0.57549	0.02650	0.01706
variables	120	280	80	121	121
constraints	80	240	40	80	80

For other values of $\varepsilon \in (0, 0.1]$ and the choice of $z_{\mathrm{s}}(0)$ almost the same runtimes are obtained for both the full problem and the lifted problem.

3.4.3 CSTR Example

In the following, we study another example that involves some more variables than the enzyme example. Inspired by an example of Cvejn [Cve07], we consider a small Continuous Stirred Tank Reactor (CSTR) in which the chemical reactions

$$A \underset{k_1^-}{\overset{k_1}{\rightleftharpoons}} B \overset{\varepsilon}{\to} C \overset{k_2}{\to} D$$

take place for given reaction rates k_1, k_1^-, k_2 and ε. For simplicity, we assume that the tank is perfectly mixed and the reaction is isothermic. Fig. 3.3 illustrates the CSTR.

Input for the reaction is only species A with a given (constant) concentration $c_{A_{\mathrm{in}}}$. This input can be controlled via a feed $q_A \in [0, q_{A_{\max}}]$. Output of the reactor is a mixture of species A, B, C and D and can also be controlled with the outlet $q \in [0, q_{\max}]$. A possible scenario is that the amount of species B should be maximized

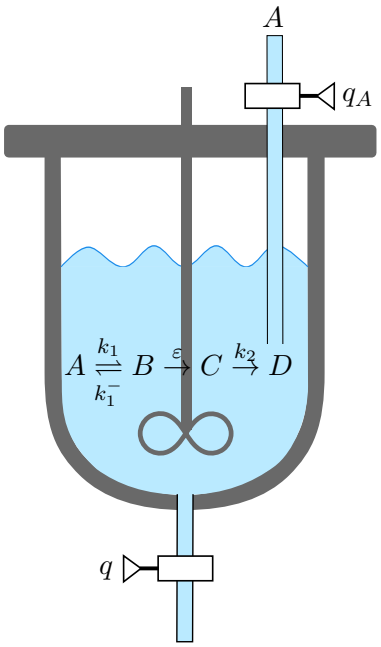

Figure 3.3: Visualization of the CSTR. Modified from [Hei+17].

in the output of the CSTR. Since the volume of the tank reactor is bounded, this leads to an optimal control problem with constraints (see (3.12)). For brevity, we omit the arguments of the functions in the ODE part of the OCP (i.e. the dependency on t).

$$\min_{c(\cdot), V(\cdot), q(\cdot), q_A(\cdot)} \quad \int_0^{500} -0.1\, q \cdot c_B + q^2 + q_A^2 \, \mathrm{d}t \tag{3.12a}$$

$$\text{s.t.} \quad c_A{}' = -k_1 c_A + k_1^- c_B + \frac{q_A}{V}\left(c_{A_{\text{in}}} - c_A\right), \tag{3.12b}$$

$$c_B{}' = k_1 c_A - (k_1^- + \varepsilon) c_B - \frac{q_A}{V} c_B, \tag{3.12c}$$

$$c_C{}' = \varepsilon c_B - k_2 c_C - \frac{q_A}{V} c_C, \tag{3.12d}$$

$$c_D{}' = k_2 c_C - \frac{q_A}{V} c_D, \tag{3.12e}$$

$$V' = q_A - q, \tag{3.12f}$$

$$c^* = c(0), \tag{3.12g}$$

$$V^* = V(0) = V(500), \tag{3.12h}$$

where $c(t) = \big(c_A(t), c_B(t), c_C(t), c_D(t)\big)^\mathsf{T}$ and $c^* = \big(c_A^*, c_B^*, c_C^*, c_D^*\big)^\mathsf{T}$. The values of the constants in OCP (3.12) are listed in Table 3.2.

Table 3.2: Constants for the CSTR example

constant	description	value
$c_{A_{\text{in}}}$	concentration of species A of inlet	1
k_1	forward reaction rate constant of $A \rightleftharpoons B$	100
k_1^-	backward reaction rate constant of $A \rightleftharpoons B$	90
k_2	reaction rate constant of $C \to D$	20
ε	reaction rate constant of $B \to C$	10^{-6}
$q_{A_{\text{max}}}$	maximum value for q_A in inlet	10^{-3}
q_{max}	maximum value for q in outlet	$1.5 \cdot 10^{-3}$
c_A^*	initial concentration of species A	10^{-3}
c_B^*	initial concentration of species B	10^{-3}
c_C^*	initial concentration of species C	0
c_D^*	initial concentration of species D	10^{-8}
V^*	initial and final volume of tank reactor	10^{-2}

Note that the ODE constraint of this OCP is not in singularly perturbed form. However, the idea of lifting in combination with the ZDP method is still applicable because its dynamics are given by a multi-scale ODE. The choice of reaction progress variables is not obvious and has combinatorial complexity. We choose B, D and the volume V mainly motivated by the reaction rates.

For $N = 140$ intervals and the initial values $c_A(0) = c_A^*$ and $c_C(0) = c_C^*$ from Table 3.2, IPOPT finds a point of local infeasibility for the nonlinear program resulting from the lifted OCP using multiple shooting and ZDP of order 2. Removing the initial value $c_A(0) = c_A^*$ constraint, the IPOPT code converges to the solution depicted in Fig. 3.4. For the plots of the lifted OCP, we took the optimal controls of the numerical solution and integrated the other states forward in time with an implicit Radau II-A integrator.

The solutions of the original system (3.4) via multiple shooting and the lifted system (3.7) (without forward integration) differ in contrast to the enzyme example. It holds

$$\begin{aligned}&\max\Big\{||c^{\text{orig}} - c^{\text{app}}||_\infty, ||q_{\text{A}}^{\text{orig}} - q_{\text{A}}^{\text{app}}||_\infty, ||q^{\text{orig}} - q^{\text{app}}||_\infty\Big\}\\ &= ||c_{\text{B}}^{\text{orig}} - c_{\text{B}}^{\text{app}}||_\infty \approx 0.049.\end{aligned}$$

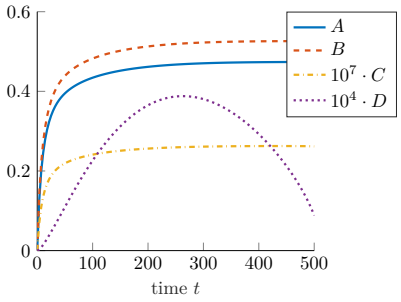

(a) Full solution species c_A, c_B, c_C and c_D of (3.4) solved by multiple shooting.

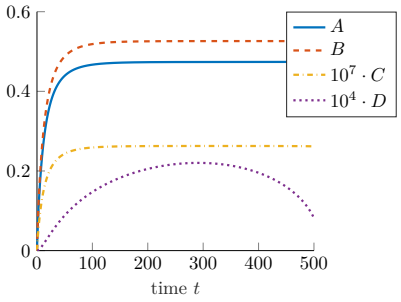

(b) Lifted solution species c_A, c_B, c_C and c_D of (3.7) using the ZDP with $m = 2$.

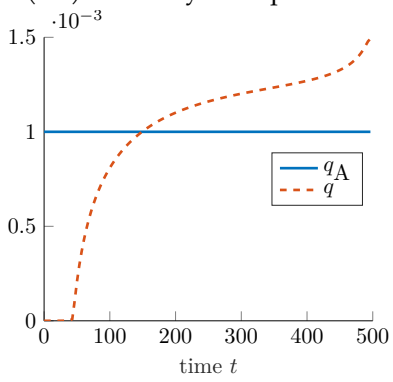

(c) Full solution controls q_A and q of (3.4) solved by multiple shooting.

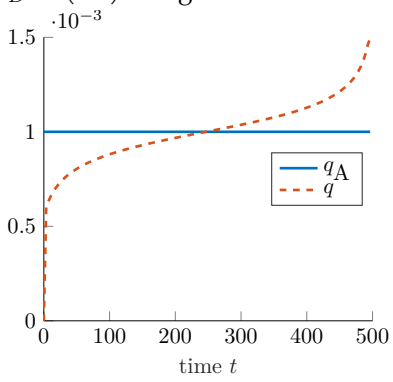

(d) Lifted solution controls q_A and q of (3.7) using the ZDP with $m = 2$.

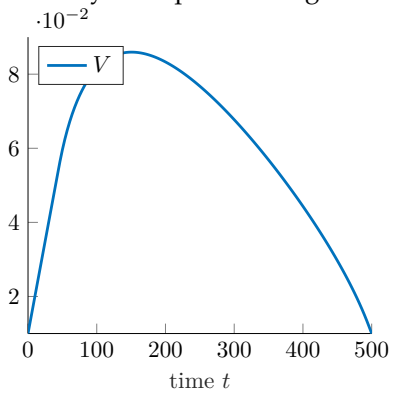

(e) Full solution volume V of Eq. (3.4) solved by multiple shooting.

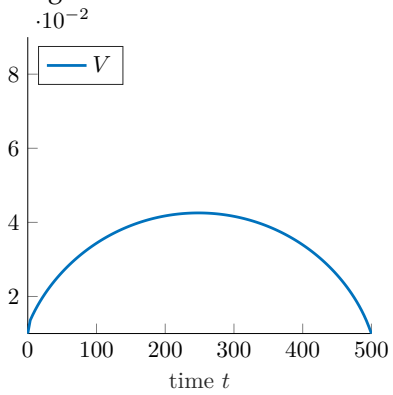

(f) Lifted volume V of (3.7) using the ZDP with $m = 2$

Figure 3.4: Numerical solution of the CSTR example. Plotted values for the "lifted" variables of (3.7) are obtained by forward integration with the calculated lifted controls. Modified from [Hei+17].

This can also be observed in Figs. 3.4a and 3.4b. Variable c_B in the lifted OCP grows more rapidly at the beginning of the time interval. IPOPT has found two different local minima (for two different nonlinear problems). The objective function values are -0.25667 for the full system and -0.25679 for the lifted system which yields an absolute difference of $1.2 \cdot 10^{-4}$ and a relative difference of about 0.047%.

The average runtimes of 10 runs for all methods mentioned above can be found in Table 3.3. Since the numerical solution of the reduced OCP (3.5) took a very long time for the enzyme example (see Section 3.4.2), we did not implement this approach for the CSTR example. The relations of the runtimes are comparable to those of the first example. For the lifted OCP including the ZDP method of order $m = 2$, we oberve a significant speed up of factor 38 in comparison with the full multiple shooting method. The discretization via collocation is the fastest method that we tested. Its mean runtime is very close to the lifted OCP with ZDP. However, it involves more than twice the number of NLP variables and constraints.

Table 3.3: Runtimes for the CSTR example in seconds for $N = 140$ and the number of variables and constraints for the underlying NLP. Used order for ZDP in reduced method is $m = 2$. We call each method 10 times and compute the mean runtimes.

	full OCP (Mul. S.)	**full OCP (Colloc.)**	**lifted OCP (TBOA)**	**lifted OCP (ZDP)**
mean runtime	5.06630	0.12384	0.25137	0.13035
std deviation	$2.6 \cdot 10^{-3}$	$4.5 \cdot 10^{-6}$	$1.8 \cdot 10^{-5}$	$1.4 \cdot 10^{-6}$
max runtime	5.14330	0.12730	0.26098	0.13256
min runtime	4.97032	0.12138	0.24634	0.12894
variables	979	2379	980	980
constraints	700	2100	700	700

Depending on the number of shooting intervals and thus control discretization intervals, the solution of the full system changes. For $N = 4000$ intervals, the solution of the full OCP via multiple shooting (see Figs. 3.5a to 3.5c) looks qualitatively more like the lifted solution for $N = 140$ than like the solution of the full OCP. The objective function value is -0.2568167. These facts point out the sensitivity of the problem as well as the benefits of the lifted OCP. Though the full and lifted solution illustrated in Fig. 3.4 are different, IPOPT converges in each case to a solution. We therefore assume that these solutions are two different local minima for the NLP resulting from the multiple shooting method for the full OCP.

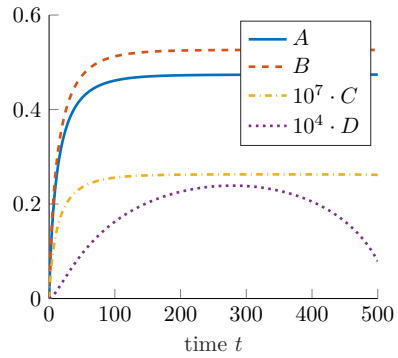

(a) Full solution species c_A, c_B, c_C and c_D of (3.4) solved by multiple shooting on $N = 4000$ intervals.

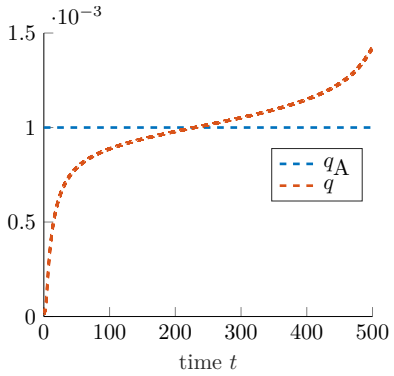

(b) Full solution controls q_A and q of (3.4) solved by multiple shooting on $N = 4000$ intervals.

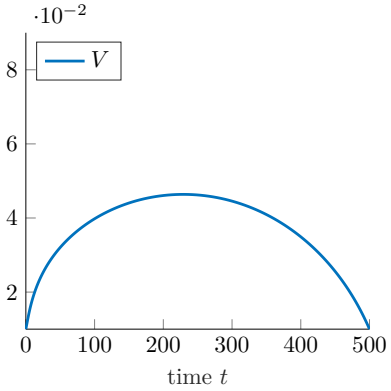

(c) Full volume V of (3.4) solved by multiple shooting on $N = 4000$ intervals.

Figure 3.5: Numerical solution of the CSTR example on $N = 4000$ intervals. Modified from [Hei+17].

Furthermore, higher-dimensional problems may be solved faster by the lifted OCP than by the full OCP discretized with collocation (or multiple shooting). The time needed to construct the NLP with CasADi is considerable for the collocation. The lifted approaches involve less variables and are consequently, easier to construct. However, their drawback for high-dimensional problems may be the tuning of parameters: Choices have to be made for the ZDP order, initial values of the slow variables, and the previously mentioned weight factor of the SIM approximation equality constraints.

4 Holomorphic Dynamical Systems and Newton Flows

In this chapter, we leave the optimal control theory and consider dynamical systems of *holomorphic* functions. The identification of $\mathbb{C} \simeq \mathbb{R}^2$ makes the theory in $\mathbb{R}^n$ of the last chapters accessible. However, the Cauchy-Riemann equations show that for holomorphic functions in $\mathbb{C}$ there is an additional structure in comparison to real-analytic functions in $\mathbb{R}^2$.

The phase portrait of holomorphic functions often includes invariant structures, called separatrices, similar to slow invariant manifolds. Thus, we study the phase portrait of holomorphic dynamical systems and its separatrices in this chapter. For motivation, we start introducing the Riemann ζ function as an example for holomorphic functions. The reader is introduced into the Riemann hypothesis and we point out a connection to holomorphic dynamical systems that goes back to an idea of Dirk Lebiedz. Afterwards, we consider Newton flows. These are holomorphic flows that represent the continuous form of the Newton-Raphson method and thus, are linked with convergence to zeros of the right-hand side. We study the behavior of holomorphic and Newton flows as the time tends to infinity. In Chapter 5, we subsequently aim at identifying and characterizing separatrices of holomorphic and Newton flows.

4.1 Holomorphic Flow of the ξ Function and the Riemann Hypothesis

In this section, we introduce the Riemann ζ function and present some properties of this function. The Riemann ζ function has a deep connection to prime numbers and was first studied for complex arguments by Riemann. This function is a central subject of many studies in the analytic number theory. Afterwards, the Riemann ξ

function is introduced as symmetric version of ζ. Both functions are central issue of the Riemann Hypothesis.

The Riemann ζ function is defined by $\zeta\colon \{z \in \mathbb{C}\colon \operatorname{Re} z > 1\} \to \mathbb{C}$ with

$$\zeta(z) \coloneqq \sum_{n=1}^{\infty} \frac{1}{n^z}. \tag{4.1}$$

The next section shows that this definition of the ζ function can be holomorphically continued to the complex plane without $z = 1$.

4.1.1 Holomorphic Continuation of the ζ Function

Although the series representation (4.1) only converges for z with real parts greater than 1, complex analysis tools yield a possible extension of ζ on the whole complex plane except of the point $z = 1$. At $z = 1$, the series diverges because it is the harmonic series. The following analytic continuation of the Riemann ζ function is based on the original Riemann paper [Rie59] and [Edw01].

A closer look on the terms of Eq. (4.1) reveals a holomorphic continuation of $\zeta(z)$ for z with $\operatorname{Re} z \leq 1$. The terms are multiplied with the gamma function, which is well defined for all complex numbers with $\operatorname{Re} z > 0$. This results in

$$\frac{1}{n^z}\Gamma(z) = \frac{1}{n^z}\int_0^\infty t^{z-1}\mathrm{e}^{-t}\,\mathrm{d}t \overset{t=\tau\cdot n}{=} \frac{1}{n^z}\int_0^\infty (\tau n)^{z-1}\mathrm{e}^{-\tau n} n\,\mathrm{d}\tau = \int_0^\infty \tau^{z-1}\mathrm{e}^{-\tau\, n}\,\mathrm{d}\tau. \tag{4.2}$$

Switching the order of integration and summation because of compact convergence, we obtain

$$\begin{aligned}\zeta(z)\Gamma(z) &\overset{(4.1)}{=} \sum_{n=1}^{\infty}\frac{1}{n^z}\Gamma(z) \overset{(4.2)}{=} \sum_{n=1}^{\infty}\int_0^\infty \tau^{z-1}\mathrm{e}^{-\tau\, n}\,\mathrm{d}\tau = \int_0^\infty \sum_{n=1}^{\infty}\tau^{z-1}\mathrm{e}^{-\tau\, n}\,\mathrm{d}\tau \\ &= \int_0^\infty \frac{\tau^{z-1}\mathrm{e}^{-\tau}}{1-\mathrm{e}^{-\tau}}\,\mathrm{d}\tau = \int_0^\infty \frac{\tau^{z-1}}{\mathrm{e}^{\tau}-1}\,\mathrm{d}\tau.\end{aligned} \tag{4.3}$$

Riemann investigates the contour integral

$$\int_\gamma \frac{(-\tau)^{z-1}}{\mathrm{e}^{\tau}-1}\,\mathrm{d}\tau, \tag{4.4}$$

where γ is a curve that starts at ∞ and goes down slightly above the real axis up to an infinitesimally small circle around 0 (in positive mathematical direction) and returns to ∞ slightly below the real axis (cf. [Edw01, p. 10]). It can be formulated as the limit for $\delta \to 0$ of the sum of these three integrals:

$$\int_{\infty}^{\delta} \frac{(-\tau)^{z-1}}{\mathrm{e}^{\tau}-1}\,\mathrm{d}\tau + \oint_{|\tau|=\delta} \frac{(-\tau)^{z-1}}{\mathrm{e}^{\tau}-1}\,\mathrm{d}\tau + \int_{\delta}^{\infty} \frac{(-\tau)^{z-1}}{\mathrm{e}^{\tau}-1}\,\mathrm{d}\tau. \tag{4.5}$$

The second term in Eq. (4.5) is by Cauchy's integral formula equal to $2\pi\mathrm{i} \cdot (-\tau)^{z}(\mathrm{e}^{\tau}-1)^{-1}$ evaluated at the midpoint 0 of the circle $|\tau| = \delta$. As a result, this integral term vanishes. The remaining terms can be simplified by means of the following calculation:

$$\begin{aligned}\int_{\gamma} \frac{(-\tau)^{z-1}}{\mathrm{e}^{\tau}-1}\,\mathrm{d}\tau &= \lim_{\delta\to 0}\left(\int_{\infty}^{\delta} \frac{\exp(s(\log\tau - \mathrm{i}\pi))}{(\mathrm{e}^{\tau}-1)\tau}\,\mathrm{d}\tau + \int_{\delta}^{\infty} \frac{\exp(s(\log\tau + \mathrm{i}\pi))}{(\mathrm{e}^{\tau}-1)\tau}\,\mathrm{d}\tau\right)\\ &= \left(\mathrm{e}^{\mathrm{i}\pi\tau} - \mathrm{e}^{-\mathrm{i}\pi\tau}\right)\int_{0}^{\infty} \frac{\tau^{z-1}}{\mathrm{e}^{\tau}-1}\,\mathrm{d}\tau \overset{(4.3)}{=} 2\mathrm{i}\sin(\pi z)\Gamma(z)\zeta(z).\end{aligned} \tag{4.6}$$

Using the functional equation

$$\Gamma(z)\Gamma(1-z) = \frac{\pi}{\sin(\pi z)},$$

we finally obtain

$$\zeta(z) \overset{(4.6)}{=} \frac{\Gamma(1-z)}{2\pi\mathrm{i}}\int_{\gamma} \frac{(-\tau)^{z-1}}{\mathrm{e}^{\tau}-1}\,\mathrm{d}\tau. \tag{4.7}$$

Eq. (4.7) is the holomorphic continuation of the Dirichlet sum (4.1). The integral (4.4) converges for all z since e^{τ} grows faster than τ^{z} for $\tau \to \infty$ and on compact domains it converges uniformly. Therefore, this integral is an entire function. It is well known that $\sin(\pi z)$ is an entire function and $\Gamma(z)$ is holomorphic in the half plane $\mathrm{Re} z > 0$. The continuation of ζ (4.7) is thus well defined for all z except all natural numbers, where $\Gamma(1-z)$ has poles. Definition (4.1) shows that $\zeta(z)$ is well defined at all natural numbers bigger than 1. Hence, the ζ continuation is defined for all $z \in \mathbb{C} \setminus \{1\}$ with a simple pole at $z = 1$. In other words, the ζ function is a

meromorphic function.

4.1.2 The Functional Equation of the ζ Function

The last section revealed that the ζ function is a meromorphic function. In this section, we uncover another property of this function. Riemann deduces a functional equation for the ζ function from the analytic continuation integral (4.7) [Rie59; Tit86]. This functional equation is the starting point to construct the ξ function which is symmetric with respect to the line $\operatorname{Re} z = 1/2$, i.e., $\xi(z) = \xi(1-z)$. We follow the argumentation of [Edw01].

Starting point for the derivation of the functional equation is the integral in the analytic continuation (4.7). Consider the domain $D_k \subset \mathbb{C}$, which is the disk $U_{2\pi k+1}(0) \coloneqq \{z \in \mathbb{C} \colon |z| < 2\pi k + 1\}$ excluding all points that lie in the "tube" $T_k \coloneqq \{z = \sigma + \mathrm{i}t \in \mathbb{C} \colon \sigma \in (0, 2\pi k + 1), |t| < \varepsilon\}$ near the real axis and excluding all disks $U_\varepsilon(2\pi k\mathrm{i})$ for $k = 1, \ldots, n$. The points $2\pi k\mathrm{i}$ are the singularities of the integrand

$$\int \frac{(-\tau)^{z-1}}{\mathrm{e}^\tau - 1}\,\mathrm{d}t$$

and at the positive real axis $(-\tau)^{z-1} = \exp((z-1)\log(-\tau))$ is not defined. We apply Cauchy's integral theorem to obtain

$$\begin{aligned} 0 &= \oint_{\partial D_k} \frac{(-\tau)^{z-1}}{\mathrm{e}^\tau - 1}\,\mathrm{d}\tau \\ &= \oint_{\partial U_{(2\pi k+1)}(0)} \frac{(-\tau)^{z-1}}{\mathrm{e}^\tau - 1}\,\mathrm{d}\tau + \oint_{\partial T_k} \frac{(-\tau)^{z-1}}{\mathrm{e}^\tau - 1}\,\mathrm{d}\tau + \sum_{n=-k}^{k} \oint_{\partial U_\varepsilon(2\pi n\mathrm{i})} \frac{(-\tau)^{z-1}}{\mathrm{e}^\tau - 1}\,\mathrm{d}\tau \end{aligned} \tag{4.8}$$

In the limit $k \to \infty$, the first integral in Eq. (4.8) vanishes because the length of integration curve is $2\pi(2\pi k + 1)$, the denominator is bounded below and the modulus of the nominator satisfies $\left|(-\tau)^{z-1}\right| \leq (2\pi k + 1)^{-\delta-1}$ for $z \leq -\delta < 0$. Thus, we first consider the special case of a real $z < 0$. Since the tube T_k converges to the above mentioned integration path γ, it holds

$$0 = \int_\gamma \frac{(-\tau)^{z-1}}{\mathrm{e}^\tau - 1}\,\mathrm{d}\tau + \sum_{n\in\mathbb{Z}} \oint_{\partial U_\varepsilon(2\pi n\mathrm{i})} \frac{(-\tau)^{z-1}}{\mathrm{e}^\tau - 1}\,\mathrm{d}\tau \tag{4.9}$$

as k tends to infinity.

Application of the residue theorem makes it possible to compute the integrals that appear in the sum of (4.9).

$$\begin{aligned}
\oint_{\partial U_\varepsilon(2\pi n\mathrm{i})} \frac{(-\tau)^{z-1}}{\mathrm{e}^\tau - 1}\,\mathrm{d}\tau &= 2\pi\mathrm{i}\,\mathrm{Res}_{2\pi n\mathrm{i}}\left(\frac{(-\tau)^{z-1}}{\mathrm{e}^\tau - 1}\right) \\
&= 2\pi\mathrm{i}\lim_{\tau\to 2\pi n\mathrm{i}}(\tau - 2\pi n\mathrm{i})\frac{(-\tau)^{z-1}}{\mathrm{e}^\tau - 1} \\
&\overset{\text{L'Hospital}}{=} 2\pi\mathrm{i}\lim_{\tau\to 2\pi n\mathrm{i}}\frac{(-\tau)^{z-2}(-\tau + (z-1)(\tau - 2\pi n\mathrm{i}))}{\mathrm{e}^\tau} \\
&= 2\pi\mathrm{i}(-2\pi n\mathrm{i})^{z-1}. \qquad (4.10)
\end{aligned}$$

Combining the last equations leads to the following functional equation of the Riemann ζ function

$$\begin{aligned}
\zeta(z) &\overset{(4.7)}{=} \frac{\Gamma(1-z)}{2\pi\mathrm{i}}\int_\gamma \frac{(-\tau)^{z-1}}{\mathrm{e}^\tau - 1}\,\mathrm{d}\tau \\
&\overset{(4.9)}{=} -\frac{\Gamma(1-z)}{2\pi\mathrm{i}}\sum_{n\in\mathbb{N}}\oint_{\partial U_\varepsilon(-2\pi n\mathrm{i})}\frac{(-\tau)^{z-1}}{\mathrm{e}^\tau - 1}\,\mathrm{d}\tau + \oint_{\partial U_\varepsilon(2\pi n\mathrm{i})}\frac{(-\tau)^{z-1}}{\mathrm{e}^\tau - 1}\,\mathrm{d}\tau \\
&\overset{(4.10)}{=} \Gamma(1-z)\sum_{n=1}^{\infty}(2\pi n\mathrm{i})^{z-1} + (-2\pi n\mathrm{i})^{z-1} \\
&= \Gamma(1-z)\sum_{n=1}^{\infty}(2\pi n)^{z-1}\frac{1}{\mathrm{i}}\left(\mathrm{i}^z + (-\mathrm{i})^z\right) \\
&= \Gamma(1-z)\sum_{n=1}^{\infty}(2\pi n)^{z-1}\frac{1}{\mathrm{i}}\left(\mathrm{e}^{z\log\mathrm{i}} + \mathrm{e}^{z\log(-\mathrm{i})}\right) \\
&= \Gamma(1-z)\sum_{n=1}^{\infty}(2\pi n)^{z-1}\frac{1}{\mathrm{i}}\left(\mathrm{e}^{z\mathrm{i}\pi/2} + \mathrm{e}^{-z\mathrm{i}\pi/2}\right) \\
&= \Gamma(1-z)\sum_{n=1}^{\infty}(2\pi n)^{z-1}2\sin\left(\frac{\pi}{2}z\right) \\
&= \Gamma(1-z)(2\pi)^{z-1}2\sin\left(\frac{\pi}{2}z\right)\sum_{n=1}^{\infty}n^{z-1} \\
&= \Gamma(1-z)(2\pi)^{z-1}2\sin\left(\frac{\pi}{2}z\right)\zeta(1-z). \qquad (4.11)
\end{aligned}$$

This functional equation extends to $z \in \mathbb{C} \setminus \mathbb{N}_0$ as well because the right-hand side of Eq. (4.11) is analytic.

4.1.3 Riemann ξ Function

The functional equation (4.11) can be reduced to a simple form by introducing the function

$$\xi(z) \coloneqq \frac{1}{2} z(z-1)\Gamma\left(\frac{z}{2}\right)\pi^{-z/2}\zeta(z),$$

which is called *Riemann ξ function* in honor of Bernhard Riemann. The functional equation now becomes

$$\xi(z) = \xi(1-z). \tag{4.12}$$

Because of this strong symmetric relation, the Riemann ξ function is often referred to as "symmetric ζ function".

On top of this simpler functional equation, the ξ function is an entire function. Multiplication of $\Gamma\left(\frac{z}{2}\right)$ with ζ cancels the simple poles at $z = -2, -4, \ldots$. The poles of $\Gamma\left(\frac{z}{2}\right)\pi^{-z/2}\zeta(z)$ at 0 and 1 vanish by multiplication with $z(z-1)$. Thus, the ξ function is entire and its zeros are exactly the non-trivial zeros of ζ.

4.1.4 Zeros of the ζ Function

In the following, we will focus on the roots of the Riemann ζ function. We start with formula (4.7). The function $\frac{z}{\mathrm{e}^z-1}$ is an analytic function near $z = 0$ with power series

$$\frac{z}{\mathrm{e}^z - 1} = \sum_{n=0}^{\infty} \frac{B_n}{n!} z^n,$$

where B_n are the *Bernoulli numbers* (cf. [Edw01]).

A short calculation shows that

$$\zeta(-n) = (-1)^n \frac{B_{n+1}}{n+1} \quad \text{for all } n = 0, 1, 2, \ldots.$$

Since the Bernoulli numbers for odd natural numbers $2n+1$, $n \in \mathbb{N}$ are zero we get

$$\zeta(-2n) = 0 \quad \text{for all } n \in \mathbb{N}.$$

These negative even integers are called the *trivial* zeros of the Riemann ζ function. All other zeros are named *non-trivial* zeros.

These non-trivial zeros are part of the Riemann hypothesis which is one of the seven millennium prize problems put forth by the Clay Mathematical Institute in 2000 (see `http://www.claymath.org/millennium-problems`).

Riemann Hypothesis. *All non-trivial zeros of the Riemann ζ function have real part 1/2.*

If the Riemann hypothesis is true, all non-trivial zeros of ζ lie on the *critical line* $\mathrm{Re}z = 1/2$. In other words, the Riemann hypothesis is equivalent to the statement that all zeros of the Riemann ξ function lie on its symmetry axis $\mathrm{Re}z = 1/2$.

This Riemann hypothesis was first mentioned in [Rie59] in 1859. Riemann claims that it is "very likely that all of the roots are real. One would of course like to have a rigorous proof of this, but I have put aside the search for such a proof after some fleeting vain attempts because it is not necessary for the immediate objective of my investigation". He defines a $\hat{\xi}$ function

$$\hat{\xi}(t) \coloneqq \xi(1/2 + \mathrm{i}t),$$

for which all roots should be real.

The ξ function can be written in the product form

$$\xi(z) = \xi(z_0) \prod_n \frac{z - \rho_n}{z_0 - \rho_n},$$

where ρ_n are the non-trivial zeros of the Riemann ζ function. The product is understood such that the zeros ρ_n and $1 - \rho_n = \bar{\rho}_n$ are paired. The validity of the product formula is not obvious and was first shown by Hadamard in 1893 [Had93]. A proof and more details are given in chapter 2 of [Edw01].

4.1.5 Riemann Hypothesis and Prime Numbers

The Riemann hypothesis fascinates many mathematicians. This is mainly explained by the connections of the ζ function to complex analysis, dynamical systems and number theory. In this subsection, we highlight the "connecting thread" to prime numbers.

Euler was one of the first mathematicians who investigated the ζ function. The *Euler product*

$$\zeta(z) = \prod_{p\,\text{prime}} \left(1 - p^{-z}\right)^{-1}$$

can be obtained by prime factorization of n in the definition of ζ and represents a direct connection of ζ to primes.

The final result of Riemann in his paper „Ueber die Anzahl der Primzahl unter einer gegebenen Grösse“ [Rie59] is about the number of primes $\pi(x)$ smaller than a given number x:

$$\pi(x) = \sum_{n=1}^{\infty} \frac{\mu(n)}{n} J\left(x^{1/n}\right),$$

where $\mu(n)$ is 0 if n is divisible by a prime square, and $(-1)^k$ if it is the product of k distinct primes. The function $J(x)$ is given by

$$J(x) = \text{Li}(x) - \sum_{\rho} \text{Li}(x^{\rho}) - \log 2 + \int_x^{\infty} \frac{\mathrm{d}t}{t(t^2-1)\log t}.$$

Here, $\text{Li}(x)$ denotes the integral logarithm $\int_2^x \frac{\mathrm{d}t}{\log t}$ and the numbers ρ are the Riemann zeros.

If all Riemann zeros were known more information about the distribution of the prime numbers would be available. It would be a cryptographic nightmare if arbitrary prime numbers could easily be computed as many encryption algorithms are based on the multiplication of two very big prime numbers that have the function of private keys. In this case, hackers would be able to guess the private keys.

4.2 Holomorphic Flow

Let us now turn back to dynamical systems. In ordinary differential equations, fixed points play an important role for the phase portrait. An idea of Dirk Lebiedz is to establish a link between the search for Riemann zeros — in general the zeros of some holomorphic function f — and dynamical systems by regarding the ODE

$$z' = \zeta(z) \quad \text{resp.} \quad z' = f(z).$$

In this section, we study this differential equation and simplifications of it. Particularly, we are interested in the structures and long-term behavior of these dynamical systems.

First, we recall the general definition of a holomorphic dynamical system (see Definition 2.6).

Definition 4.1. A *holomorphic IVP* is a relation of the form

$$\begin{aligned} z'(t) &= f(t, z(t)) \quad \text{for all } (t, z) \in U \\ z(t_0) &= z_0, \end{aligned}$$

where $f : U \to \mathbb{C}^n$ is holomorphic in an open subset $U \subset \mathbb{C}^{n+1}$ containing (t_0, z_0).

In the following, we only consider autonomous holomorphic ODEs because we are interested in the zero set of holomorphic functions. When such functions are used in the context of dynamical systems, this leads naturally to autonomous ODEs. Moreover, we consider t to be a real variable in the following sections (until Section 5.5), i.e., we restrict the solution of a holomorphic IVP] onto $U \cap \mathbb{R} \times \mathbb{C}^n$.)

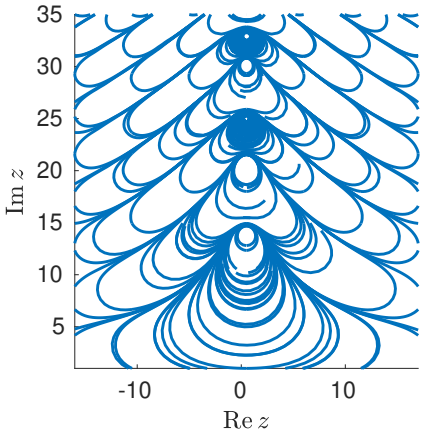

Figure 4.1: Holomorphic flow of $z' = \xi(z)$. Phase portrait is restricted to the rectangle $\{z \in \mathbb{C} : \operatorname{Re} z \in [-16, 17], \operatorname{Im} z \in [0, 35]\}$.

First, we consider the holomorphic flow of the Riemann ξ function $z' = \xi(z)$. For this differential equation no analytical solution formula is known. Figure 4.1 shows the phase portrait of the Riemann ξ function. The symmetry of the portrait with respect to the line $\operatorname{Re} z = 1/2$ is clearly evident and the optical confirmation of the

functional equation. All shown trajectories are periodic orbits which only differ in the encircled zero of the ξ function. There are some lines that separate the trajectories around a pair of "neighbored" equilibria (i.e., for a chosen equilibrium the other one has minimum distance of all other equilibria). These separating lines are subject of the following section.

4.2.1 Separatrices

When considering holomorphic flows, e.g. $z' = \cosh\left(z - \frac{1}{2}\right)$ (see Fig. 4.2), it becomes evident that there are special trajectories called *separatrices* which divide the whole bundle of trajectories into different regions of the same qualitative stability behavior. It appears evident that trajectories in the neighborhood bundle at these trajectories, i.e., locally the Euclidean distance between a trajectory and such a separatrix decreases. This makes the phase portrait look similar to slow invariant manifolds [HL18; LU16] (see Section 5.1). An introduction and short overview of these separatrices is given in this section that can be found in [HL19].

In Fig. 4.1, the phase portrait is full of periodic orbits around the Riemann zeros. Broughan defines the open set of periodic orbits around a specific Riemann zero to be a *band* [Bro05, Definition 5.1]. Towards the boundary of such bands, the density of trajectories seems to increase. The maximum bundling occurs at the boundary of these bands. More general, we can say that separatrices divide regions of distinct stability behavior of the phase space. By stability behavior, we mean that in such regions, all trajectories are for instance periodic orbits around the same center or converge to the same fixed point. However, an appropriate and precise mathematical definition of separatrices is a controversial topic (cf. [Bro03b], Section 2 for a brief overview of definitions). In the context of holomorphic flows, the following Definition 4.2 is reasonable and well suited in our context as we will see later.

Definition 4.2 (Separatrix [Bro03b])**.** A trajectory γ is a *positive* (*negative*) *separatrix* for the holomorphic flow (5.1) if for $z \in \gamma$, the maximum interval of existence of the path starting at z and following the holomorphic flow (5.1) in positive (negative) time is finite.

Although, this definition is not based on the separation of stability regions in the phase space, Broughan [Bro03a; Bro03b; BB04; Bro05] shows that the boundary

of these stability regions consists of trajectories with finite maximum interval of existence, and thus separatrices. To be more precise, he analyzes the phase portrait regions around centers, foci, nodes and elliptic sectors. He proves the boundaries of these regions to be the union of separatrices. Thus, the maximum interval of trajectories with initial point on such a boundary has to be finite.

More theory on separatrices and their characterization is presented in Chapter 5.

4.2.2 Holomorphic Flow of $\cosh(z - 1/2)$

It is challenging to investigate the holomorphic flow of the Riemann ξ function because the Riemann zeros are unknown and the definition of ξ is complicated. Numerical evaluation of the Riemann ξ function needs an efficient evaluation of (4.12) and (4.7). Because this calls for a further (numerical) analysis and might be a computationally intense job, we consider an approach to analyze holomorphic flows that are simpler but still closely related to ξ. In this section, we present a simplification of ξ that generates a phase portrait with periodic orbits around centers as well. Furthermore, there is an analytical connection between this simplification and ξ.

The next definition is used to specify what is meant by holomorphic flows that have "similar" phase portraits.

Definition 4.3 (Topologically equivalent flows [Per00, Definition 2, p. 183])**.** Let $f \in C^1(U_1, K^n)$ and $g \in C^1(U_2, K^n)$ be two continuously differentiable functions defined on two open sets $U_1, U_2 \subset K^n$ with $K = \mathbb{R}$ or $K = \mathbb{C}$. Then, two autonomous differential equations

$$z' = f(z) \tag{4.13}$$

and

$$z' = g(z) \tag{4.14}$$

are said to be *topologically equivalent* if there is a homeomorphism $H \colon U_1 \to U_2$ which maps trajectories of (4.13) to trajectories of (4.14) and preserves their orientation in time.

Now, let us take a closer look at $f(z) = \cosh(z - 1/2)$. Figure 4.2 illustrates the phase portrait of the cosh function. At first glance, the portrait is topologically

equivalent to the phase portrait of ξ. It consists of periodic solutions orbiting (infinitely many) zeros of cosh. The flow is analyzed in more detail later.

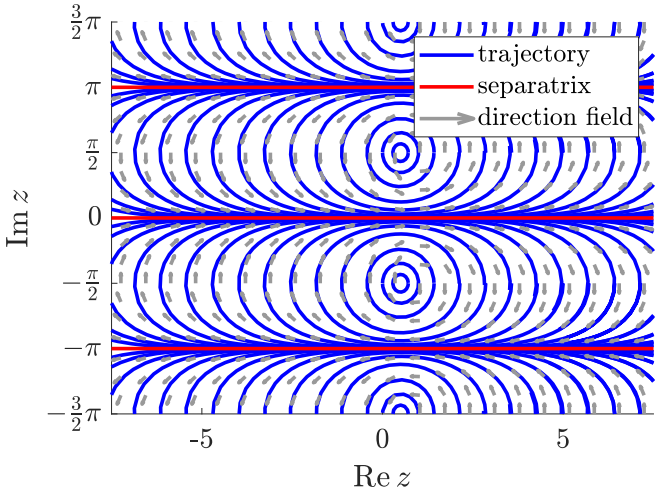

Figure 4.2: Holomorphic flow of $z' = \cosh(z - 1/2)$. "Ordinary" trajectories in blue, separatrix in red and direction field in gray, i.e., the normalized vector field. See [HL19].

Further, the cosh function satisfies the functional equation

$$f(z) = \cosh\left(z - \frac{1}{2}\right) = \cosh\left(-z + \frac{1}{2}\right) = \cosh\left(1 - z - \frac{1}{2}\right) = f(1 - z).$$

The last two aspects are necessary for a good "simplification" of ξ but do not point out whether f and ξ are connected via an analytic or algebraic equation. Riemann himself (cf. [Edw01] and[Rie59]) reveals that

$$\xi(z) = \int_1^\infty 4 \frac{\mathrm{d}\left[x^{3/2}\psi'(x)\right]}{\mathrm{d}x} x^{-1/4} \cosh\left(\frac{1}{2}\left(z - \frac{1}{2}\right)\log(x)\right) \mathrm{d}x,$$

where

$$\psi(x) = \sum_{n=1}^{\infty} e^{-n^2\pi x}.$$

Broughan shows in [Bro05, Theorem 6.1] that if a holomorphic function f defined in some open set $\Omega \subset \mathbb{C}$ transforms trajectories of $z' = \xi(z)$ to trajectories of

$z' = \cosh(z)$, then $f'(z)\xi(z) = \cosh\big(f(z)\big)$. The function f satisfies the third order differential equation

$$\xi f' f''' + \xi' f' f'' + \xi'' f'^2 = \xi f''^2 + \xi f'^4$$

and may be represented by

$$f(z) = \sinh^{-1} \tan \int_0^z \frac{1}{\xi(z)}\, \mathrm{d}z.$$

The next section shows the cosh function can even be "simplified" to generate a topologically equivalent flow if the cosh flow is restricted to two bands.

4.2.3 Holomorphic Flow of $z^2 + 1$

For the qualitative (topological) analysis of the holomorphic cosh flow, it suffices to analyze a (double) strip $S_n \coloneqq \big\{z \in \mathbb{C} \colon \mathrm{Im} z \in [2(n-1)\pi, 2n\pi)\big\}$ for an arbitrary $n \in \mathbb{N}$. This can even be simplified by the following observation. If $w' = w^2 + 1$ has a solution $w(t)$, then $\tilde{z}(t) \coloneqq \log w(t/2)$ satisfies the following ordinary differential equation:

$$\begin{aligned}
\tilde{z}'(t) &= \frac{1}{2}\frac{w'(t/2)}{w(t/2)} = \frac{1}{2}\frac{w^2(t/2)+1}{w(t/2)} = \frac{1}{2}\Big(w(t/2) + \big(w(t/2)\big)^{-1}\Big) \\
&= \frac{1}{2}\big(\exp(\log w(t/2)) + \exp(-\log w(t/2))\big) \\
&= \frac{1}{2}\Big(\exp\big(\tilde{z}(t)\big) + \exp\big(-\tilde{z}(t)\big)\Big) = \cosh\big(\tilde{z}(t)\big).
\end{aligned}$$

Consequently $z(t) = \frac{1}{2} + \tilde{z}(t)$ satisfies

$$z'(t) = \tilde{z}'(t) = \cosh\big(\tilde{z}(t)\big) = \cosh\left(z(t) - \frac{1}{2}\right).$$

Hence,

$$z(t) = \frac{1}{2} + \log\left(\tan\left(\frac{1}{2}(t+c)\right)\right), \quad c \in \mathbb{C}$$

is the general solution of the cosh flow and the period of $z(\cdot)$ is 2π independently from the initial value if $z(0) = z_0 \notin \mathbb{R} + 2k\pi\mathrm{i}$ for $k \in \mathbb{Z}$. If the initial value z_0 equals $\alpha + 2k\pi\mathrm{i}$ for $\alpha \in \mathbb{R}$ and $k \in \mathbb{Z}$, then the maximum interval of existence is finite, i.e.,

the corresponding trajectory is a separatrix.

The occurrence of the logarithm explains how infinitely many fixed points of cosh are related to only two zeros of z^2+1. Depending on the branches of the logarithm, the phase portrait of z^2+1 is transformed and "concatenated" where each branch differs by an imaginary part of $2k\pi\mathrm{i}$ in the sense that

$$\log(z) = \mathrm{Log}(z) + 2k\pi\mathrm{i} \quad \text{for a } k \in \mathbb{Z},$$

where Log is the main branch of the complex logarithm.

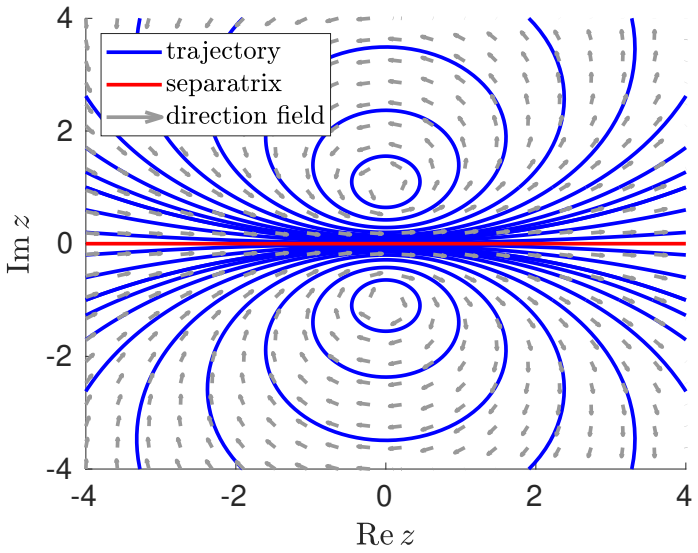

Figure 4.3: Holomorphic flow of $z' = z^2+1$ for $\mathrm{Re}\, z \in [-4,4]$ and $\mathrm{Im}\, z \in [-4,4]$. Trajectories for some chosen initial values are illustrated in blue. The separatrix dividing the upper plane $\mathrm{Im} z > 0$ from the lower one is depicted in red. See [HL19].

Figure 4.3 shows the phase portrait of $z' = f(z) = z^2+1$. The finite fixed points are given by $z = \mathrm{i}$ and $z = -\mathrm{i}$. Since $f'(\pm\mathrm{i}) = \pm 2\mathrm{i}$, these fixed points are centers. The plot in Fig. 4.3 indicates that all trajectories are periodic orbits encircling either $z = \mathrm{i}$ or $z = -\mathrm{i}$. There is one exception: the real axis is a trajectory but of course not periodic. The solution formula $z(t) = \tan(t+c)$ directly shows that the real axis is a separatrix. This separatrix is discussed in more detail in Chapter 5.

The analytical general solution of the flow

$$z' = z^2 + 1, \quad z(0) \coloneqq z_0 \in \mathbb{C},$$

is given by $z(t) = \tan(t+c)$, where the complex constant $c = c_1 + \mathrm{i}c_2 \in \mathbb{C}, c_1, c_2 \in \mathbb{R}$ fixes the initial value $z_0 = \tan(c)$. Splitting the tan function into real and imaginary part

$$\tan(t+c) = \tan(t + c_1 + \mathrm{i}c_2) = \frac{\sin(2t + 2c_1) + \mathrm{i}\sinh(2c_2)}{\cos(2t + 2c_1) + \cosh(2c_2)}$$

shows the π-periodicity of the trajectories if $c \notin \mathbb{R}$.

These trajectories are not only periodic orbits but circles in $\mathbb{R}^2$. To see this, we calculate the curvature (see Proposition 5.1) of a trajectory $z(t) = \tan(t+c)$ for an arbitrary constant $c = c_1 + \mathrm{i}c_2 \in \mathbb{C}$. Using the identity

$$\begin{aligned}\cosh^2(c_2) - \sin^2(t + c_1) &= \frac{1}{2}\Big(2\cosh^2(c_2) - 1 + 1 - 2\sin^2(t + c_1)\Big) \\ &= \frac{1}{2}\big(\cosh(2c_2) + \cos(2t + 2c_1)\big)\end{aligned}$$

the curvature is given by

$$\begin{aligned}\kappa\big(z(t)\big) &= \frac{|\mathrm{Im} f'\big(z(t)\big)|}{|f\big(z(t)\big)|} = \frac{|2\mathrm{Im} z(t)|}{|z^2(t) + 1|} = \frac{2|\mathrm{Im}\tan(t+c)|}{|\tan^2(t+c) + 1|} \\ &= |2\mathrm{Im} z(t)||\cos^2(t+c)| = |2\mathrm{Im} z(t)||\cos(t+c)|^2 \\ &= |2\mathrm{Im} z(t)|\Big(\cos^2(t + c_1)\cosh^2(c_2) + \sin^2(t + c_1)\sinh^2(c_2)\Big) \\ &= |2\mathrm{Im} z(t)|\Big(\cos^2(t + c_1)\cosh^2(c_2) + \sin^2(t + c_1)(\cosh^2(c_2) - 1)\Big) \\ &= |2\mathrm{Im} z(t)|\Big(\cosh^2(c_2) - \sin^2(t + c_1)\Big) \\ &= |2\mathrm{Im} z(t)|\frac{1}{2}\big(\cosh(2c_2) + \cos(2t + 2c_1)\big) \\ &= |\mathrm{Im}\tan(t+c)|\big(\cosh(2c_2) + \cos(2t + 2c_1)\big) \\ &= \frac{|\sinh(2c_2)|}{\cosh(2c_2) + \cos(2t + 2c_1)}\big(\cosh(2c_2) + \cos(2t + 2c_1)\big) = |\sinh(2c_2)|.\end{aligned}$$

Since all trajectories have a constant curvature they consist of circles (and a straight line if $c_2 = 0 \Leftrightarrow c \in \mathbb{R}$). In order to determine the radius and center of the circles, we choose the initial value $z_0 = a_0 + \mathrm{i}b_0 \in \mathbb{C}$ arbitrarily. The orbit circle through

$z_0 = z(0)$ evolves with respect to the time t as

$$z(t) = \frac{\sin(2t + 2c_1) + \mathrm{i}\sinh(2c_2)}{\cos(2t + 2c_1) + \cosh(2c_2)},$$

where $z_0 = \tan(c_1 + \mathrm{i}c_2)$.

In order the calculate the geometric center of the circles, we pick two pairs of points on each circle. We calculate the center of the circle using perpendicular bisectors of the segments connecting the pairs. The first two points are

$$a_0 + \mathrm{i}b_0 = z_0 = \tan(c) = \tan(c_1 + \mathrm{i}c_2) = \frac{\sin(2c_1) + \mathrm{i}\sinh(2c_2)}{\cos(2c_1) + \cosh(2c_2)}$$

and

$$z(-4c_1) = \frac{\sin(-2c_1) + \mathrm{i}\sinh(2c_2)}{\cos(-2c_1) + \cosh(2c_2)} = \frac{-\sin(2c_1) + \mathrm{i}\sinh(2c_2)}{\cos(2c_1) + \cosh(2c_2)}.$$

The perpendicular bisector of the segment from $z(0) = z_0$ to $z(-4c_1)$ is the imaginary axis $\mathrm{Re}z = 0$. The points

$$z(-c_1) = \mathrm{i}\frac{\sinh(2c_2)}{\cosh(2c_2) + 1}$$

and

$$z\left(\frac{\pi}{2} - c_1\right) = \mathrm{i}\frac{\sinh(2c_2)}{\cosh(2c_2) - 1}$$

are located on the imaginary axis as well. Thus, the center of the circle $z(\cdot)$ is given by

$$M(z_0) \coloneqq \frac{1}{2}\left(z(-c_1) + z\left(\frac{\pi}{2} - c_1\right)\right) = \mathrm{i}\coth(2c_2) = \mathrm{i}\frac{a_0^2 + b_0^2 + 1}{2b_0},$$

where the last equation holds because

$$\coth(2c_2) = \coth\left(2\,\mathrm{Im}\arctan(a_0 + \mathrm{i}b_0)\right) = \coth\left(\mathrm{artanh}\left(\frac{2b_0}{a_0^2 + b_0^2 + 1}\right)\right).$$

Since the radius of the reciprocal value of the curvature, we obtain

$$r(z_0) = \sqrt{\left(\frac{{a_0}^2 + {b_0}^2 + 1}{2b_0}\right)^2 - 1} = \sqrt{\coth(2c_2) - 1} = \frac{1}{|\sinh(2c_2)|}.$$

To sum up, the phase space of $z^2 + 1$ consists of circles that do not intersect and have their centers on the imaginary axis. The circles are not concentric and the bigger the absolute value of imaginary part of the geometric center of the circles at $M(z_0) = \mathrm{i}\frac{a_0^2+b_0^2+1}{2b_0}$ the larger is the radius.

4.3 Newton Flow

The flow of the holomorphic functions ξ, cosh and $z^2 + 1$ leads to periodic orbits around centers. However, we could benefit from a dynamical system where the trajectories directly converge to zeros of the corresponding right-hand side (flow generating vector field). One way to get such a system is to define a Newton flow that is a continuous version of Newton's method. In this section, we introduce and analyze Newton flows. Moreover, we point out how to overcome difficulties that go along with singularities in Newton flows.

Definition 4.4 (Newton Flow)**.** The *Newton Flow* for a holomorphic function $f\colon \Omega \to \mathbb{C}$ on an open set $\Omega \subset \mathbb{C}$ is defined by

$$z' = -\frac{f(z)}{f'(z)}, \quad z(0) = z_0. \tag{4.15}$$

In order for the flow to be well-defined, z_0 must not be a zero of the derivative of f. For the sake of brevity, the zero set of a function h is denoted by

$$\mathcal{Z}_h \coloneqq \big\{z \in \mathbb{C}\colon h(z) = 0\big\} = h^{-1}\big(\{0\}\big),$$

i.e., for the Newton flow $z_0 \notin \mathcal{Z}_{f'}$. In the following we consider $\Omega \coloneqq \mathbb{C} \setminus \mathcal{Z}_{f'}$.

Let $z(t)$ be a solution of the Newton flow. Then $f'(z)z' = -f(z)$. Since the left-hand side of this equation is the derivative of $f\big(z(t)\big)$ w.r.t. t, it holds

$$f\big(z(t)\big) = f(z_0)\mathrm{e}^{-t}. \tag{4.16}$$

If $z(t)$ exists for all $t \geq 0$, then (4.16) proves that $\lim\limits_{t\to\infty} f\big(z(t)\big) = 0$. Figure 4.4 illustrates the Newton flow for $f(z) = \cosh(z - 1/2)$. Most trajectories converge to a zero at $z_k = \frac{1}{2} + \frac{2k+1}{2}\pi\mathrm{i}$, $k \in \mathbb{Z}$. However, the trajectories $\mathrm{Im}z = k\pi$ for $k \in \mathbb{Z}$ are exceptions. Because they separate the phase space into the basins of attraction of the zeros z_k, they are named *separatrices* (see Definition 4.2).

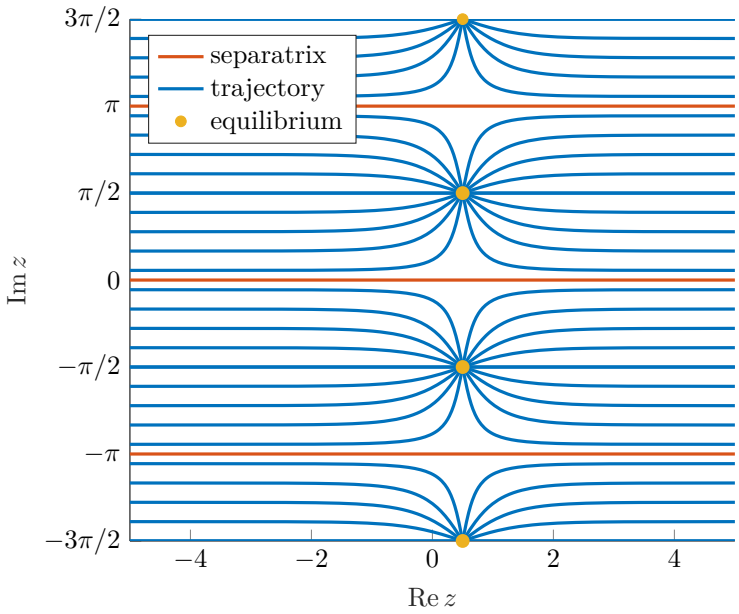

Figure 4.4: Newton flow of $z' = f(z) := \cosh(z - 1/2)$. Blue trajectories converge to a zero of f (yellow ball). Red lines are separatrices that divide the phase space into the basins of attraction of the zeros of f.

Equation (4.16) shows that the trajectory through z_0 preserves the phase/argument of f at z_0. Therefore, trajectories of the Newton flow are called *lines of constant phase*.

The next Proposition 4.5 shows in addition that essentially all lines of constant phase of f are Newton flow trajectories.

Proposition 4.5. *Let $\gamma\colon I \to \mathbb{C}$ be a complex differentiable, regular curve on the interval $I = [t_0, t_f] \subset \mathbb{R}$ with $t_0 < t_f$. Let $f\colon \mathbb{C} \to \mathbb{C}$ be a holomorphic function with $f \neq 0$. If γ is a line of constant phase for f, i.e.,*

$$\operatorname{Arg}\Big(f\big(\gamma(t)\big)\Big) = \operatorname{Arg}\Big(f\big(\gamma(t_0)\big)\Big) \quad \text{for all } t \in I,$$

and $f\big(\gamma(t)\big) \cdot f'\big(\gamma(t)\big) \neq 0$ for all $t \in I$, then there is a closed interval J and a parametrization $\phi\colon J \to I$ such that $\gamma \circ \phi$ is a solution of the Newton flow (4.15).

Proof. Let $f\colon \mathbb{C} \to \mathbb{C}$ be a holomorphic function and $\gamma\colon I \to \mathbb{C}$ a differentiable,

regular curve on the interval $I = [t_0, t_f]$ such that $\operatorname{Arg}\Big(f\big(\gamma(t)\big)\Big) \equiv \phi_0$ for a $\phi_0 \in (-\pi, \pi]$ and all $t \in I$.

Since

$$f\big(\gamma(t)\big) = \Big|f\big(\gamma(t)\big)\Big| \, \mathrm{e}^{\mathrm{i}\phi_0},$$

the expression

$$\frac{f\big(\gamma(t)\big)}{f\big(\gamma(t_0)\big)} = \frac{|f\big(\gamma(t)\big)|}{|f\big(\gamma(t_0)\big)|}$$

is positive for all $t \in I$. Thus, the function $\theta(t) \coloneqq -\log\Big(f\big(\gamma(t)\big)/f\big(\gamma(t_0)\big)\Big)$ with $\theta(t_0) = 0$ is well defined, differentiable and further

$$\theta'(t) = -\frac{f'\big(\gamma(t)\big)\gamma'(t)}{f\big(\gamma(t)\big)}.$$

It was assumed that $f\big(\gamma(t)\big) \cdot f'\big(\gamma(t)\big)$ does not vanish on I and γ is regular. Thus, the derivative $\theta'(t)$ does not become zero on I and θ is a bijective mapping from I onto its image $J \coloneqq \theta(I)$. If we define $\phi \coloneqq \theta^{-1}$, then $\hat{\gamma} = \gamma \circ \phi$ satisfies for $s = \phi^{-1}(t) = \theta(t)$

$$f\big(\hat{\gamma}(s)\big) = f\big(\gamma(t)\big) \overset{\text{Def of } \phi}{=} f\big(\gamma(t_0)\big)\mathrm{e}^{-\theta(t)} = f\big(\hat{\gamma}(0)\big)\mathrm{e}^{-s}.$$

Applying the chain rule on $f(\hat{\gamma})$ for the differentiable function $\hat{\gamma} = \gamma \circ \phi$ shows that $\hat{\gamma}$ is a trajectory of the Newton flow. □

Limit Behavior of Trajectories As seen before, trajectories with infinite maximum interval of existence converge to a zero of f. But what does the limit behavior of all other trajectories look like? For this purpose we define a finite ω-limit set and prove a proposition (Proposition 4.8) that answers this question.

Definition 4.6. Let $z(t)$ be a trajectory of a flow $z'(t) = g\big(z(t)\big)$ for a holomorphic function $g\colon \Omega \to \mathbb{C}$ with finite maximum interval of existence $I = (t_-, t_+)$, i.e., $t_+ < \infty$ and $z(0) = z_0$. We define the *finite-time ω-limit set* of z_0 to be

$$\omega_{t_+}(z_0) \coloneqq \left\{z \in \mathbb{C}\colon \exists\, t_n \nearrow t_+ \ (n \to \infty) \text{ such that } z(t_n) \to z \text{ as } n \to \infty\right\}.$$

The following Proposition 4.7 shows some topological properties of this finite-time ω-limit set.

Proposition 4.7. *Let $z(t)$ be a trajectory of the Newton flow* (4.15) *with finite maximum interval of existence $I = (t_-, t_+)$. Let $z(t)$ be bounded as $t \nearrow t_+$. Then $\omega_{t_+}(z_0)$ is closed, non-empty, compact and connected.*

Proof. The proof is analogous to the proof for the same properties of the ω-limit set. See e.g. [Tes04, Lemmata 6.6 and 6.7]. □

The next Proposition 4.8 shows that all bounded Newton flow trajectories "converge" to a zero of f or f' in forward-time.

Proposition 4.8 (cf. [WF18; JJT80])**.** *Let $z(\cdot)$ be a solution trajectory of the Newton flow* (4.15) *in $\Omega := \mathbb{C} \setminus \mathcal{Z}_{f'}$ with maximum interval of existence $I = (t_-, t_+)$. Then exactly one of the following statements is satisfied:*

(*a*) *$z(t)$ is unbounded as $t \to t_+$.*

(*b*) *There is a zero $z^* \in \mathcal{Z}_f$ such that $z(t) \to z^*$ as $t \to t_+ = \infty$.*

(*c*) *There is a zero $z^* \in \mathcal{Z}_{f'} \setminus \mathcal{Z}_f$ such that $z(t) \to z^*$ as $t \to t_+ < \infty$.*

Proof. The following proof is based on [WF18]. Another proof is given in [JJT80]. Jongen et al. even show that bounded Newton flow trajectories with $t_+ < \infty$ converge to a point $z^* \in \mathcal{Z}_{f'} \setminus \mathcal{Z}_f$. Let $z(t)$ be a bounded solution trajectory of the Newton flow (4.15) with maximum interval of existence $I = (t_-, t_+)$. If $t_+ = \infty$, we know from (4.16) that there is a strict Lyapunov function, i.e., a continuous function $V : \Omega \to \mathbb{R}$ such that $V\big(w(t)\big)$ is strictly decreasing for all non-constant solutions $w(t)$ of the Newton flow (4.15). This Lyapunov function is given by

$$V\big(w(t)\big) = \Big|f\big(w(t)\big)\Big| = \Big|f\big(w(0)\big)\Big|\,\mathrm{e}^{-t}.$$

Thus, the ω-limit set $\omega(z)$ is included in $\mathcal{Z}_f$. f has only isolated fixed points because it is a holomorphic function and $\omega(z)$ is connected. Thus $\omega(z) = z^*$ for a $z^* \in \mathcal{Z}_f$.

If $t_+ < \infty$, the theory of dynamical systems tells (see [PW10, Theorem 6.2.1]) that $\liminf_{t \to t_+} \operatorname{dist}(z(t), \partial\Omega) = \liminf_{t \to t_+} \operatorname{dist}(z(t), \mathcal{Z}_{f'}) = 0$. There is a sequence $(t_n)_{n \in \mathbb{N}}$ such that $t_n \nearrow t_+$ and $\lim_{n \to \infty} \inf_{z \in \mathcal{Z}_{f'}} |z(t_n) - z| = 0$. Since $z(t_n)$ is bounded, there is subsequence (t_{n_k}) such that $z(t_{n_k}) \to z^* \in \mathbb{C}$ for a $z^* \in \mathbb{C}$ as $k \to \infty$.

Next, we show that $z^* \in \mathcal{Z}_{f'}$: By definition of the infimum, there exist $z_k \in \mathcal{Z}_{f'}$ with

$$|z(t_{n_k}) - z_k| \leq \inf_{z \in \mathcal{Z}_{f'}} |z(t_{n_k}) - z| + \frac{1}{k} \to 0 \quad \text{as} \quad k \to \infty.$$

Consequently, $\lim_{k\to\infty} z_k = \lim_{k\to\infty} z(t_{n_k}) = z^*$. Since $\mathcal{Z}_{f'}$ is closed, $z^* \in \mathcal{Z}_{f'}$.

It remains to show, that $z(t)$ converges to $z^* \in \mathcal{Z}_{f'}$. Suppose now, there is another sequence $(s_k)_{k\in\mathbb{N}} \nearrow t_+$ and a zero $\tilde{z} \in \mathcal{Z}_{f'} \setminus \{z^*\}$ such that $z(t_k) \to \tilde{z}$ as $k \to \infty$. With Proposition 4.7 it follows that $\omega_{t_+}(z_0)$ is connected and includes z^* and $\tilde{z}$. Consequently, it includes an accumulation point $\hat{z} \in \omega_{t_+}(z_0)$. But $f'(\hat{z})$ has to be zero and by the identity theorem for holomorphic functions, f is constant which means $\Omega = \emptyset$. So, the assumption must be wrong and the statement follows. □

Corollary 4.9. *Every bounded separatrix of the Newton flow* (4.15) *converges to a zero of* f'.

Proposition 4.8 implies that bounded Newton flow trajectories which are complete (i..e, with infinite maximum interval of existence) converge to a zero of f. Moreover, the next Proposition 4.10 additionally shows that all simple zeros of f are asymptotically stable.

Proposition 4.10. *Let z^* be a simple zero of f, i.e., $z_0 \in \mathcal{Z}_f \setminus \mathcal{Z}'_f$. Then z^* is an asymptotically stable node.*

Proof. Let z^* be a simple zero of f. The derivative of $g(z) \coloneqq -\frac{f(z)}{f'(z)}$ at $z = z^*$ is given by

$$g'(z^*) = -\frac{\big(f'(z^*)\big)^2 - f(z^*)f''(z^*)}{\big(f'(z^*)\big)^2} = -1.$$

If regarded in $\mathbb{R}^2$, the Cauchy-Riemann differential equations yield

$$J_g(z^*) = \begin{pmatrix} -1 & 0 \\ 0 & -1 \end{pmatrix}.$$

Thus, z^* is an asymptotically stable node. □

Behavior Near Zero of f' So far it was shown that bounded incomplete trajectories (i.e., trajectories with finite maximum interval of existence) converge to a

zero of f'. In this paragraph, the behavior of the flow near a simple zero of f' is analyzed in more detail.

First, we start by citing a theorem of Broughan, which characterizes the holomorphic flow near a simple pole of the right-hand side to be qualitatively the same as the flow near a saddle.

Theorem 4.11 (Theorem 2.2 in [Bro03a])**.** *If $f\colon \Omega \to \mathbb{C}$ has a simple pole in the open set $\Omega \subset \mathbb{C}$ at $z = a \in \Omega$ then, for some $\varepsilon > 0$, the flow of $z' = f(z)$ has the same orbits in $U_\varepsilon(a) \setminus \{a\}$ as a saddle.*

Proposition 4.12. *Let $z(t)$ be a trajectory with finite maximum interval of existence $I = (t_-, t_+)$ that is bounded as $t \nearrow t_+$. According to Proposition 4.8 $z(t)$ converges to a $z^* \in \mathcal{Z}_{f'}$. If $z^* \in \mathcal{Z}_{f'} \setminus \big(\mathcal{Z}_f \cup \mathcal{Z}_{f''}\big)$, then there is an $\varepsilon > 0$ such that the Newton flow* (4.15) *has the same orbits in $U_\varepsilon(z^*) \setminus \{z^*\}$ as a saddle.*

Proof. W.l.o.g. let $z^* = 0$. Laurent series expansion of f and f' show that $-\frac{f(z)}{f'(z)}$ has a pole at 0 with residue $-\frac{f(0)}{f''(0)} \neq 0$. The claims follows finally with Theorem 4.11. □

Although the plots of Fig. 4.2 and its analogies to the theory of slow invariant manifolds might suggest that the bundling behavior of separatrices in forward or backward time is accompanied by time scale separation, this is not the case.

Proposition 4.13. *There is no time scale separation in the flow of holomorphic functions. To be more precise, if λ_1 and λ_2 are the eigenvalues of the Jacobian of f in $\mathbb{R}^2$, then*

$$\frac{\mathrm{Re}(\lambda_2)}{\mathrm{Re}(\lambda_1)} = 1,$$

if $\mathrm{Re}(\lambda_1) \neq 0$.

Proof. Let $f(z) = f(x + iy) = u(x, y) + \mathrm{i}v(x, y)$ be a holomorphic function. If transformed to $\mathbb{R}^2$, the derivative of f is the Jacobian

$$J_f(x, y) = \begin{pmatrix} u_x(x, y) & u_y(x, y) \\ v_x(x, y) & v_y(x, y) \end{pmatrix} = \begin{pmatrix} u_x(x, y) & u_y(x, y) \\ -u_y(x, y) & u_x(x, y) \end{pmatrix}$$

because of the Cauchy-Riemann equations. Its eigenvalues are $\lambda_{1,2} = u_x(x, y) \pm \mathrm{i}u_y(x, y)$. □

The three following examples illustrate the previously described characteristics and properties of Newton flows.

4.3.1 Newton Flow of $z^2 + 1$

The most basic example presented for the Newton flow of holomorphic functions with phase portraits related to the ξ Newton flow is $f\colon \Omega \to \mathbb{C}, z \mapsto f(z) = z^2 + 1$. Its Newton flow is given by the differential equation

$$z' = -\frac{z^2 + 1}{2z}, \quad z(0) = z_0.$$

The only zero of $f'(z) = 2z$ is located at $z = 0$. Thus, $\mathcal{Z}_{f'} = \{0\}$ and $\Omega = \mathbb{C} \setminus \{0\}$. Using (4.16), we obtain the solution of this ODE by

$$z(t) = \pm\sqrt{(z_0^2 + 1)\mathrm{e}^{-t} - 1}. \tag{4.17}$$

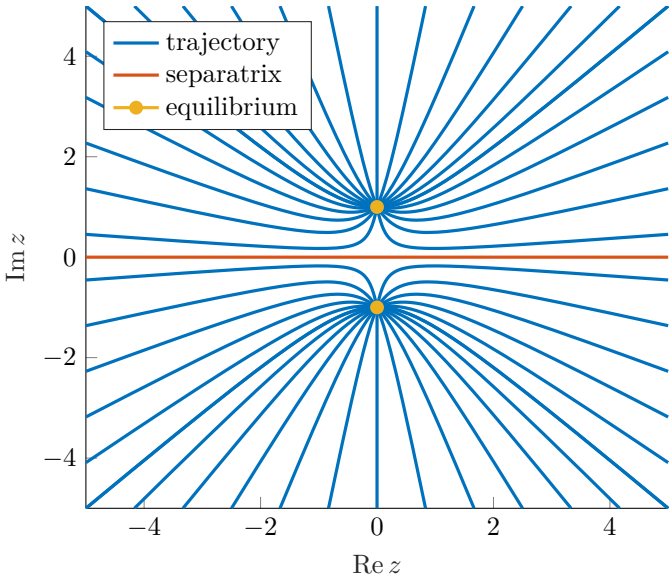

Figure 4.5: Newton flow of $z' = z^2 + 1$. Blue trajectories converge either to $z = \mathrm{i}$ or $z = -\mathrm{i}$. Red separatrix divides the basins of attraction of $z = \pm\mathrm{i}$.

In Fig. 4.5, several trajectories of the phase space are depicted. All plotted trajectories except for the real axis converge to a zero of $f(z)$, i.e., to $z = \pm\mathrm{i}$. Trajectories

with real valued initial values (i.e. separatrices) converge in finite time to the origin which is the simple zero of $f'(z)$. There are no unbounded solutions in forward time as (4.17) shows. The phase space near $z = 0$ looks indeed like a saddle point.

4.3.2 Newton Flow of cosh

The Newton flow of $f\colon \Omega \to \mathbb{C}, z \mapsto f(z) = \cosh(z - 1/2)$ is given by

$$z' = -\coth(z - 1/2), \quad z(0) = z_0.$$

The zeros of $f'(z) = \sinh(z - 1/2) = \sinh(x - 1/2 + \mathrm{i}y) = \sinh(x - 1/2)\cos(y) + \mathrm{i}\cosh(x - 1/2)\sin(y)$ are located at $z = 1/2 + k\pi\mathrm{i}$ for $k \in \mathbb{Z}$. Thus, $\mathcal{Z}_{f'} = \bigcup_{k\in\mathbb{Z}} \{1/2 + k\pi\mathrm{i}\}$ and $\Omega = \mathbb{C} \setminus \bigcup_{k\in\mathbb{Z}} \{1/2 + k\pi\mathrm{i}\}$.

Using (4.16), we obtain the solution of this ODE:

$$\begin{aligned} z(t) &= \frac{1}{2} + \operatorname{arcosh}\left(\cosh(z_0 - 1/2)\mathrm{e}^{-t}\right) \\ &= \frac{1}{2} + \log\left(\cosh(z_0 - 1/2)\mathrm{e}^{-t} + \sqrt{\cosh^2(z_0 - 1/2)\mathrm{e}^{-2t} - 1}\right). \end{aligned} \tag{4.18}$$

In Fig. 4.4, several trajectories of the phase space are depicted. All plotted trajectories except for the straight lines $S_k \coloneqq \{z \in \mathbb{C}\colon \operatorname{Im} z = k\pi, \text{ for a } \in \mathbb{Z}\}$ converge to a zero of $f(z)$, i.e., to $z = \frac{1}{2} + \frac{2k+1}{2}\pi\mathrm{i}$. The separatrices S_k each converge to $1/2 + k\pi\mathrm{i}$ for a $k \in \mathbb{Z}$, which are simple zeros of $f'(z)$. There are no unbounded solutions as (4.18) demonstrates. The phase space behavior near the zeros of $f'(z)$ is again homeomorphic to that of a saddle point.

4.3.3 Newton Flow of ξ

For the Newton flow of the Riemann ξ function no analytical solution is known. This makes it difficult to determine the open region $\Omega \approx \mathbb{C} \setminus \mathcal{Z}_{f'}$, where the Newton flow of ξ is well defined. An overview on numerical methods for the evaluation of ξ and the calculation of ξ zeros is given by Gourdon and Sebah [GS03]. Among others, Odlyzko [Odl19] calculates the first $10^5\xi$ zeros with high numerical precision. The first zeros are located approximately at $\rho_1 \approx 14.135$, $\rho_2 \approx 21.022$, $\rho_3 \approx 25.011$, $\rho_4 \approx 30.425$ and $\rho_5 \approx 32.935$.

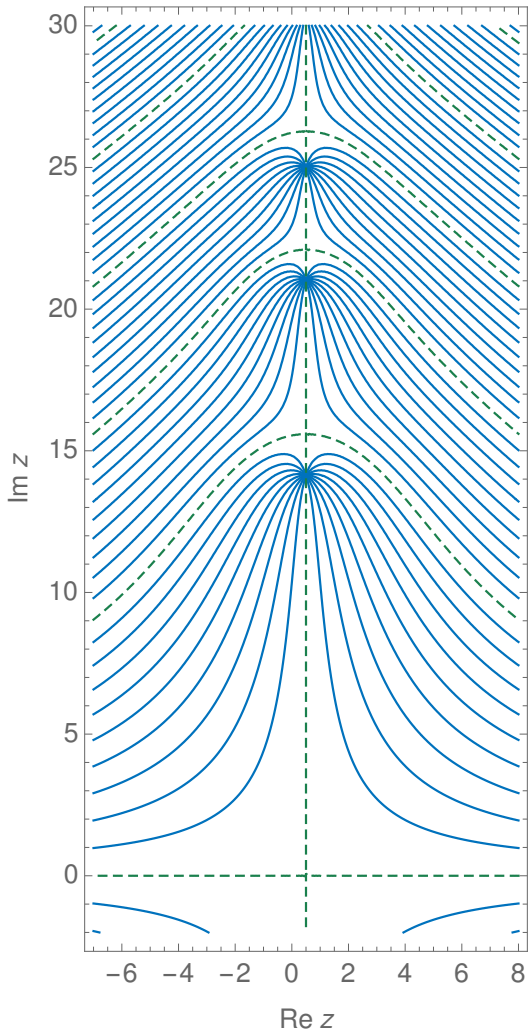

Figure 4.6: Newton flow of ξ function. Several lines of constant phase are depicted in blue. The green, dashed lines are the lines where ξ is real valued. In [Ari03] those lines are called x-rays. Modified from [HL19].

Equation (4.16) shows that Newton flow trajectories are lines of constant phase. Several phases are depicted in Fig. 4.6. All trajectories in the plotted domain are bounded in forward time. Trajectories with an initial value z_0 such that $f(z_0) \in \mathbb{R}$ are colored in green. The green lines which are not on the axis $\operatorname{Re} z = 1/2$ divide the attraction regions of the first non-trivial Riemann zeros and seem to be the separatrices. As it is not clear how to determine the maximum interval of existence

for these lines, we cannot prove them to be separatrices in the sense of Definition 4.2.

The green line $\operatorname{Re} z = 1/2$ crosses the other green lines. As seen before, bounded trajectories of the Newton flow converge to a zero of ξ or ξ' (see Corollary 4.9). Since regular trajectories cannot intersect, the intersection points of the green lines have to be zeros of ξ'. The saddle-point behavior of the trajectories at these intersection points supports this fact. The following Proposition 4.14 and Corollary 4.15 show that the ξ function is real on the critical axis. Hence, a pair of Riemann ξ zeros on the critical axis implies a zero of ξ' on the critical axis between them.

Proposition 4.14. *Let $f\colon \mathbb{C} \to \mathbb{C}$ be a holomorphic function. Then $g(z) \coloneqq \overline{f(\overline{z})}$ is a holomorphic function and $f = g$ if and only if $f(\mathbb{R}) \subset \mathbb{R}$.*

Proof. The Cauchy-Riemann equations for f directly imply the validity of the Cauchy-Riemann equations for g. Thus, g is a holomorphic function. If $f = g$, then it holds

$$f(x) = g(x) = \overline{f(\overline{x})} = \overline{f(x)} \quad \Rightarrow\ f(x) \in \mathbb{R}, \quad \text{for all } x \in \mathbb{R}.$$

Otherwise let $f(\mathbb{R}) \subset \mathbb{R}$. Then f and g coincide on all $x \in \mathbb{R}$. The identity theorem for holomorphic functions implies that $f = g$. □

Corollary 4.15. *The Riemann ξ function is real valued on the critical axis* $\operatorname{Re} z = \frac{1}{2}$.

Proof. It is easy to see that $\xi(\mathbb{R}) \subset \mathbb{R}$. According to Proposition 4.14 $\xi(z) = \overline{\xi(\overline{z})}$. Thus it holds

$$\xi(1/2 + \mathrm{i}t) = \xi\big(1 - (1/2 - \mathrm{i}t)\big) = \xi(1/2 - \mathrm{i}t) = \xi(\overline{1/2 + \mathrm{i}t}) = \overline{\xi(1/2 + \mathrm{i}t)}.$$

□

4.3.4 Desingularizing the Newton Flow

The main goal of this section is to prevent singular behavior at roots of f' by replacing with a new root of f (actually by transformation of the right-hand side f such that new function has more roots than f). The challenging part is to preserve all trajectories but those converging to a root of f'. If successful, trajectories

converging to a zero of f' afterwards have *infinite* maximum interval of existence and thus are no longer separatrices in the sense of Definition 4.2.

Jongen, Jonker and Twilt [JJT80; JJT88] suggest a desingularization for the Newton flow of meromorphic functions. The desingularized Newton flow is given by:

$$z' = -(1 + |f(z)|^4)^{-1} f(z)\overline{f'(z)}. \tag{4.19}$$

Since the right-hand side of (4.19) differs from the right-hand side of the corresponding Newton flow (4.15) only by a factor of a real number $\alpha(z) \in \mathbb{R}$ depending on $z \in \Omega$, the Newton flow trajectories are desingularized Newton flow trajectories as well. So the phase portrait does not change while the time parametrization of the solution curves varies in general.

Lemma 4.16 (Desingularization Lemma [JJT88])**.** *For each nonconstant meromorphic function f, a real analytic vector field $\bar{\mathcal{N}}(f)$ exists, defined on whole $\mathbb{C}$, with the properties:*

(1) *Trajectories for the Newton flow $\mathcal{N}(f) = -\frac{f(z)}{f'(z)}$ are also trajectories for $\bar{\mathcal{N}}(f)$.*

(2) *A critical point for f is an equilibrium for $\bar{\mathcal{N}}(f)$.*

(3) $\bar{\mathcal{N}}(f) = -\bar{\mathcal{N}}(1/f)$.

Proof. See [JJT88]. □

Benzinger [Ben91] studies plane autonomous systems with rational vector fields, i.e., ODEs of the form $z' = R(z) = p(z)/q(z)$, where R is any rational function in the complex plane. His main novelty is to represent this dynamical system as a Newton flow

$$z' = R(z) = -\frac{f(z)}{f'(z)},$$

for a function f which can be written as

$$f(z) = C\mathrm{e}^{P_0(z)} \prod_{j=1}^{J} (z - z_j)^{A_j} \mathrm{e}^{P_j\left(1/(z-z_j)\right)},$$

with polynomials $P_0, \ldots, P_J$ and complex constants C and $A_1, \ldots, A_J$ such that $P_j(0) = 0$ for all $j = 1, \ldots, J$.

This Newton flow representation is used by Benzinger to analyze the long-term behavior of the dynamical system using the Riemann sphere. Desingularization of

the Newton flow as well as orthogonal vector fields (closely related to imaginary and complex time; see Section 5.5) are basic concepts for proving his statements.

In the following, we use the transformation (4.19) neglecting the real factor $(1+|f(z)|^4)^{-1}$:

$$z' = -\overline{f'(z)}f(z). \tag{4.20}$$

In both the systems (4.19) and (4.20), it is obvious that all zeros of f' turn into critical points. Since equilibria cannot be reached in finite time (otherwise one could leave them in reverse time) and the phase portrait is conserved, all bounded trajectories have infinite maximum interval of existence. We will make use of this fact in Section 5.3 and particularly in Subsection 5.3.5.

The following example demonstrates the desingularization of the cosh flow.

Example 4.17 (Desingularized cosh Flow)**.** For the Newton flow of $f(z) = \cosh(z - 1/2)$ it holds

$$f(z) = -\coth(z-1/2) = -\coth(x-1/2+\mathrm{i}y) = -\frac{\sinh(2x-1)-\mathrm{i}\sin(2y)}{\cosh(2x-1)-\cos(2y)}$$

Its desingularized flow is given by

$$\begin{aligned} z' &= -\overline{\sinh(z-1/2)}\cosh(z-1/2) \\ &= -\big(\sinh(x-1/2)\cos(y) - \mathrm{i}\cosh(x-1/2)\sin(y)\big) \\ &\quad \cdot \big(\cosh(x-1/2)\cos(y) + \mathrm{i}\sinh(x-1/2)\sin(y)\big) \\ &= -\sinh(x-1/2)\cosh(x-1/2) + \mathrm{i}\sin(y)\cos(y) \\ &= -\frac{1}{2}\sinh(2x-1) + \mathrm{i}\frac{1}{2}\sin(2y). \end{aligned}$$

Obviously, the (former) separatrices $y = k\pi$ for $k \in \mathbb{Z}$ converge to the equilibria $z = 1/2 + k\pi$.

To conclude this section, we show an analogous result to (4.16).

Proposition 4.18. *Let $z(t)$ be the solution of the desingularized Newton flow for a holomorphic function $f\colon \Omega \to \mathbb{C}$. Then it holds*

$$f\big(z(t)\big) = f\big(z(0)\big)\exp\left(-\int_0^t \left|f'\big(z(\tau)\big)\right|^2 \mathrm{d}\tau\right).$$

Proof. Differentiation of $f\big(z(t)\big)$ w.r.t. t yields

$$f'\big(z(t)\big)z'(t) = -\left|f'\big(z(t)\big)\right|^2 f\big(z(t)\big).$$

This implies the desired result. □

Hence, Proposition 4.18 indicates how the time t in the solution curve of a Newton flow $z(t)$ changes when the Newton flow becomes desingularized.

5 Characterization of Separatrices

In Chapter 4, we introduced one-dimensional complex autonomous dynamical systems

$$z' = \frac{\mathrm{d}z}{\mathrm{d}t} = f(z), \quad z(0) = z_0 \in \mathbb{C}, \tag{5.1}$$

where $f : \mathbb{C} \to \mathbb{C}$ is a holomorphic function. Examining the phase space of these systems, specific structures called separatrices (for a definition see Section 4.2.1) turned out to be geometrically accompanied by a bundling of trajectories in the sense that the distance between two trajectories becomes small near separatrices. We have already observed a similar behavior for slow invariant manifolds in the context of real, multi-scale systems. Thus, the first aim of this chapter is to apply manifold approximation methods on separatrices to find characteristics of separatrices.

We then move on to search for other characterizations of separatrices. For the holomorphic flows (5.1) many studies have been performed, e.g. see [Bro03a; Bro03b; BB04; Bro05] and for corresponding Newton flows, e.g., see [Neu+14; Sch+18]

$$z' = -\frac{f(z)}{f'(z)}, \quad z(0) = z_0 \in \mathbb{C},$$

also and in particular in a context where $f(z)$ is number-theoretically significant like the Riemann $\zeta(z)$- or $\xi(z)$-functions. A brief introduction of the ζ and ξ functions is given in Chapter 4. The recent work of Schleich et al. [Sch+18] suggests that the behavior of Newton flow separatrices at infinity provides us with information about the exact location of the equilibria of holomorphic flows. In the case of the Riemann ξ functions these zeros are the non-trivial zeroes of $\xi(z)$. Thus, the study of separatrices at infinity might represent an important step toward the Riemann hypothesis.

It is the intention of this chapter to characterize separatrices (at infinity and in the complex plane) using geometric and topological characteristics. As already mentioned, we first study slow invariant manifold techniques in the context of

holomorphic dynamical systems. Afterwards, we investigate separatrices at infinity. We show that equilibria of polynomial holomorphic flows at infinity have at least an incoming or outgoing separatrix. Moreover, we reveal the utility of Lyapunov exponents for the identification of separatrices, in particular for the desingularized Newton flow. For separatrices between two center fixed points, the winding number of periodic orbits is shown to change its sign at the separatrix. Hence, this is a topological property that characterizes separatrices in specific circumstances. At the end of this chapter, complex time reveals new possibilities for a separatrix characterization. Sections 5.2, 5.4 and 5.5 can be found in [HL19] or are modifications of it.

5.1 Numerical Separatrix Approximation with SIM Methods

When the phase space of multiple time scale dynamical systems and holomorphic flows is considered, a common feature of separatrices and slow invariant manifolds is the bundling behavior of nearby solution trajectories (cf. Chapter 1). Although holomorphic flows do not have multiple time scales (see Proposition 4.13), this section applies numerical approximation methods for the SIM to holomorphic dynamical systems. The idea behind is that many SIM approximation techniques are designed to exploit geometric characteristics of trajectories like curvature, attraction of nearby trajectories (and thus bundling behavior), and invariance. The aim of this section is to get a deeper insight and understanding of properties that are characteristic for separatrices. The research of this section is of experimental nature. We discuss the utility of several manifold approximation techniques for the separatrix characterization.

A basic concept of many SIM approximation methods is *curvature*. Thus, we begin by expressing the concept of curvature of curves in the context of holomorphic dynamical systems.

Proposition 5.1. *Let $z(t) \notin \mathcal{Z}_f$ be the solution of the holomorphic ODE $z'(t) = f\big(z(t)\big)$. Then the curvature κ of the solution curve $z(t)$ at time t is given by*

$$\kappa\big(z(t)\big) = \frac{|\mathrm{Im} f'\big(z(t)\big)|}{|f\big(z(t)\big)|}.$$

Proof. Using the 2-D curvature formula

$$\kappa = \frac{\left|\det \begin{pmatrix} x' & x'' \\ y' & y'' \end{pmatrix}\right|}{\left\|(x', y')^{\mathsf{T}}\right\|^3}$$

and the $\mathbb{R}^2$-identification $f(z) = u(x, y) + \mathrm{i}v(x, y)$ gives the expected formula. See also [Bro03a]. □

In the following subsections, we apply methods developed for the SIM approximation to holomorphic flows. The application on Newton flows is analyzed in the bachelor thesis of André Mayer [May18]. Hence, we only consider the holomorphic $z^2 + 1$, cosh and ξ flows as examples but not their corresponding Newton flows. Although, Newton and holomorphic flows are in general different concerning stability properties, the results of [May18] are similar to what follows.

5.1.1 Flow Curvature Method

The Flow Curvature Method (FCM) introduced in Section 2.4.2 is based on higher curvatures of solution trajectories. In real space $\mathbb{R}^n$, the flow curvature manifold is given by the set of points $z \in \mathbb{R}^n$ satisfying the equation

$$\Phi_{\text{FCM}}(z) \coloneqq \det\Big(z'(t), z''(t), \ldots, z^{(n)}(t)\Big) = 0.$$

For a two-dimensional system of ODEs the function $\Phi_{\text{FCM}}(z)$ vanishes if and only if either z' or the curvature

$$\kappa = \frac{\Phi_{\text{FCM}}(z)}{\left\|z'(t)\right\|^{\frac{3}{2}}}$$

of a solution trajectory of $z'(t) = f\big(z(t)\big)$ vanishes. In the context of one-dimensional complex dynamics, Proposition 5.1 shows that the curvature of the solution curves equals 0 if and only if the derivative $f'\big(z(t)\big)$ is real along the solution $z(t)$. Thus, for 1-D holomorphic flows, the FCM is the zero set of $\operatorname{Im} f'(z)$. We do not consider the fixed points of the flow, i.e., the points where z' vanishes as part of the FCM.

Example 5.2 (FCM for $z^2 + 1$)**.** For the holomorphic flow of $f(z) = z^2 + 1$, the

derivative $f'(z) = 2z$ is real if and only if $z \in \mathbb{R}$. Thus, the FCM approximation is the real axis and coincides with the separatrix exactly. At second glance, this corresponds exactly to the results of Section 4.2.3: We have shown that all trajectories regarded as 2-D curves have constant curvature. While the real axis has zero curvature, all other trajectories are circles (with positive absolute curvature).

Example 5.3 (FCM for cosh)**.** In case of $f(z) = \cosh(z - 1/2)$, a short calculation yields

$$\begin{aligned} f'(z) &= \sinh\left(z - \frac{1}{2}\right) = \sinh\left(x - \frac{1}{2} + \mathrm{i}y\right) \\ &= \sinh\left(x - \frac{1}{2}\right)\cos(y) + \mathrm{i}\cosh\left(x - \frac{1}{2}\right)\sin(y). \end{aligned}$$

Thus, the FCM solution set is given by

$$\left\{z \in \Omega = \mathbb{C} \setminus \mathcal{Z}_f \colon \sin(y) = 0\right\} = \left\{z \in \Omega = \mathbb{C} \setminus \mathcal{Z}_f \colon \operatorname{Im} z = k\pi,\ k \in \mathbb{Z}\right\}.$$

As already seen for $z^2 + 1$, FCM is an exact criterion for the separatrix in these two examples because the separatrix is the only trajectory without curvature.

Example 5.4 (FCM for ξ)**.** For the holomorphic flow of ξ, no analytic representation for the FCM is known, because ξ' is not easily evaluable. A numerical approximation of the FCM calculated by Mathematica is depicted in Fig. 5.1. Although the FCM differ from the separatrices, the FCM lines seem to capture the essence of the separatrices. However, the ξ flow lines and the FCM lines "intersect" near $z = 1/2 + 22\mathrm{i}$. Zooming into the Mathematica solution reveals numerical inaccuracy near the critical line $\operatorname{Re} z = 1/2$.

5.1.2 Zero Derivative Principle

We briefly recall the Zero-Derivative-Principle (ZDP) introduced in Section 2.4.1. First, the set of variables $z = (z_1, z_2)^\mathsf{T} = (x, y)^\mathsf{T}$ is divided into the set of reaction progress variables RPV $\subset \{1, 2\}$. In this case, it only will make sense to choose exactly one reaction progress variable. The remaining indices are stored in the set nRPV $= \{1, 2\} \setminus$ RPV. Let I be an index set (e.g., $I =$ RPV or $I =$ nRPV). By z_I, we denote

$$z_I \coloneqq \{z_i \colon i \in I\}.$$

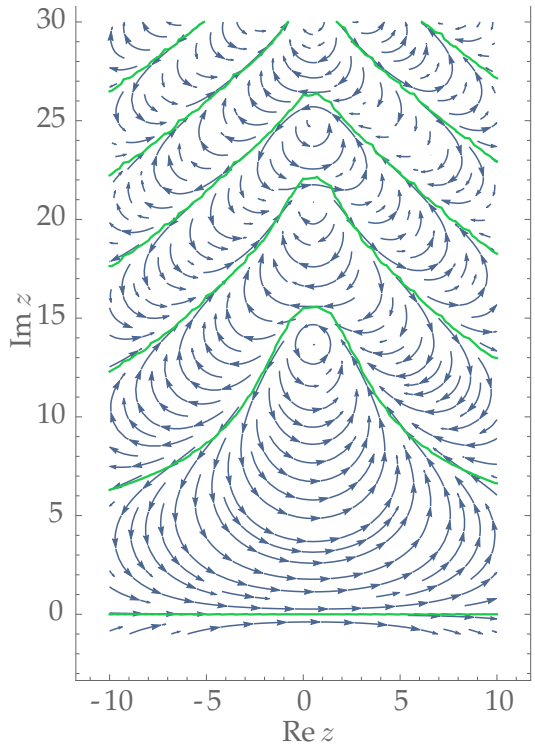

Figure 5.1: Flow lines for holomorphic ξ flow calculated by Mathematica. The green line is a numerical approximation of the line where ξ' is real.

For a fixed number $m \in \mathbb{N}$ (that determines the order of SIM approximation in case of slow-fast systems; cf. Section 2.4.1), we solve the following equation with respect to the reaction progress variables:

$$\frac{\mathrm{d}^m}{\mathrm{d}t^m} z_{\mathrm{nRPV}}(t) = 0, \quad \text{for a } m \in \mathbb{N}.$$

The RPV choice is a-priori not clear because there is no time scale separation (see Proposition 4.13) in holomorphic flows. As elucidated in Section 2.4.1, the choice of RPVs only affects the order of approximation for slow-fast systems. Thus, we compute and compare all possible choices for RPVs.

For 1-D holomorphic flows, we can choose either $z_{\mathrm{RPV}} = x$ or $z_{\mathrm{RPV}} = y$. If using the first order ZDP, i.e. $m = 1$, this methods results in the sets Im $f(z) = 0$ and Re $f(z) = 0$. Thus it determines where the vector field is purely imaginary resp. real. This corresponds to the x-rays of f (see [Ari03]). We test $m = 2$ as well and

use the same examples as for the FCM tests. Higher orders $m > 2$ are omitted because calculations become more difficult and the outcome does not change in nature.

Example 5.5 (ZDP for $z^2 + 1$)**.** For $m = 1$, the ZDP approach yields

$$\begin{aligned} x' = u = \mathrm{Re} f(z) = 0 \Leftrightarrow x^2 - y^2 + 1 = 0 \\ y' = v = \mathrm{Im} f(z) = 0 \Leftrightarrow 2xy = 0 \end{aligned}$$

Thus in the first case, the ZDP gives a hyperbola and in the second case both, the real and imaginary axis. The approximation resulting from $y' = 0$ with RPV x is better suited in this case because it contains the analytical separatrix.

If $m = 2$ is used for the ZDP order, we get

$$\begin{aligned} x'' = (D_x u)u + (D_y u)v = 0 \Leftrightarrow 2x(x^2 - 3y^2 + 1) = 0 \\ y'' = (D_x v)u + (D_y v)v = 0 \Leftrightarrow 2y(3x^2 - y^2 + 1) = 0. \end{aligned}$$

Hence, the ZDP calculates the hyperbola $x^2 - 3y^2 + 1 = 0$ and the imaginary axis if y is chosen as RPV. For x as RPV we obtain the hyperbola $3x^2 - y^2 + 1 = 0$ and the real axis. Since the separatrix is the real axis $y = 0$, the ZDP only contains the separatrix (for $m = 1$ and $m = 2$), if x is chosen as RPV. It calculates more lines than just the separatrix (imaginary axis resp. a hyperbola). This requires additional conditions or assumptions in order to filter the separatrix out of the ZDP approximation.

Example 5.6 (ZDP for cosh)**.** For

$$\begin{aligned} f(z) &= \cosh(z - 1/2) = \cosh(x - 1/2)\cos(y) + \mathrm{i}\sinh(x - 1/2)\sin(y) \\ &= u(x, y) + \mathrm{i}v(x, y), \end{aligned}$$

the ZDP results for $m = 1$ in the sets $\left\{z \in \mathbb{C} \colon \mathrm{Im}\ z = \frac{2k+1}{2}\pi,\ k \in \mathbb{Z}\right\}$ using x as RPV resp. $\left\{z \in \mathbb{C} \colon \mathrm{Re}\ z = \frac{1}{2} \text{ or } \mathrm{Im}\ z = k\pi,\ k \in \mathbb{Z}\right\}$ using y as RPV.

We omit the calculations for $m = 2$ but want to point out that the separatrices are included in the ZDP solutions with x as RPV.

Example 5.7 (ZDP for ξ)**.** In Fig. 5.2, the ZDP solution sets for $m = 1$ are illustrated. The green line corresponds to y as RPV. The orange line corresponds to x as

RPV. Figure 5.2 clearly shows that both approximations do not coincide with the separatrices which are located in between the green and orange line (in the shown compact set for z).

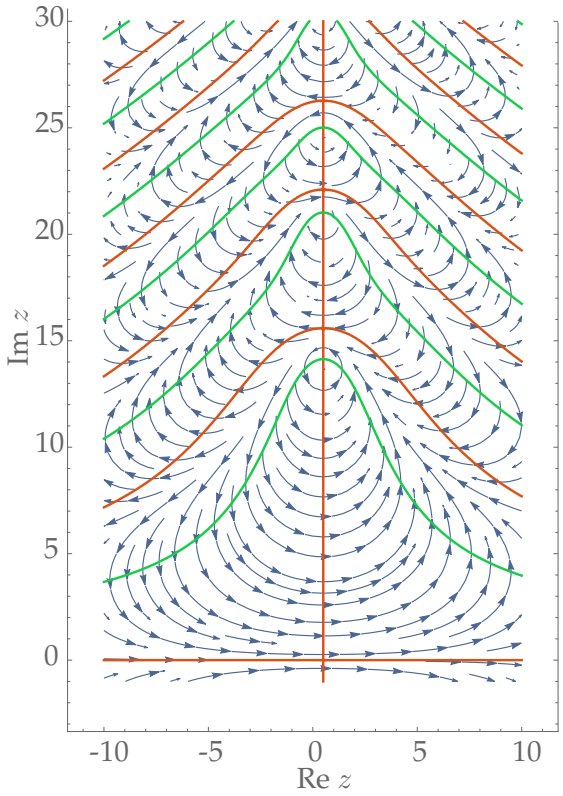

Figure 5.2: Flow lines for holomorphic ξ flow calculated by Mathematica. On the orange line f attains real values and on the green line imaginary values. Separatrices are in between the orange and green curves for this compact subset $[-10, 10] \times [-1, 30] \ni z$.

5.1.3 Trajectory-Based Optimization Approach

We apply the Trajectory-Based Optimization Approach (TBOA) introduced in Section 2.4.3 to holomorphic and Newton flows. To calculate non-reaction progress variables for fixed values z^*_{RPV}, the TBOA solves the following variational problem (in backward mode):

$$\begin{aligned} \min_{z(\cdot)} \quad & \psi(z) \coloneqq \left\|\ddot{z}(t_0)\right\|^2 \\ \text{s.t.} \quad & z'(t) = f\big(z(t)\big), \qquad \text{for } t \in [t_0, t_\mathrm{f}], \\ & z_\mathrm{RPV}(t_\mathrm{f}) = z^*_\mathrm{RPV}. \end{aligned}$$

Motivated by the results of the previous SIM approximation methods, we choose $z_\mathrm{RPV} = x$ as reaction progress variable. Since, the separatrices for the $z^2 + 1$, cosh, and ξ flows cannot be represented as graph over y (see Figs. 4.1 to 4.3), this choice of z_RPV is better suited for these examples.

In the local approach, i.e., the limiting case $t_0 = t_\mathrm{f}$, the ODE constraint becomes redundant. The non-local TBOA is the solution of the following problem (with $f(z) = z^2 + 1$).

$$\begin{aligned} \min_{z(\cdot)} \quad & \left\|\ddot{z}(t_0)\right\|^2 \\ \text{s.t.} \quad & z'(t) = f\big(z(t)\big), \qquad \text{for } t \in [t_0, t_\mathrm{f}], \\ & x(t_\mathrm{f}) = \operatorname{Re} z(t_\mathrm{f}) = x^*. \end{aligned} \tag{5.2}$$

Though a solution of the ODE constraint might be available, problem (5.2) is often hard to solve analytically. Nevertheless, we use a little mathematical trick to obtain at least necessary conditions for the solution of (5.2). For this purpose, we artificially write (5.2) in the form of an optimal control problem. In the second step, we apply Pontryagin's minimum principle (Theorem 3.5).

One possibility to handle (5.2) as optimal control problem is to replace the final state $y(t_\mathrm{f})$ by the artificially introduced boundary control $u(t_\mathrm{f})$. An equivalent formulation of problem 5.2 is then given by

$$\begin{aligned} \min_{z(\cdot),\, u(\cdot)} \quad & \psi\big(z(0)\big) \coloneqq \left\|\ddot{z}(t_0)\right\|^2 \\ \text{s.t.} \quad & z'(t) = f\big(z(t)\big), \qquad \text{for } t \in [t_0, t_\mathrm{f}], \\ & x(t_\mathrm{f}) = \operatorname{Re} z(t_\mathrm{f}) = x^*, \\ & y(t_\mathrm{f}) = \operatorname{Im} z(t_\mathrm{f}) = u(t_\mathrm{f}). \end{aligned}$$

For the derivation of necessary optimality conditions, Lagrangian multipliers $\lambda = (\lambda_x, \lambda_y)$ and $\mu = (\mu_x, \mu_y)$ are introduced to define the Lagrangian of this OCP

as (cf. Section 5 in Lebiedz and Unger [LU16])

$$J \coloneqq \psi\big(z(0)\big) + \int_{t_0}^{t_\mathrm{f}} \lambda^\mathsf{T}(t) \Big(f\big(z(t)\big) - z'(t) \Big) \,\mathrm{d}t + \mu_x\big(x(t_\mathrm{f}) - x^*\big) + \mu_y\big(y(t_\mathrm{f}) - u(t_\mathrm{f})\big).$$

The first variation of this Lagrangian can be calculated as

$$\begin{aligned}\delta J = \psi'\big(z(0)\big) \cdot \delta z_{|t_0} + \mu \cdot \delta z_{|t_\mathrm{f}} + \begin{pmatrix} x(t_\mathrm{f}) - x^* \\ y(t_\mathrm{f}) - u(t_\mathrm{f}) \end{pmatrix} \cdot \delta\mu \\ + \int_{t_0}^{t_\mathrm{f}} \Big[f'(z)^\mathsf{T}\lambda \cdot \delta z - \lambda \cdot \delta z' + \big(f(z) - z'\big) \cdot \delta\lambda \Big] \,\mathrm{d}t - \mu_y \cdot \delta u_{|t_\mathrm{f}}.\end{aligned}$$

Applying the partial integration formula

$$\int_{t_0}^{t_\mathrm{f}} \lambda \cdot \delta z' \,\mathrm{d}t = \lambda \cdot \delta z_{|t_\mathrm{f}} - \lambda \cdot \delta z_{t_0} - \int_{t_0}^{t_\mathrm{f}} \lambda' \cdot \delta z \,\mathrm{d}t$$

yields

$$\begin{aligned}\delta J = \Big(\psi'\big(z(0)\big) + \lambda\Big) \cdot \delta z_{|t_0} + (\mu - \lambda) \cdot \delta z_{|t_\mathrm{f}} + \begin{pmatrix} x(t_\mathrm{f}) - x^* \\ y(t_\mathrm{f}) - u(t_\mathrm{f}) \end{pmatrix} \cdot \delta\mu \\ + \int_{t_0}^{t_\mathrm{f}} \Big[\big(f'(z)^\mathsf{T}\lambda + \lambda'\big) \cdot \delta z + \big(f(z) - z'\big) \cdot \delta\lambda \Big] \,\mathrm{d}t - \mu_y \cdot \delta u_{|t_\mathrm{f}}.\end{aligned} \tag{5.3}$$

Finally, (5.3) implies the following necessary optimality conditions obtained by setting $\delta J = 0$. They are written in the form of the following boundary value problem:

$$\begin{aligned} z'(t) &= f\big(z(t)\big), && t \in [t_0, t_\mathrm{f}] \\ \lambda'(t) &= -f'\big(z(t)\big)^\mathsf{T}\lambda(t), && t \in [t_0, t_\mathrm{f}] \\ x(t_\mathrm{f}) &= x^*, \\ \lambda(t_0) &= -\psi'\big(z(0)\big), \\ \lambda_y(t_\mathrm{f}) &= 0, \end{aligned} \tag{5.4}$$

where $\lambda = (\lambda_x, \lambda_y)$.

In the following examples, we solve (5.4) instead of (5.2) whenever an analytical solution of (5.2) is not available.

Example 5.8 (TBOA for z^2+1)**.** The local TBOA approach minimizes the objective function $\psi(x,y) = \left\|x''(t_\mathrm{f}) + y''(t_\mathrm{f})\right\|_2^2$ where depending on the choice for RPV either $x(t_\mathrm{f})$ or $y(t_\mathrm{f})$ is fixed. Based on the results of the ZDP in Example 5.5, the use of x as RPV seems evident. For fixed RPV $x(t_\mathrm{f}) = x^*$, the vanishing gradient condition for

$$\psi_{x^*}(y) \coloneqq \psi(x^*, y) = \left\| 2x^*\big((x^*)^2 - 3y^2 + 1\big) + \mathrm{i}2y\big(3(x^*)^2 - y^2 + 1\big)\right\|_2^2$$

results in the critical point $y_1 = 0$. If $x^* \in (-\frac{1}{6}\sqrt{3}, \frac{1}{6}\sqrt{3})$, then the points

$$y_{2,3} = \pm\frac{1}{3}\sqrt{-9(x^*)^2 + 6 + 3\sqrt{1 - 12(x^*)^2}}$$

and

$$y_{4,5} = \pm\frac{1}{3}\sqrt{-9(x^*)^2 + 6 - 3\sqrt{1 - 12(x^*)^2}}$$

are critical as well. y_1, y_2 and y_3 are local minima. y_4 and y_5 are local maxima. Comparing the functions values $\psi(y_k)$ for $k = 1, 2, 3$, $y_1 = 0$ turns out to be the global minimum. If $x^* = 0$, the points $y_{2,3} = \pm 1$ are global minima as well. To sum up, the local TBOA calculates the separatrix $y = 0$ as well as the equilibria at $\pm(0, 1)$.

Let us now consider the non-local case, i.e., $t_0 < t_\mathrm{f}$. We do not have an analytical solution of (5.2) with $f(z) = z^2 + 1$ at hand. Instead, the first order conditions (5.4) are applied to $f(z) = z^2 + 1$ and $\psi(z) = \left\|z''(t_0)\right\|_2^2$. This leads to the following boundary value problem:

$$\begin{aligned}
z'(t) &= z^2(t) + 1, && t \in [t_0, t_\mathrm{f}] \\
\lambda'(t) &= -\begin{pmatrix} 2x & -2y \\ 2y & 2x \end{pmatrix}^\mathsf{T} \lambda(t), && t \in [t_0, t_\mathrm{f}] \\
x(t_\mathrm{f}) &= x^*, && \\
\lambda_x(t_0) &= -8(3x_0^5 + 6x_0^3y_0^2 + 3x_0y_0^4 + 4x_0^3 + x_0), && \\
\lambda_y(t_0) &= -8(3x_0^4y_0 + 6x_0^2y_0^3 + 3y_0^5 - 4y_0^3 + y_0), &&
\end{aligned} \tag{5.5}$$

$$\lambda_y(t_\mathrm{f}) = 0,$$

where $z(t_0) = (x_0, y_0)^\mathsf{T}$.

Note that

$$\psi(z) = \left\|2zz'\right\|_2^2 = \left\|2z(z^2+1)\right\|_2^2 = 4x^2(x^2-3y^3+1)^2 + 4y^2(3x^2-y^2+1)^2$$

and thus

$$\psi'(x,y) = 8\begin{pmatrix} 3x^5+6x^3y^2+3xy^4+4x^3+x \\ 3x^4y+6x^2y^3+3y^5-4y^3+y \end{pmatrix}.$$

Solving (5.5) yields

$$\lambda_x(t) = \frac{c_1}{\tan^2(t+c_2)+1},\ \lambda_y(t) = 0,\ x(t) = \tan(t+c_2),\ y(t) = 0$$

with c_1 and c_2 being real constants that depend on x^*. It immediately follows that only the separatrix $y = 0$ satisfies this necessary condition.

Example 5.9 (TBOA for cosh)**.** For $f(z) = \cosh(z-1/2)$ it holds

$$z'' = \sinh(z-1/2)\cosh(z-1/2) = 2\sinh(2z-1).$$

Hence, the local TBOA approach minimizes

$$\psi_{x^*}(y) \coloneqq \psi(x^*, y) = \frac{1}{4}\left\|\sinh(2x^*-1)\cos(2y) + \mathrm{i}\cosh(2x^*-1)\sin(2y)\right\|_2^2,$$

which can be simplified to

$$\psi_{x^*}(y) = \frac{1}{4}\big(\cosh^2(2x^*-1) - \cos^2(2y)\big).$$

The local and global minima are located at $y = k\frac{\pi}{2}$ for $k \in \mathbb{Z}$. Since the separatrices are at $y = k\pi$, the TBOA does not only compute separatrices but the "spurious solutions" $y = (2k+1)\frac{\pi}{2}$, i.e., incorrect solutions. In this case, the spurious solutions are not trajectories. The curvature of every periodic orbit of the holomorphic cosh flow is minimal when crossing a spurious solution (see also Fig. 4.2).

For the non-local TBOA with RPV x, we solve the first order conditions (5.4).

With $f(z) = \cosh(z - 1/2)$ and

$$\psi(z) = \left\|z''(t_0)\right\|_2^2 = \frac{1}{4}\big(\cosh^2(2x^* - 1) - \cos^2(2y)\big),$$

this results in the BVP

$$\begin{aligned}
z'(t) &= \cosh\big(z(t) - 1/2\big), && t \in [t_0, t_\mathrm{f}] \\
\lambda'(t) &= -\overline{\sinh\big(z(t) - 1/2\big)}\lambda(t), && t \in [t_0, t_\mathrm{f}] \\
x(t_\mathrm{f}) &= x^*, \\
\lambda(t_0) &= \frac{1}{2}\big(\sinh(4x_0 - 2) + \mathrm{i}\sin(4y_0)\big) \\
\lambda_y(t_\mathrm{f}) &= \mathrm{Im}\big(y(t_\mathrm{f})\big) = 0,
\end{aligned} \tag{5.6}$$

with $z(t_0) = (x_0, y_0)^\mathsf{T}$.

An analytical solution of (5.6) is unknown. However, it is possible to prove that for each $k \in \mathbb{Z}$ there is a solution for $y(t) = k\pi$ for all $t \in [t_0, t_\mathrm{f}]$. In other words, the separatrices are solutions of (5.6). For a fixed value of $k \in \mathbb{Z}$, the additional constraint $y(t) = k\pi$ implies that the solution of (5.6) satisfies

$$x(t) = \frac{1}{2} + \log\left(\tan\left(\frac{1}{2}c_1(-1)^k + \frac{1}{2}(-1)^k t\right)\right),$$

with a real constant c_1 and $\lambda_y(t) = 0$ for all $t \in [t_0, t_\mathrm{f}]$.

In general, there is no solution of (5.6) satisfying the spurious solution $y(t_\mathrm{f}) = (2k+1)\frac{\pi}{2}$ of the local TBOA. To see this, we set $x(t_0) = 1/2$ and $y(t_\mathrm{f}) = \tau \in (0, \pi)$. As a consequence, $t_\mathrm{f} = \frac{\pi}{2}$ and x^* are implicitly fixed. Thus, it is possible to solve the ODEs for $z(t)$ and consequently for $\lambda(t)$ using the initial values $\lambda(t_0)$ as listed above comparing $\lambda(t_\mathrm{f})$ with the desired value $\lambda_y(t_\mathrm{f}) = 0$.

The following Fig. 5.3 depicts the imaginary part of $\lambda(\frac{\pi}{2})$ for different values of $y(t_0) = \tau$. The red line shows $\lambda_y(\frac{\pi}{2})$ which equals zero if and only if $y(t_0) = \tau$ is a multiple of $\frac{\pi}{4}$. For $\tau = \tau_1 := \frac{\pi}{4}$ and $\tau = \tau_2 := \frac{3\pi}{4}$, we obtain approximately $x_1^* \approx 1.3814$ and $x_2^* \approx -0.3814$. This proves that the spurious solution $y(t_\mathrm{f}) = (2k+1)\frac{\pi}{2}$ of the local TBOA can only be a spurious solution of the non-local TBOA for $x^* \in \{x_1^*, x_2^*\}$.

We have no strict proof but are convinced that the choice of $x(t_0) = 1/2$ does not influence $\lambda_y(t_\mathrm{f})$ once $y(t_\mathrm{f})$ is fixed.

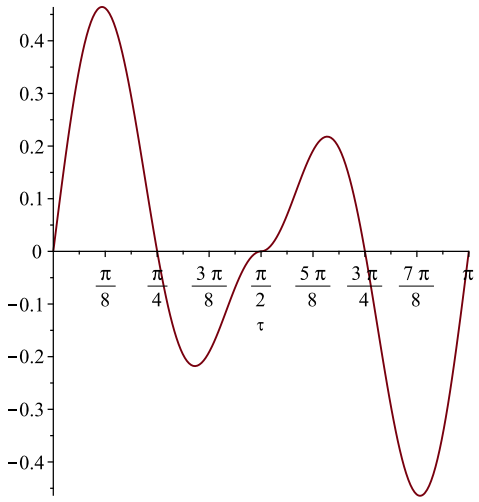

Figure 5.3: Values for $\lambda(t_f) = \lambda(\frac{\pi}{2})$ solving (5.6) with the initial values $z(t_0) = 1/2 + \mathrm{i}\tau$. Red line shows the imaginary part of $\lambda(\frac{\pi}{2})$ obtained by Maple.

The TBOA for the ξ flow is not considered because an analytical solution (even for the local version) cannot be calculated. For numerical results concerning curvature-based optimization approaches like the TBOA, see Section 5.5.3.

This section has reviewed three SIM approximation techniques in the context of holomorphic flows. With the ξ flow and its two simplifications $z^2 + 1$ and cosh, it was attempted to calculate separatrices and provide us with a deeper understanding of them. All approximation methods — the FCM, ZDP, and TBOA — detected the separatrices for z^2+1 and cosh correctly. However, all methods have minor drawbacks. Figure 5.1 suggests that the FCM likely not characterizes the separatrices exactly. The ZDP performs better if x is chosen as RPV but calculates in any case not only the separatrices but also spurious solutions. Similar to the ZDP, the local version of the TBOA produces spurious solutions. The non-local version excluded most of the spurious solutions while keeping the separatrices. Due to the sophisticated analysis, results for the ξ flow were either numerical or omitted.

It is very likely that the good performance of SIM approximations for the computation of separatrices is based on the bundling behavior of trajectories near the SIMs and separatrices. Another reason is that the $z^2 + 1$ and cosh flows might be oversimplifications in the sense that all separatrices are straight lines there. This and the difficulty of the ξ analysis call for a development of new tools to

characterize separatrices. In the next section, we introduce a new point of view on separatrices.

5.2 Critical Points at Infinity

Since separatrices have (by Definition 4.2) finite maximum interval of existence, the vector field of an entire function f cannot be bounded on separatrices. Otherwise, one could enlarge the interval of existence. Therefore, a positive separatrix (see Definition 4.2) for entire functions f must reach out to infinity in phase space. This motivates the investigation of the qualitative behavior of holomorphic flows at infinity.

Mapping the complex phase space to the Poincaré sphere provides insight into the dynamics of the flow at infinity [Per00]. Other transformations can reveal characteristics at infinity as well. The global phase space behavior of polynomial vector fields f is well studied. We prove for polynomial systems that critical points at infinity must have at least one incoming or outgoing trajectory which is a separatrix. Thus, separatrices are closely related to heteroclinic or homoclinic orbits connecting critical points at infinity. This refers to the work of Davis and Skodje [DS99] and Al-Khateeb et al. [Al-+09] for dynamical systems in $\mathbb{R}^n$ and their slow invariant manifolds.

In this section, techniques for investigation of the behavior of dynamical systems at infinity are presented. We follow the introductions of Perko [Per00], Meiss [Mei07], Roeder [Roe03], Gingold and Solomon [GS13] into this topic. We use the identification $\mathbb{C} \simeq \mathbb{R}^2$ and consider two-dimensional real dynamical systems. The content of this chapter can be found in [HL19].

In the following subsections, three mappings of the form $T\colon \mathbb{R}^2 \to R$ are presented, where $R \subset \mathbb{R}^2$ or $R \subset S^2 \subset \mathbb{R}^3$. Points at infinity are then introduced as a subset of the boundary ∂R. In order to analyze the behavior at infinity, the dynamics $z' = f(z)$ with $z \in \mathbb{R}^2$ are transformed into dynamics in R by using T. Applying the chain rule to $T(z) = \rho$ yields the dynamics in R

$$\rho' = T'\big(T^{-1}(\rho)\big) \cdot f\big(T^{-1}(\rho)\big). \tag{5.7}$$

These new dynamics are then investigated for the behavior near and at infinity.

5.2.1 Infinity in Polar Coordinates

There are several possibilities to compactify and analyze complex-valued dynamical systems. A first one relies on polar coordinates (r, θ) and regards the limit $r \to \infty$ (cf. [Roe03]). Roeder shows the utility of this transformation in [Roe03]. We take advantage of this transformation in Section 5.2.5. Consider a polynomial, two-dimensional real dynamical system of the form

$$\begin{aligned} x' &= \tfrac{\mathrm{d}x}{\mathrm{d}t} &&= P(x,y) = P_0(x,y) + P_1(x,y) + \cdots + P_d(x,y) \\ y' &= \tfrac{\mathrm{d}y}{\mathrm{d}t} &&= Q(x,y) = Q_0(x,y) + Q_1(x,y) + \cdots + Q_d(x,y), \end{aligned} \tag{5.8}$$

where P and Q are polynomials in x and y with $P_i(x,y)$ resp. $Q_i(x,y)$ being the homogeneous polynomial of degree i in P resp. Q.

The mapping $T_{\text{polar}} \colon \mathbb{R}^2 \setminus \{0\} \to (0,\infty) \times (-\pi, \pi]$ maps 2-D coordinates $(x,y)^\mathsf{T}$ to polar coordinates

$$\begin{pmatrix} r \\ \phi \end{pmatrix} = T_{\text{polar}}(x,y) \coloneqq \begin{pmatrix} \sqrt{x^2+y^2} \\ \operatorname{atan2}(y,x) \end{pmatrix}.$$

The function atan2$\colon \mathbb{R}^2 \setminus \{0\} \to (-\pi, \pi]$ is defined by the arctan function:

$$\operatorname{atan2}(y,x) = \begin{cases} \arctan\left(\frac{y}{x}\right) & \text{if } x > 0 \\ \arctan\left(\frac{y}{x}\right) + \pi & \text{if } x < 0, y \geq 0 \\ \arctan\left(\frac{y}{x}\right) - \pi & \text{if } x < 0, y < 0 \\ \frac{\pi}{2} & \text{if } x = 0, y > 0 \\ -\frac{\pi}{2} & \text{if } x = 0, y < 0. \end{cases}$$

Using the inverse mapping $T^{-1}_{\text{polar}}(r,\phi) = (r\cos\phi, r\sin\phi)^\mathsf{T}$, the following system is obtained:

$$r' = \cos\theta\, P(r\cos\theta, r\sin\theta) + \sin\theta\, Q(r\cos\theta, r\sin\theta) \tag{5.9a}$$

$$= \sum_{k=0}^{d} r^k \left(\cos\theta P_k(\cos\theta, \sin\theta) + \sin\theta Q_k(\cos\theta, \sin\theta)\right) \tag{5.9b}$$

$$\theta' = \frac{1}{r}\left(-\sin\theta P(r\cos\theta, r\sin\theta) + \cos\theta Q(r\cos\theta, r\sin\theta)\right) \tag{5.9c}$$

$$= \frac{1}{r} \sum_{k=0}^{d} r^k \left(-\sin\theta P_k(\cos\theta, \sin\theta) + \cos\theta Q_k(\cos\theta, \sin\theta) \right) \tag{5.9d}$$

For taking the limit $r \to \infty$, r is replaced by $s = \frac{1}{r}$ and then the limit $s \to 0+$ is considered

$$s' = -s^2 \sum_{k=0}^{d} s^{-k} \left(\cos\theta P_k(\cos\theta, \sin\theta) + \sin\theta Q_k(\cos\theta, \sin\theta) \right) \tag{5.10a}$$

$$\theta' = s \sum_{k=0}^{d} s^{-k} \left(-\sin\theta P_k(\cos\theta, \sin\theta) + \cos\theta Q_k(\cos\theta, \sin\theta) \right). \tag{5.10b}$$

We denote the degrees of the right-hand side of (5.10a) in s by $2 - I$ and of (5.10b) by $1 - J$. As we will see, behavior at infinity depends on the number $\hat{k} \coloneqq I - J$ (see Theorem 5.14).

Defining the transformation $\tilde{T}_{\text{polar}} \colon \mathbb{R}^2 \setminus \{0\} \to (0, \infty) \times (-\pi, \pi] =: R_{\text{polar}}$ with $\tilde{T}_{\text{polar}}(x, y) = (s, \theta)^{\mathsf{T}} = \left(\frac{1}{\sqrt{x^2+y^2}}, \text{atan2}(y, x) \right)^{\mathsf{T}}$, points at infinity correspond to the inverse image of $s = 0$, i.e., to the set $\{0\} \times (-\pi, \pi] \subset \partial R_{\text{polar}}$.

5.2.2 Poincaré Sphere

The aim of the Poincaré sphere is the same as for the Riemann sphere: compactification of the 2-D plane resp. complex plane. The stereographic projection of the plane onto the surface of a unit ball transfers infinity to the north pole. Thus, infinity can be handled like a finite point. However, there is a major drawback of the Riemann sphere: infinity is just a single point. Thus, if infinitely many separatrices exist, they accumulate at this single point of infinity. This might turn the study of infinity into a painful task. An alternative is the projection to the Poincaré sphere that represent infinity by infinitely many (finite) points. To project a point (x^*, y^*) of the dynamical system (5.8) onto a point (X^*, Y^*, Z^*) on the northern hemisphere (Poincaré sphere)

$$S^2_+ = \left\{ (X, Y, Z) \in \mathbb{R}^3 \colon X^2 + Y^2 + Z^2 = 1, Z \geq 0 \right\},$$

the (x, y) plane is pinned in 3D coordinates to the plane $(x, y, 1)$. The corresponding point (X^*, Y^*, Z^*) is then obtained by calculating the intersection point of the

straight line through the origin and $(x^*, y^*, 1)$, and the surface of the northern hemisphere as shown in Fig. 5.4.

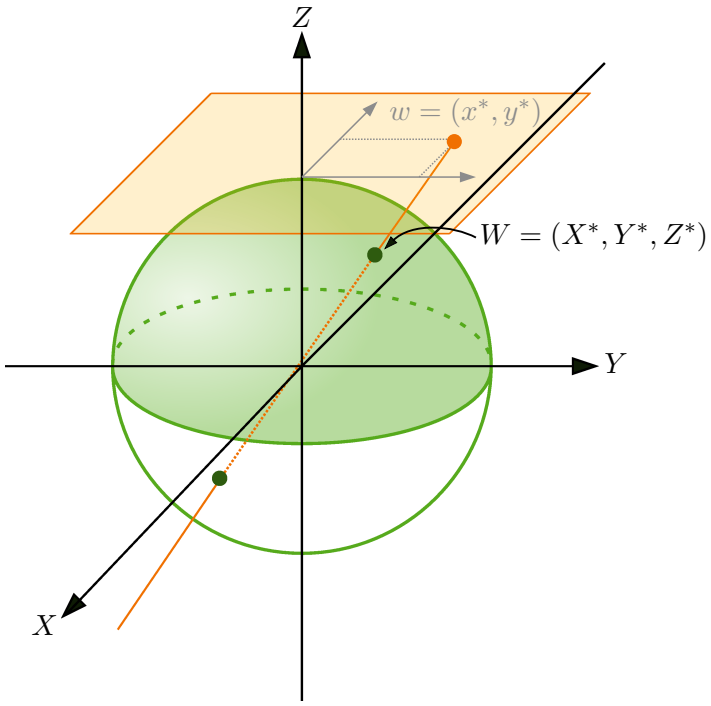

Figure 5.4: Construction of Poincaré sphere. See [HL19].

In short mathematical notation, the transformation can be written as mapping $T_{\text{PS}}\colon \mathbb{R}^2 \to S^2_+ =: R_{\text{PS}}$ such that

$$(X, Y, Z)^\mathsf{T} = T_{\text{PS}}(x, y) \coloneqq \left(\frac{x}{\sqrt{1 + x^2 + y^2}}, \frac{y}{\sqrt{1 + x^2 + y^2}}, \frac{1}{\sqrt{1 + x^2 + y^2}} \right)^\mathsf{T}$$
$$(x, y)^\mathsf{T} = T^{-1}_{\text{PS}}(X, Y, Z) = \left(\frac{X}{Z}, \frac{Y}{Z} \right)^\mathsf{T}.$$

Using this transformation, infinity corresponds to the set $\{(X, Y, 0) \in \mathbb{R}^3 \colon X^2 + Y^2 = 1\} \subset S^2_+ = R_{\text{PS}}$.

Direct calculations show that the dynamics on the Poincaré sphere are given by

$$\begin{aligned} X' &= Z\left((1-X^2)P\left(\tfrac{X}{Z},\tfrac{Y}{Z}\right) - XYQ\left(\tfrac{X}{Z},\tfrac{Y}{Z}\right)\right) \\ Y' &= Z\left((1-Y^2)Q\left(\tfrac{X}{Z},\tfrac{Y}{Z}\right) - XYP\left(\tfrac{X}{Z},\tfrac{Y}{Z}\right)\right) \\ Z' &= -Z^2\left(XP\left(\tfrac{X}{Z},\tfrac{Y}{Z}\right) + YQ\left(\tfrac{X}{Z},\tfrac{Y}{Z}\right)\right) \end{aligned}$$

In the following, the degree of the polynomials P and Q is assumed to be a natural number $d \in \mathbb{N}$. We are interested in the case $Z = 0$ which corresponds to infinity. Since $P\left(\frac{X}{Z},\frac{Y}{Z}\right) = \mathcal{O}(Z^{-d})$ as $Z \to 0$ (and $Q\left(\frac{X}{Z},\frac{Y}{Z}\right) = \mathcal{O}(Z^{-d})$ as well), the flow might be incomplete if $d > 1$. In order to restore the completeness of trajectories, we introduce a new time variable τ defined by

$$\tau(t) = \int_0^t Z^{1-d}(s)\,\mathrm{d}s. \tag{5.11}$$

τ is a differentiable function and strictly monotonous because $Z(s) > 0$. Thus, it is a bijective mapping with $\frac{\mathrm{d}\tau}{\mathrm{d}t} = Z^{1-d}(t)$. In the following, we will not only use the different time variables t and τ but similar time transformations like for τ. For better readability, we "misuse" the differential notation $\frac{\mathrm{d}\tau}{\mathrm{d}t} = Z^{1-d}(t)$ or $\mathrm{d}\tau = Z^{1-d}(t)\,\mathrm{d}t$ without explicit definition of the rescaled time like in (5.11). But that does not mean it is not well defined.

Switching to this rescaled time $\tau = \tau(t)$ yields a topologically equivalent differential equation system (see Definition 4.3). The differential equations can be calculated using the chain rule (see (5.7)):

$$\dot{X} \coloneqq \frac{\mathrm{d}X}{\mathrm{d}\tau} = \frac{\mathrm{d}X}{\mathrm{d}t}\frac{\mathrm{d}t}{\mathrm{d}\tau} = (1-X^2)P^*(X,Y,Z) - XYQ^*(X,Y,Z) \tag{5.12a}$$

$$\dot{Y} \coloneqq \frac{\mathrm{d}Y}{\mathrm{d}\tau} = \frac{\mathrm{d}Y}{\mathrm{d}t}\frac{\mathrm{d}t}{\mathrm{d}\tau} = (1-Y^2)Q^*(X,Y,Z) - XYP^*(X,Y,Z) \tag{5.12b}$$

$$\dot{Z} \coloneqq \frac{\mathrm{d}Z}{\mathrm{d}\tau} = \frac{\mathrm{d}Z}{\mathrm{d}t}\frac{\mathrm{d}t}{\mathrm{d}\tau} = -Z\left(XP^*(X,Y,Z) + YQ^*(X,Y,Z)\right), \tag{5.12c}$$

where $P^*(X,Y,Z) = Z^dP\left(\frac{X}{Z},\frac{Y}{Z}\right)$ and $Q^*(X,Y,Z) = Z^dQ\left(\frac{X}{Z},\frac{Y}{Z}\right)$. For $Z = 0$, τ is not a bijection. However, the transformed system preserves the limiting behavior as $Z \to 0$ because the dominating highest order terms of P and Q are still involved. Evaluating $Z = 0$ in Eq. (5.12) directly reveals the dynamics on the equator, which

are given by

$$\dot{X} = \frac{\mathrm{d}X}{\mathrm{d}\tau} = -Y\left(XQ_d(X,Y) - YP_d(X,Y)\right) \tag{5.13a}$$

$$\dot{Y} = \frac{\mathrm{d}Y}{\mathrm{d}\tau} = X\left(XQ_d(X,Y) - YP_d(X,Y)\right), \tag{5.13b}$$

where $P_d(X,Y) = \lim_{Z\to 0} P^*(X,Y,Z)$ and $Q_d(X,Y) = \lim_{Z\to 0} Q^*(X,Y,0)$ are the terms with exactly degree d in P and Q. Thus, fixed points at infinity must satisfy the following equation

$$XQ_d(X,Y) - YP_d(X,Y) = 0. \tag{5.14}$$

Since this equation is homogeneous of degree $d+1$, an equilibrium $(X,Y,0)$ induces the antipodal (diametrically opposite) point $(-X,-Y,0)$ to be a fixed point as well. The antipodal point is the same type of fixed point. However, the direction of the flow reverses if the natural number d is even.

In algebraic mathematics, every pair of antipodal points (not only at the equator) is uniquely identified by the straight line through the origin and these points. This leads to definition of the projective plane. For more information, see e.g. [Hul12].

Aiming to characterize the type of an equilibrium $(X,Y,0)$ at infinity, it can be useful to transform the system in the neighborhood of the equilibrium to the tangent plane at this fixed point. In differential geometry this corresponds to a change of the local chart (cf. Definition 2.29). For instance, if $X \neq 0$, the mapping defined by the relations

$$\beta = \frac{Y}{X}, \gamma = \frac{Z}{X}$$

projects (X,Y,Z) onto the (β,γ)-plane and corresponding dynamics with respect to a rescaled time $\mathrm{d}s = X^{d-1}\,\mathrm{d}\tau$

$$\begin{aligned} \beta' &= \tfrac{\mathrm{d}\beta}{\mathrm{d}s} = \gamma^d Q\left(\tfrac{1}{\gamma}, \tfrac{\beta}{\gamma}\right) - \beta\gamma^d P\left(\tfrac{1}{\gamma}, \tfrac{\beta}{\gamma}\right) \\ \gamma' &= \tfrac{\mathrm{d}\gamma}{\mathrm{d}s} = -\gamma^{d+1} P\left(\tfrac{1}{\gamma}, \tfrac{\beta}{\gamma}\right). \end{aligned} \tag{5.15}$$

A fixed point $(\beta_0, 0)$ in this new system (5.15) corresponds to a fixed point $\pm\left(\frac{1}{\sqrt{1+\beta_0^2}}, \frac{\beta_0}{\sqrt{1+\beta_0^2}}, 0\right)$ on the Poincaré sphere.

Analogously, in the case $Y \neq 0$ (e.g. for $X = 0$), the mapping

$$\alpha = \frac{X}{Y}, \gamma = \frac{Z}{Y}$$

projects (X, Y, Z) onto the (α, γ)-plane with according dynamics with respect to a rescaled time $\mathrm{d}s = Y^{d-1}\,\mathrm{d}\tau$

$$\begin{aligned} \alpha' &= \tfrac{\mathrm{d}\alpha}{\mathrm{d}s} = \gamma^d P\left(\tfrac{\alpha}{\gamma}, \tfrac{1}{\gamma}\right) - \alpha\gamma^d Q\left(\tfrac{\alpha}{\gamma}, \tfrac{1}{\gamma}\right) \\ \gamma' &= \tfrac{\mathrm{d}\gamma}{\mathrm{d}s} = -\gamma^{d+1} Q\left(\tfrac{\alpha}{\gamma}, \tfrac{1}{\gamma}\right). \end{aligned} \tag{5.16}$$

A fixed point $(\alpha_0, 0)$ in this new system (5.16) corresponds to a fixed point $\pm\left(\frac{\alpha_0}{\sqrt{1+\alpha_0^2}}, \frac{1}{\sqrt{1+\alpha_0^2}}, 0\right)$ on the Poincaré sphere.

5.2.3 Compactification of $\mathbb{R}^2$

A third possibility for the compactification might be the following approach (cf. [GS13]). Let U be the unit ball $U \coloneqq U_1(0) = \left\{p \in \mathbb{R}^2 \colon \|p\| < 1\right\}$. Consider the mapping $T_{\text{comp}} \colon \mathbb{R}^2 \to U =: R_{\text{comp}}$ defined by

$$p = T_{\text{comp}}(z) \coloneqq \frac{2z}{1 + \sqrt{1 + 4\|z\|^2}}, \quad z \in \mathbb{R}^2.$$

Its inverse mapping is given by

$$z = T_{\text{comp}}^{-1}(p) = \frac{p}{1 - \|p\|^2}.$$

This mapping can be continued (see Gingold [Gin04]) to the boundary ∂U, which is mapped to a set of points p_∞ at infinity that differ in their "direction" p at infinity. For this purpose, we define what a direction at infinity is.

Definition 5.10 (cf. [GS13])**.** A continuous function $h : (t_-, t_+) \to \mathbb{R}^2$ *diverges in direction $p \in \partial U$ to infinity* (*or diverges to p_∞*) — in notation $\lim\limits_{t \nearrow t_+} h(t) = p_\infty$ — iff

$$\lim_{t \nearrow t_+} \left\|h(t)\right\| = \infty \quad \text{and}$$

$$\lim_{t \nearrow t_+} \frac{h(t)}{\left\|h(t)\right\|} = p.$$

Having this definition at hand, we define the "infinity direction set" to be

$$\mathrm{ID} \coloneqq \left\{ p_\infty \colon \ \|p\| = 1 \right\}.$$

In the sense of Definition 5.10, infinity corresponds for the mapping T_{comp} to the boundary $\partial U = \partial R_{\text{comp}}$. Gingold shows that the continuation of T_{comp} maps $\bar{\mathbb{R}}^2 \coloneqq \mathbb{R}^2 \cup \mathrm{ID}$ bijective onto $\bar{U} = U \cup \partial U$.

Remark 5.11. $\bar{\mathbb{R}}^2$ can be equipped with the chordal metric in order to become a complete metric space. See [GS13] for more details.

Transformation of the dynamical system (5.8) with T_{comp} leads to a new differential equations systems on the compact unit ball $\bar{U} \subset \mathbb{R}^2$. According to [GS13, Proposition 7], these new dynamics in U satisfy:

$$p' = \begin{pmatrix} p_1' \\ p_2' \end{pmatrix} = \frac{(1+\|p\|^2)I - 2pp^\mathsf{T}}{(1+\|p\|^2)(1-\|p\|^2)^{-1}} \begin{pmatrix} P\left(\frac{p_1}{1-\|p\|^2}, \frac{p_2}{1-\|p\|^2}\right) \\ Q\left(\frac{p_1}{1-\|p\|^2}, \frac{p_2}{1-\|p\|^2}\right) \end{pmatrix}$$

Transforming the time t to τ with $\mathrm{d}t = (1+\|p\|^2)(1-\|p\|^2)^{d-1}\,\mathrm{d}\tau$ results in the dynamical system

$$\dot{p} = \frac{\mathrm{d}p}{\mathrm{d}\tau} = (1-\|p\|^2)^d \left[(1+\|p\|^2) \begin{pmatrix} P(\cdot,\cdot) \\ Q(\cdot,\cdot) \end{pmatrix} - 2 \left(p^\mathsf{T} \begin{pmatrix} P(\cdot,\cdot) \\ Q(\cdot,\cdot) \end{pmatrix} \right) \cdot p \right], \tag{5.17}$$

where we omitted the arguments of P and Q for brevity. They are evaluated at $\left(\frac{p_1}{1-\|p\|^2}, \frac{p_2}{1-\|p\|^2}\right)$. Finally, for $p \in \partial U$, we obtain

$$\begin{aligned} \dot{p_1} &= 2P_d(p_1,p_2) - 2\left(p_1 P_d(p_1,p_2) + p_2 Q_d(p_1,p_2)\right) p_1 \\ &= 2(1-p_1^2)P_d(p_1,p_2) - 2p_2 p_2 Q_d(p_1,p_2) \\ \dot{p_2} &= 2Q_d(p_1,p_2) - 2\left(p_1 P_d(p_1,p_2) + p_2 Q_d(p_1,p_2)\right) p_2 \\ &= -2p_1 p_2 P_d(p_1,p_2) + 2(1-p_2^2)Q_d(p_1,p_2), \end{aligned}$$

which is twice the right-hand side of (5.13). So the compactification via mapping T_{comp} is very similar to the transformations to the Poincaré sphere and subsequently projection to the plane containing the equator of the sphere.

5.2.4 Definition of Critical Points at Infinity

Next, we define critical points at infinity using the above mentioned compactifications. For the Poincaré sphere, the definition is based on Eq. (5.14):

Definition 5.12 (Critical Point at Infinity)**.** A *critical point at infinity* for the system (5.8) is a point $p \in \partial U$ such that

$$p_1 Q_d(p_1, p_2) - p_2 P_d(p_1, p_2) = 0.$$

Proposition 5.13. *Let p be in ∂U. Then the following statements are equivalent*

(*a*) *p is a critical point at infinity for the system* (5.8)*,*

(*b*) *There is a real number $\alpha \in \mathbb{R}$ such that* $\begin{pmatrix} P_d(p_1, p_2) \\ Q_d(p_1, p_2) \end{pmatrix} = \alpha \begin{pmatrix} p_1 \\ p_2 \end{pmatrix}$*,*

(*c*) $\begin{pmatrix} P_d(p_1, p_2) \\ Q_d(p_1, p_2) \end{pmatrix} = \begin{pmatrix} p_1 \\ p_2 \end{pmatrix}^{\mathsf{T}} \begin{pmatrix} P_d(p_1, p_2) \\ Q_d(p_1, p_2) \end{pmatrix} \begin{pmatrix} p_1 \\ p_2 \end{pmatrix}$ *— this statement is used for definition of critical points at infinity in* [*GS13*].

Proof. (a) is equivalent to

$$\det \begin{pmatrix} p_1 & P_d(p_1, p_2) \\ p_2 & Q_d(p_1, p_2) \end{pmatrix} = 0.$$

This holds exactly when (b) holds. (c) is an equation of the form $y = (p^{\mathsf{T}} y)p = pp^{\mathsf{T}} y$, which is an eigenvalue problem of the matrix pp^{T} of rank 1 with eigenvalue 1. Since $p = pp^{\mathsf{T}} p$, the vector p lies in the image of the matrix pp^{T}. Now it follows

$$\left\{ y \in \mathbb{R}^2 \colon y = p^{\mathsf{T}} y p \right\} = \{ \alpha p \colon \alpha \in \mathbb{R} \}.$$

Therefore, (b) and (c) are equivalent. □

Proposition 5.13 shows that essentially both, the transformations T_{PS} of [Per00] and T_{comp} of [GS13] yield the same points of infinity. The third presented transformation T_{polar} using polar coordinates can detect if the equator of the Poincaré sphere, i.e., the points of infinity, consists entirely of critical points.

Theorem 5.14 (cf. [Roe03, Theorem 2])**.** *Consider the polynomial system* (5.8) *and its transformed system* (5.9) *with polar coordinates. We denote the polynomial degrees of* $\mathrm{d}r/\mathrm{d}t$ *by* I *and* $\mathrm{d}\theta/\mathrm{d}t$ *by* J*. Let* $\hat{k} \coloneqq I - J$*. If* $\hat{k} \geq 2$*, the equator of the Poincaré sphere consists entirely of fixed points. If* $\hat{k} \leq 1$*, then: If there is no critical point at infinity, the equator of the Poincaré sphere is a cycle trajectory. Otherwise there are finitely many critical points at infinity.*

Proof. See [Roe03, Theorem 2]. □

5.2.5 Heteroclinic Orbits as Separatrix Generators

For vector fields f arising in the context of two-time-scale systems, 1-D SIMs are special trajectories sharing a phase portrait similar to separatrices. 1-D SIMs are invariant, attractive curves. In their neighborhood, other trajectories are attracted onto these SIMs either in forward or backward time direction.

Al-Khateeb et al. [Al-+09] conjecture and make plausible that the 1-D SIMs are heteroclinic orbits that start in critical points (finite or infinite) of saddle type with exactly one unstable direction (based on [DS99]). In 2-D real dynamical systems, the stable and unstable manifolds of a saddle can be considered as separatrices respectively SIMs. Therefore, it seems natural to investigate whether separatrices are heteroclinic, homoclinic orbits or none of them.

In the following we restrict ourselves to 1-D complex polynomial differential systems, so we can apply the theory of the last sections.

Lemma 5.15. *Let* $f(z) = \sum_{k=0}^{d} \alpha_k z^k$ *be a complex polynomial of degree* $d \geq 1$*, i.e.,* $\alpha_d \neq 0$ *and* $\alpha_k = a_k + \mathrm{i}b_k \in \mathbb{C}, a_k, b_k \in \mathbb{R}$ *for all* $k = 0, 1, \ldots, d$*. Then, the differential*

equation $z' = f(z)$ can be identified in $\mathbb{R}^2$ by the differential equation system

$$\begin{aligned} x' = P(x,y) &= \sum_{k=0}^{d} P_k(x,y) \coloneqq \sum_{k=0}^{d} a_k\xi_k(x,y) - b_k\eta_k(x,y) \\ y' = Q(x,y) &= \sum_{k=0}^{d} Q_k(x,y) \coloneqq \sum_{k=0}^{d} a_k\eta_k(x,y) + b_k\xi_k(x,y), \end{aligned} \tag{5.18}$$

where

$$\begin{aligned} \xi_k(x,y) &\coloneqq \sum_{\ell=0}^{\lfloor k/2 \rfloor} \binom{k}{2\ell} (-1)^\ell x^{k-2\ell} y^{2\ell}, \\ \eta_k(x,y) &\coloneqq \sum_{\ell=0}^{\lfloor (k-1)/2 \rfloor} \binom{k}{2\ell+1} (-1)^\ell x^{k-2\ell-1} y^{2\ell+1}. \end{aligned}$$

Furthermore, if the equator of the Poincaré sphere consists of infinitely many critical points, then d is an odd number and $\alpha_d = a_d$ is a real number.

Proof. Let $f(z) = \sum_{k=0}^{d} \alpha_k z^k$ be a complex polynomial of degree $d \geq 1$. Because of

$$(x + \mathrm{i}y)^k = \xi_k(x,y) + \mathrm{i}\,\eta_k(x,y),$$

it holds

$$\alpha_k(x + \mathrm{i}y)^k = a_k\xi_k(x,y) - b_k\eta_k(x,y) + \mathrm{i}\big(a_k\eta_k(x,y) + b_k\xi_k(x,y).$$

Thus, transformation (5.18) follows immediately. We consider the polar coordinate setting of (5.9) and determine the integers $I \in \{1, 2, \ldots, d\}$ and $J \in \{-1, 0, \ldots, d-1\}$ in this special case. Recall that I and J represent the degrees in r and θ of the vector field polynomial. First, notice that $\xi_k(1,0) = 1$ and $\eta_k(1,0) = 0$. If k is an even number, then $\xi_k(0,1) = (-1)^{\frac{k}{2}}$ and $\eta_k(0,1) = 0$. If k is an odd number, then $\xi_k(0,1) = 0$ and $\eta_k(0,1) = (-1)^{\frac{k-1}{2}}$. Inserting $\theta = 0$ in (5.9), yields

$$r' = \sum_{k=0}^{d} r^k P_k(1,0) = \sum_{k=0}^{d} r^k a_k$$

$$\theta' = \frac{1}{r}\sum_{k=0}^{r} r^k Q_k(1,0) = \frac{1}{r}\sum_{k=0}^{r} r^k b_k.$$

If $a_d \neq 0$ then $I = d$. If $b_d \neq 0$, $J = d-1$.

Inserting $\theta = \frac{\pi}{2}$ in (5.9), yields

$$\begin{aligned} r' &= \sum_{k=0}^{d} r^k Q_k(0,1) = \sum_{k=0}^{d} r^k \big(a_k \eta_k(0,1) + b_k \xi_k(0,1)\big) \\ \theta' &= -\frac{1}{r}\sum_{k=0}^{d} r^k P_k(0,1) = -\frac{1}{r}\sum_{k=0}^{d} r^k \big(a_k \xi_k(0,1) - b_k \eta_k(0,1)\big) \end{aligned}$$

If d is even, we obtain

$$\begin{aligned} r' &= r^d b_d (-1)^{\frac{d}{2}} + \sum_{k=0}^{d-1} r^k (a_k \eta_k(0,1) + b_k \xi_k(0,1)) \\ \theta' &= -\frac{1}{r}\left(r^d a_d (-1)^{\frac{d}{2}} + \sum_{k=0}^{d-1} r^k \big(a_k \xi_k(0,1) - b_k \eta_k(0,1)\big)\right) \end{aligned}$$

Table 5.1 concludes which numerical values $\hat{k} = I - J$ may assign.

Table 5.1: Values for $\hat{k} = I - J$ with respect to d and α_d.

	$a_d = 0$	$b_d = 0$	$a_d \cdot b_d \neq 0$
d even	$\hat{k} = d-(d-1) = 1$	$\hat{k} = d-(d-1) = 1$	$\hat{k} = d-(d-1) = 1$
d odd	$\hat{k} = I-(d-1) \leq 1$	$\hat{k} = d - J \geq 1$	$\hat{k} = d-(d-1) = 1$

It shows, that $\hat{k} \geq 2$ only if d is odd and $b_d = 0$. The statement now follows applying Theorem 5.14. □

With the next theorem, we show that critical points of polynomial holomorphic flows at infinity are connected to separatrices. Furthermore, the sign of α in Proposition 5.13 corresponds to the direction of the separatrix.

Theorem 5.16 (cf. Theorem 18 of [GS13]). *Let $p \in \partial U$ be a critical point at infinity of system* (5.18) *with polynomial degree $d \geq 2$ satisfying*

$$\begin{pmatrix} P_d(p_1, p_2) \\ Q_d(p_1, p_2) \end{pmatrix} = \alpha \begin{pmatrix} p_1 \\ p_2 \end{pmatrix},$$

for a $\alpha \in \mathbb{R}$ (cf. Proposition 5.13). Then, p is generic, i.e., $\alpha \neq 0$. If $\alpha > 0$ ($\alpha < 0$), there is a separatrix that ends (starts) at the critical point p at infinity.

Proof. Let p be a critical point at infinity with corresponding $\alpha \in \mathbb{R}$. At first, we show that $\alpha \neq 0$. Assume that $\alpha = 0$. Thus it holds

$$\begin{aligned} 0 = P_d(p_1, p_2) &= a_d \xi_d(p_1, p_2) - b_d \eta_d(p_1, p_2) \\ 0 = Q_d(p_1, p_2) &= a_d \eta_d(p_1, p_2) + b_d \xi_d(p_1, p_2) \end{aligned}$$

which is equivalent to

$$\begin{pmatrix} 0 \\ 0 \end{pmatrix} = \begin{pmatrix} a_d & -b_d \\ b_d & a_d \end{pmatrix} \begin{pmatrix} \xi_d(p_1, p_2) \\ \eta_d(p_1, p_2) \end{pmatrix}.$$

The matrix in this equation is regular. Otherwise $\alpha_d = a_d + \mathrm{i} b_d$ would be zero and using Lemma 5.15 yields $(p_1 + \mathrm{i} p_2)^d = \xi_d(p_1, p_2) + \mathrm{i}\eta_d(p_1, p_2) = 0$. This contradicts $p \in \partial U$. The assumption $\alpha = 0$ must have been wrong.

Because of Proposition 5.13, we can apply Theorem 18 resp. Theorem 14 of [GS13]. There it is shown that the vector field is incomplete. More precisely, the authors show that there is a matrix A and a polynomial vector function V in the variables u,p, and $u - p$ such that (5.17) is equivalent to

$$\frac{\mathrm{d}(u - p)}{\mathrm{d}\tau} = A(u - p) + V,$$

with A equals to

$$2(I - pp^{\mathsf{T}}) \left[J_d(p) - 2 \begin{pmatrix} P_{d-1}(p_1, p_2) \\ Q_{d-1}(p_1, p_2) \end{pmatrix} p^{\mathsf{T}} \right] - 2p^{\mathsf{T}} \begin{pmatrix} P_d(p_1, p_2) \\ Q_d(p_1, p_2) \end{pmatrix} I,$$

where J_d denotes the Jacobian of the vector field $\begin{pmatrix} P_d(p_1, p_2) \\ Q_d(p_1, p_2) \end{pmatrix}$. The function V

satisfies

$$V = \mathcal{O}\left(\|u-p\|^2\right) \quad \text{as} \quad \|u-p\| \to 0.$$

Further,

$$-2p^{\mathsf{T}} \begin{pmatrix} P_d(p_1,p_2) \\ Q_d(p_1,p_2) \end{pmatrix} = -2\alpha$$

is an eigenvalue of A for the left eigenvector p. W.l.o.g. let $\alpha > 0$. Then there is at least one trajectory $u^*(t)$ with $\lim_{t \nearrow t_+} u^*(t) = p_\infty$ for a finite value $t_+ < \infty$. Thus, u^* is a separatrix in the sense of Definition 4.2 that ends at the critical point p at infinity. □

In the case of polynomial flows where the highest coefficient α_d is real (for instance if $f(z) = z^2 + 1$), Theorem 5.16 and the proof of Lemma 5.15 imply the following statements.

Corollary 5.17. *Let $z' = f(z) = \sum_{k=0}^{d} \alpha_k z^k$ be a one-dimensional complex polynomial flow with $\alpha_d = a_d \in \mathbb{R}, d \geq 1$. Then $p = \pm(1,0)$ is a fixed point at infinity and no (limit) cycle at infinity can exist. If $d \geq 2$, there exists a separatrix in the phase portrait. If d is even, there are only finitely many fixed points at infinity.*

Proof. The calculations in the proof of Lemma 5.15 imply that

$$\begin{pmatrix} P_d(1,0) \\ Q_d(1,0) \end{pmatrix} = \begin{pmatrix} 1 \\ 0 \end{pmatrix}.$$

Hence, $(1,0)$ and its antipodal point $(-1,0)$ are critical points at infinity. In the case $d \geq 2$, Theorem 5.16 shows the existence of a separatrix that starts or ends at $p = (1,0)$. Theorem 5.14 implies that for $\alpha_d = a_d$ and d even, there are at most finitely many fixed points at infinity. □

Remark 5.18. It is necessary in Theorem 5.16 to require that $d > 1$. The example $f(z) = z, P(x,y) = x, Q(x,y) = y$ with solution trajectories $x(t) = x(0)\mathrm{e}^t, y(t) = y(0)\mathrm{e}^t$ shows that no separatrices are present.

Example 5.19 (Global Phase Portrait of z^2+1)**.** We apply the theory of this section to investigate the phase space behavior of the dynamical system

$$z' = f(z) = z^2 + 1; \quad z, f(z) \in \mathbb{C} \tag{5.19}$$

which can be regarded as two-dimensional, real ODE

$$x' = x^2 - y^2 + 1$$
$$y' = 2xy.$$

Figure 5.5 illustrates the two-dimensional phase portrait of (5.19) and gives a first impression of the phase space in the bounded region $[-4, 4] \times [-4, 4]$. The phase space consists of periodic orbits around $z = \pm\mathrm{i}$. The only exception is the real axis which seems to diverge to infinity (into a fixed point at infinity).

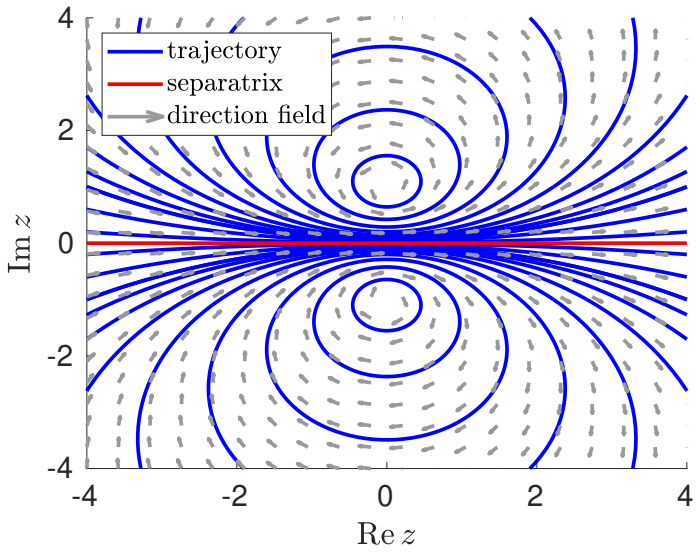

Figure 5.5: Holomorphic flow of $z' = z^2 + 1$. Trajectories in blue, separatrix in red, direction field (normalized vector field) in gray. See [HL19].

The following calculations and applications of the previously presented theorems and statements verify the observations from Fig. 5.6. The finite fixed points are given by $(0, 1)$ and $(0, -1)$. The Jacobian

$$\begin{pmatrix} 2x & -2y \\ 2y & 2x \end{pmatrix}$$

reveals that $(0, 1)$ and $(0, -1)$ are centers with different direction of the flows.

Periodic orbits around these centers are plotted with orange color in Fig. 5.6.

Application of Theorem 5.16 guarantees the existence of a separatrix and according to Corollary 5.17 $p_{1,2} = \pm(1,0)$ are two (of finitely many) critical points at infinity. Explicit calculation of the critical points at infinity is carried out by solving

$$0 = XQ_2(X,Y) - YP_2(X,Y) = Y(X^2+Y^2) = Y$$

and thus are given by $(X,Y,Z) = \pm(1,0,0)$. These two infinite critical points are depicted as green balls in Fig. 5.6 and are the only two equilibria at infinity.

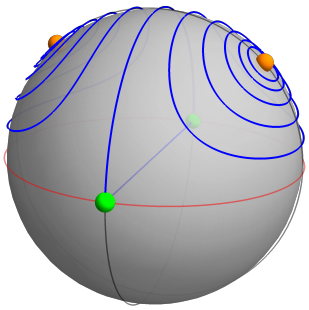

Figure 5.6: Global phase portrait of z^2+1 on the Poincaré sphere. See [HL19].

To determine the type of these equilibria at infinity, the transformed ODE

$$\begin{aligned} \dot{\beta} &= \gamma^2 Q\left(\tfrac{1}{\gamma}, \tfrac{\beta}{\gamma}\right) - \beta\gamma^2 P\left(\tfrac{1}{\gamma}, \tfrac{\beta}{\gamma}\right) &&= \beta + \beta^3 - \beta\gamma^2 \\ \dot{\gamma} &= -\gamma^3 P\left(\tfrac{1}{\gamma}, \tfrac{\beta}{\gamma}\right) &&= -\gamma + \beta^2\gamma - \gamma^3. \end{aligned}$$

is considered. The Jacobian evaluated at $(\beta,\gamma) = (0,0)$ is given by

$$\begin{pmatrix} 1 & 0 \\ 0 & -1 \end{pmatrix}.$$

Consequently, the critical point $(X,Y,Z) = (1,0,0)$ is a saddle point. The equilibrium $(X,Y,Z) = (-1,0,0)$ is a saddle point with opposite direction of the flow because the degree $d = 2$ of the regarded polynomials of the right-hand side is an even number. For the sake of completeness, we would like to add that

$$\begin{pmatrix} P_2(\pm1,0) \\ Q_2(\pm1,0) \end{pmatrix} = \begin{pmatrix} 1 \\ 0 \end{pmatrix} = \pm 1 \cdot \begin{pmatrix} \pm 1 \\ 0 \end{pmatrix},$$

i.e., $\alpha = \pm 1$. Thus, we have an incoming separatrix for $(1, 0)$ and an outgoing separatrix for $(-1, 0)$.

Next, a potential approach for the numerical calculation of separatrices is given below. An eigenvector corresponding to the stable eigenvalue -1 of $(\beta, \gamma) = (0, 0)$ is $e_2 = (0, 1)^\mathsf{T}$. Perturbation of this fixed point into this direction with magnitude ε leads to

$$p_\varepsilon = (0, 0)^\mathsf{T} + \varepsilon e_2 = (0, \varepsilon)^\mathsf{T}.$$

Mapping this point back to the Poincaré sphere yields

$$(X_\varepsilon, Y_\varepsilon, Z_\varepsilon) = \left(\frac{1}{\sqrt{1+\varepsilon^2}}, 0, \frac{\varepsilon}{\sqrt{1+\varepsilon^2}} \right).$$

A back transformation to the (x, y) coordinates results in the point $(x_\varepsilon, y_\varepsilon) = \left(\frac{1}{\varepsilon}, 0\right)$. Since $y_\varepsilon = 0$, the perturbed point is already on the separatrix and propagation in backward time directly calculates the separatrix numerically.

For practical purposes, this approach may have the drawback that it relies on the calculation of critical points at infinity. Nevertheless, it shows a way how separatrices can be numerically calculated.

The next example turns back to the context of slow invariant manifolds and shows that in general even (real) polynomial ODEs can lead to numerical difficulties since incomplete trajectories exist. This requires a special treatment of such trajectories.

Example 5.20 (Michaelis-Menten-Henri example)**.** The Michaelis-Menten-Henri enzyme mechanism introduced in Example 2.27 is given by the chemical reaction mechanism

$$S + E \rightleftharpoons C \to P + E, \tag{5.20}$$

where S is a substrate, E is an enzyme, C the corresponding substrate-enzyme-complex and P a product. Simplifying the ODE (cf. [Mur93]) which underlies (5.20) results in the following ODE (in Section 3.4.2 we chose $\kappa = 1$ and $\beta = 0.5$).

$$\begin{aligned} \dot{x}(t) &= -x(t) + \big(x(t) + \kappa - \beta\big)\, y(t) \\ \varepsilon \dot{y}(t) &= x(t) - \big(x(t) + \kappa\big)\, y(t). \end{aligned}$$

Although the underlying ODEs of mass-action-type chemical reaction mechanisms have polynomial right-hand sides, in general two-dimensional, chemical ODEs

cannot be interpreted as real and imaginary part of a complex polynomial as right-hand side because they have to satisfy additional constraints (cf. Lemma 5.15). Application of the theory of this section is thus limited. Fixed points at infinity have to satisfy Proposition 5.13(c), i.e.,

$$\begin{pmatrix} P_2(x,y) \\ Q_2(x,y) \end{pmatrix} = \begin{pmatrix} x \\ y \end{pmatrix}^{\mathsf{T}} \begin{pmatrix} P_2(x,y) \\ Q_2(x,y) \end{pmatrix} \begin{pmatrix} x \\ y \end{pmatrix}$$

$$\Leftrightarrow \qquad \begin{pmatrix} xy \\ -\frac{xy}{\varepsilon} \end{pmatrix} = \begin{pmatrix} x^2 y(x - \frac{y}{\varepsilon}) \\ xy^2(x - \frac{y}{\varepsilon}) \end{pmatrix}.$$

A short calculation reveals that the fixed points at infinity are

$$\begin{pmatrix} x \\ y \end{pmatrix} \in \left\{ \pm \begin{pmatrix} 0 \\ 1 \end{pmatrix}, \pm \begin{pmatrix} 1 \\ 0 \end{pmatrix}, \pm \frac{1}{\sqrt{1+\varepsilon^2}} \begin{pmatrix} \varepsilon \\ -1 \end{pmatrix} \right\}.$$

Only the infinite fixed points $\pm \frac{1}{\sqrt{1+\varepsilon^2}}(\varepsilon, -1)^{\mathsf{T}}$ are generic, i.e.,

$$\begin{pmatrix} x \\ y \end{pmatrix}^{\mathsf{T}} \begin{pmatrix} P_2(x,y) \\ Q_2(x,y) \end{pmatrix} \neq 0.$$

Theorem 18 in [GS13] concludes that for those fixed points there is at least one incoming resp. outgoing trajectory that has finite maximum interval of existence (a separatrix). The bottom line is that the ODE for the Michaelis-Menten enzyme mechanism is incomplete.

We close this section with the global phase portrait of $\cosh(z - 1/2)$. Although it is not a polynomial system, we show a possibility to apply the results of this section to this non-polynomial function.

Example 5.21 (Global Phase Portrait of $\cosh(z - 1/2)$)**.** The theory of the transformation to the Poincaré sphere is not applicable for cosh since it is not a polynomial. However, the global phase portrait of $z' = \cosh(z - 1/2)$ can be described using the phase portrait of $z' = z^2 + 1$. The transformation $w(t) = \exp\big(z(2t) - 1/2\big)$ turns every solution trajectory of $z' = \cosh(z - 1/2)$ into a solution trajectory of $w' = w^2 + 1$. Essentially, the inverse transformation is the logarithm. As a consequence, the global phase portrait of $z' = z^2 + 1$ is homeomorphic to the phase

portrait of $z' = \cosh(z - 1/2)$ in each strip $S_k \coloneqq \{z \in \mathbb{C} \colon 2k\pi \leq \operatorname{Im} z < 2(k+1)\pi\}$ for $k \in \mathbb{Z}$, where the logarithm is bijective.

5.3 Lyapunov Exponents

The theory of Lyapunov exponents goes back to Lyapunov's doctoral thesis (for an English translation see [Lya92]) and is one of the first systematic studies about stability and long-term behavior of ODE solutions. Lyapunov applies a small perturbation to the initial value of an IVP and then analyzes how the solution changes in the long run. In this respect, his theory can be understood as global analysis of trajectories. In the following section, we study to what extent Lyapunov's theory provides us with a deeper understanding of separatrices and SIMs. The introduction to Lyapunov Exponents in this section is based on [Mei07].

5.3.1 Motivation

Let $\Omega \subset \mathbb{R}^n$ and $f \colon \Omega \to \mathbb{R}^n$ be a Lipschitz continuous function with global Lipschitz constant L. Consider the ODE

$$z'(t) = f\big(z(t)\big) \tag{5.21}$$

and a reference trajectory $z_{\text{ref}}(t)$ which solves (5.21) for a given initial value $z_{\text{ref}}(0) = z_{\text{ref}}^{(0)} \in \Omega$. (Later we turn back to holomorphic functions f and $\Omega \subset \mathbb{C}$. For the moment, we replace $\mathbb{C}$ by its identification $\mathbb{R}^2$.)

Let $z(t)$ be another arbitrary trajectory (which is a solution of (5.21) with $z(0) = z^{(0)} \in \Omega$). Gronwall's inequality (see [Tes04, Theorem 2.6]) restricts the difference of both trajectories to grow at most

$$\left\| z_{\text{ref}}(t) - z(t) \right\| \leq \exp(Lt) \left\| z_{\text{ref}}^{(0)} - z^{(0)} \right\|, \tag{5.22}$$

where L is the Lipschitz constant of f. Thus, it is expected that in the long-term, i.e., for t big enough

$$\left\| z_{\text{ref}}(t) - z(t) \right\| \approx \exp(\lambda t) \left\| z_{\text{ref}}^{(0)} - z^{(0)} \right\|,$$

for an undetermined constant λ. Roughly speaking, the Lyapunov exponent λ is a quantity that describes the speed of divergence of those two regarded trajectories. A mathematical precise definition is given in the following subsection.

5.3.2 Definition

The definition of Lyapunov exponents requires a mathematical handling of infinitesimally close trajectories. Appropriate tools for studying these geometric properties are provided by the field of differential geometry (see Section 2.3).

For simplicity, we first consider the $\mathbb{R}^n$ and later move to the more abstract setting of smooth manifolds. Let Ω be a subset of $\mathbb{R}^n$. At first, we fix a trajectory by picking an initial value $z^* \in \Omega$. We call the unique solution curve of Eq. (5.21) with initial value z^* the *reference trajectory*, denoted by z_{ref}. Perturbing the initial value z^*, we investigate the dynamics of

$$z^* + \varepsilon v_0, \quad \varepsilon \in \mathbb{R}_+, v_0 \in \mathbb{R}^n.$$

Taylor approximation in ε of a in ε continuously differentiable flow mapping $\Phi(t, z^* + \varepsilon v_0)$ that starts at $z^* + \varepsilon v_0$ yields

$$\Phi(t, z^* + \varepsilon v_0) = \Phi(t, z^*) + \varepsilon D_z \Phi(t, z^*) v_0 + o(\varepsilon), \tag{5.23}$$

where $D_z\Phi$ is the differential of the flow map with respect to the state z. Thus, the initial perturbation vector v_0 evolves to

$$v(t) = D_z \Phi(t, z^*) v_0 + o(1) \quad \text{as} \quad \varepsilon \to 0. \tag{5.24}$$

Hence, the sensitivities $D_z\Phi(t, z^*)$ of the ODE solution with respect to the initial value z^* map the initial perturbation v_0 approximately to $v(t)$.

In general, $D_z\Phi$ is analytically not known. For its numerical computation, we derive a ODE for $v(t)$ in the following, which can be solved with a standard numerical ODE solver. Since $\Phi(t, z^*)$ yields a solution of Eq. (5.21), a further Taylor expansion of f about $\Phi(t, z^*)$ leads to

$$\begin{aligned} f\big(\Phi(t, z^*)\big) + \varepsilon v'(t) &= \frac{\mathrm{d}}{\mathrm{d}t}\big(\Phi(t, z^*) + \varepsilon v(t)\big) \overset{(5.23)}{=} \frac{\mathrm{d}}{\mathrm{d}t}\big(\Phi(t, z^* + \varepsilon v_0) + o(\varepsilon)\big) \\ = f\big(\Phi(t, z^* + \varepsilon v_0)\big) + o(\varepsilon) &\overset{(5.23)}{=} f\big(\Phi(t, z^*) + \varepsilon v(t) + o(\varepsilon)\big) + o(\varepsilon) \end{aligned}$$

$$\overset{\text{Taylor}}{=} f\big(\Phi(t,z^*)\big) + \varepsilon f'\big(\Phi(t,z^*)\big)v(t) + o(\varepsilon).$$

This shows that to first order in ε, we have

$$v'(t) \approx f'\big(\Phi(t,z^*)\big)v(t) = f'\big(z_{\text{ref}}(t)\big)v(t), \qquad v(0) = v_0.$$

The linearization

$$v'(t) = f'\big(\Phi(t,z^*)\big)v(t) = f'\big(z_{\text{ref}}(t)\big)v(t), \qquad v(0) = v_0 \tag{5.25}$$

is denoted *variational ODE* of f w.r.t. the reference trajectory $z_{\text{ref}}(t)$. Since, we are interested in the limit $\varepsilon \to 0$, the variational ODE contains the essential information for the evolution of the perturbation $v(t)$.

Proposition 5.22. *Assuming Φ to be twice continuously differentiable w.r.t. z, the solution of the variational ODE* (5.25) *is given by* (*cf.* (5.24))

$$v(t) \coloneqq D_z\Phi(t,z^*)v_0.$$

Proof. Since Φ is twice continuously differentiable w.r.t. to z, it holds

$$\begin{aligned} v'(t) &= \frac{\mathrm{d}}{\mathrm{d}t} D_z\Phi(t,z^+)v_0 = D_z \frac{\mathrm{d}}{\mathrm{d}t}\Phi(t,z^*)v_0 = D_z f\big(\phi(t,z^*)\big)v_0 \\ &= f'\big(\Phi(t,z^*)\big)D_z\Phi(t,z^*)v_0 = f'\big(\Phi(t,z^*)\big)v(t) \end{aligned}$$

and $v(0) = D_z\Phi(0,z)v_0 = Iv_0 = v_0$. □

In a more general setting, $M = \Omega$ is a smooth manifold and $p \in M$. The initial perturbation direction v_0 corresponds to a tangent vector. Consequently, $v(t)$ should be a point in the tangent space $T_{\Phi(t,z^*)}M$. Then, (5.25) can be interpreted as follows. The Jacobian $f'\big(z_{\text{ref}}(t)\big)$ linearly maps the perturbation vector $v(t) \in T_{\Phi(t,z^*)}M$ to its rate of change vector. As motivated before, we expect that in many cases there is a real number λ such that for t sufficiently large

$$\big\|v(t)\big\| \approx \mathrm{e}^{\lambda t}\,\|v_0\|\,.$$

The following definition clarifies the actual meaning of λ in the relation above.

Definition 5.23 (Lyapunov Exponent)**.** Let $z_{\text{ref}}(t)$ be a solution of the holomorphic flow $z' = f(z)$ in an open set $\Omega \subset \mathbb{C}$ (possibly a Newton flow). The *Lyapunov Exponent* $\lambda(v_0)$ for a given initial perturbation $v(0) = v_0$ is defined as

$$\lambda(v_0) \coloneqq \limsup_{t\to\infty} \frac{1}{t} \log \left\| v(t) \right\|,$$

where $v(t)$ is the solution of the variational ODE (5.25) w.r.t. $z_{\text{ref}}(t)$.

Note that in Definition 5.23, the initial perturbation is infinitesimal. Thus, v^0 is more an initial perturbation direction than a vector.

Moreover, Lyapunov exponents have the following properties which can be used for a more abstract definition (see [Bar17]).

Proposition 5.24. *The Lyapunov exponent $\lambda\colon T_{z^*}M \to \mathbb{R}\cup\{-\infty\}$ satisfies the following statements.*

(*i*) $\lambda(\alpha v) = \lambda(v)$ *for all* $v \in T_{z^*}M$ *and* $\alpha \in \mathbb{R} \setminus \{0\}$.

(*ii*) $\lambda(v + w) \leq \max\{\lambda(v), \lambda(w)\}$ *for all* $v, w \in T_{z^*}M$.

(*iii*) $\lambda(0) = -\infty$.

Proof. See Barreira [Bar17]. □

It should be mentioned that equality in (ii) holds for $\lambda(v) \neq \lambda(w)$.

5.3.3 Lyapunov Exponents and the TBOA

The variational ODE (5.25) already appears in the first order conditions for the TBOA (5.4). The Lagrangian multipliers λ in (5.4) solve the *adjoint* variational ODE $\lambda' = -\overline{f'(z_{\text{ref}})}\lambda$ where the right-hand side has opposite sign and involves the conjugate of f'. The Lagrangian multipliers $\lambda(t)$ can be used to define a *dual Lyapunov exponent*. For more information on dual Lyapunov exponents see Barreira [Bar17].

Another connection to Lyapunov exponents is hidden in the objective function of the TBOA. Since $z''(t_0) = f'(z_0) \cdot f(z_0)$, the objective function can be written as $\left\| v'(0) \right\|$ for the initial perturbation in direction of the flow: $v_0 = v(0) = f(z_0)$.

Following the notation of this section, $v(t)$ is the (primal) Lyapunov exponent. This makes the strong correlation of the TBOA and Lyapunov exponents clear. In a sense, the TBOA implicitly computes finite-time Lyapunov exponents.

Dietrich and Lebiedz (personal communication, 2019) use this backward time Lyapunov exponents to determine the SIM by distinguishing the long-term behavior of trajectories. Adding a few assumptions links the Lyapunov exponents to the previously described phase space splitting depending on the different time scales (cf. Section 2.2). In this context, the SIM can be defined as a so-called Lyapunov set of the slowest backwards time-scale. This is subject to current work in the PhD thesis of Dietrich and may yield a way to get a unique SIM.

5.3.4 Lyapunov Exponents for the Newton Flow

As its name might suggests, the separatrix in $\mathbb{R}^2$ has the property of dividing two trajectories that are close to each other but on two different sides of the separatrix. Picking an arbitrary trajectory near a separatrix and calculation of the Lyapunov exponents for all possible initial perturbation vectors v_0 may allow to decide where the separatrix is located exactly. This is the central issue of this subsection.

For one-dimensional complex differential equations, the variational ODE (5.25) has the simple solution

$$v(t) = \frac{f\big(z_{\text{ref}}(t)\big)}{f\big(z_{\text{ref}}^{(0)}\big)} v_0 \tag{5.26}$$

as differentiation shows

$$v'(t) = \frac{f'\big(z_{\text{ref}}(t)\big) z'_{\text{ref}}(t)}{f\big(z_{\text{ref}}^{(0)}\big)} v_0 = f'\big(z_{\text{ref}}(t)\big) \frac{f\big(z_{\text{ref}}(t)\big)}{f\big(z_{\text{ref}}^{(0)}\big)} v_0 = f'\big(z_{\text{ref}}(t)\big) v(t).$$

This allows us to analytically calculate Lyapunov exponents in the following subsections. We start with a closer consideration of Newton flows.

Newton Flow Consider the Newton flow

$$z' = f(z) \coloneqq -\frac{g(z)}{g'(z)} \tag{5.27}$$

for a holomorphic function $g\colon \Omega \subset \mathbb{C} \to \mathbb{C}$ (i.e., we consider the manifold $M = \Omega$). Suppose it has a solution $z_{\text{ref}}(t)$ for the initial value $z_{\text{ref}}(0) = z_{\text{ref}}^{(0)}$. As seen in (4.16),

it holds

$$g\big(z_{\text{ref}}(t)\big) = g\big(z_{\text{ref}}^{(0)}\big)\mathrm{e}^{-t}.$$

Inserting this equation into the solution (5.26) gives

$$v(t) = \frac{f\big(z_{\text{ref}}(t)\big)}{f(z_{\text{ref}}^{(0)})}v_0 = \frac{g(z_{\text{ref}}^{(0)})\mathrm{e}^{-t}}{g'\big(z_{\text{ref}}(t)\big)} \cdot \frac{g'(z_{\text{ref}}^{(0)})}{g(z_{\text{ref}}^{(0)})}v_0 = \frac{\mathrm{e}^{-t}}{g'\big(z_{\text{ref}}(t)\big)}g'\big(z_{\text{ref}}^{(0)}\big)v_0.$$

Using the complex logarithm formulas of the principal branch

$$\log z = \log|z| + \mathrm{i}\,\arg(z), \quad \Rightarrow \log|z| = \mathrm{Re}\big(\log z\big)$$

$$\mathrm{Re}\left(\log\frac{\mathrm{e}^{-t}}{g'\big(z_{\text{ref}}(t)\big)}\right) = \mathrm{Re}\left(-t - \log g'\big(z_{\text{ref}}(t)\big) + 2k\pi\mathrm{i}\right) = -t - \mathrm{Re}\log g'\big(z_{\text{ref}}(t)\big),$$

for some $k \in \mathbb{Z}$, we get

$$\frac{1}{t}\log\big\|v(t)\big\| = -1 - \frac{1}{t}\left(\mathrm{Re}\log g'\big(z_{\text{ref}}(t)\big) - \mathrm{Re}\log g'\big(z_{\text{ref}}^{(0)}\big) - \mathrm{Re}\log v_0\right).$$

Therefore, the Lyapunov exponent depends only on the real part of $\log g'\big(z_{\text{ref}}(t)\big)$.

In principle, there are two cases to distinguish. The first corresponds to an infinite maximum positive interval of existence $I = (t_-, t_+)$ for the reference trajectory, i.e., $t_+ = \infty$. If additionally $z_{\text{ref}}(t)$ is bounded it converges to a zero of g according to Proposition 4.8. Provided that this zero is simple, $\mathrm{Re}\log g'\big(z_{\text{ref}}(t)\big)$ converges as $t \to t_+$ and thus, the Lyapunov exponent is $\lambda = -1$.

The second case corresponds to separatrices. Their finite maximum interval of existence $I = (t_0, t_+)$ prevents us from taking the limit $t \to \infty$. Hence, Lyapunov exponents are not well defined for separatrices. A possible way out of this dilemma is to either set Lyapunov exponents to infinity for separatrices or to desingularize the Newton Flow (see the following Section 5.3.5).

5.3.5 Lyapunov Exponents for the Desingularized Newton Flow

The desingularized Newton flow of a function g introduced in Section 4.3.4 has the same trajectories as the Newton (5.27) flow with a different property for the separatrices. These now converge to a zero of g' as $t \to \infty$. Though the desingularized separatrices have infinite maximum intervals of existence in the

desingularized flow, we call them, for convenience, still *separatrices*. This section studies the calculation of Lyapunov exponents in the desingularized Newton flow and its consequences for the characterization of separatrices.

Starting point is again (4.20), i.e., the flow of $z'(t) = -\overline{g'(z)}g(z)$. In the light of (dual) Lyapunov exponents, this differential equation is closely related to the adjoint variational ODE with initial perturbation in direction of the vector field g. In order to clarify this, define $\mu(t)$ by the adjoint variational ODE $\mu'(t) = -\overline{g'\big(z(t)\big)}\mu(t)$ with initial perturbation $\mu(0) = g\big(z(0)\big)$. Then it holds

$$z'(0) = -\overline{g'\big(z(0)\big)}g\big(z(0)\big) = \mu'(0).$$

However, $\mu(t)$ and $z(t)$ generally differ in the long run.

The Newton flow (5.27) has the problem that Lyapunov exponents are not be defined for separatrices. Hence, we consider what the desingularization implies for the Lyapunov exponents. As seen in Section 4.3.4, all bounded trajectories have infinite maximum interval of existence. With [Tes04, Theorem 2.12] it follows that the solution of the variational ODE (5.25) exists globally. Therefore, the desingularized Newton flow overcomes the difficulties of the Newton flow and Lyapunov exponents can be defined for separatrices as well.

In the following we analyze the desingularized Newton flow of z^2+1 and calculate the corresponding Lyapunov exponents. Explicit calculations for $\cosh(z-1/2)$ and $\xi(z)$ are difficult.

Example 5.25 (Desingularized z^2+1 flow)**.** Recall that for the (non-desingularized) Newton flow, all Lyapunov exponents were -1 for bounded trajectories with infinite maximum interval of existence if they converge to a simple zero of g. For these special trajectories, the Lyapunov exponent was independent of the initial perturbation direction $v_0 \neq 0$.

The desingularized Newton flow of z^2+1 has the form

$$z'(t) = -2\overline{z(t)}\big(z^2(t)+1\big)$$

and can be transformed into the following $\mathbb{R}^2$ differential equations

$$\begin{aligned} x'(t) &= -2x(t)\big(x(t)^2 + y(t)^2 + 1\big), \\ y'(t) &= -2y(t)\big(x(t)^2 + y(t)^2 - 1\big). \end{aligned}$$

Maple computes the solution of this differential system for general initial values $x(0) = x_0 \neq 0$ and $y(0) = y_0$ to be

$$\begin{aligned} x(t) &= \pm 2\mathrm{e}^{-4t}\big(h(t)\big)^{-\frac{1}{2}}, \quad y(t) = \pm 2\frac{|y_0|}{|x_0|}\big(h(t)\big)^{-\frac{1}{2}}, \\ h(t) &:= 4\frac{-x_0^2\mathrm{e}^{-8t} + (x_0^2 - y_0^2 + 1)\mathrm{e}^{-4t} + y_0^2}{x_0^2}, \end{aligned} \tag{5.28}$$

where the function $h(t)$ is introduced to display the solution formulas shorter. Function h assigns only positive values. For $t = 0$, it holds

$$h(0) = 4\frac{-x_0^2 + (x_0^2 - y_0^2 + 1) + y_0^2}{x_0^2} = \frac{4}{x_0^2} > 0.$$

Furthermore, differentiation of $h(t)$ shows that the only extremum of h is a maximum at $t^* = -\frac{1}{4}\big(\log(x_0^2 - y_0^2 + 1) - \log(2x_0^2)\big)$, whenever t^* is well defined. Moreover, we compute

$$\lim_{t\to\infty} h(t) = 4\frac{y_0^2}{x_0^2} \geq 0.$$

This shows that (5.28) is well defined for all $t \geq 0$. For $x_0 = 0$ and $y_0 \neq 0$, the solution of the desingularized Newton flow is given by

$$x(t) = 0, \quad y(t) = \left(1 - \frac{y_0^2 - 1}{y_0^2}\mathrm{e}^{-4t}\right)^{-\frac{1}{2}}.$$

Solution of the Variational ODE The variational ODE is given by

$$\begin{pmatrix} v_x' \\ v_y' \end{pmatrix} = \begin{pmatrix} -6x^2 - 2y^2 - 2 & -4xy \\ -4xy & -2x^3 - 6y^2 + 2 \end{pmatrix} \begin{pmatrix} v_x \\ v_y \end{pmatrix}. \tag{5.29}$$

Its solution for $x_0 \neq 0$ was computed by Maple to be

$$v_x(t) = \exp\left(-6\int_0^t \tilde{h}(\tau)\,\mathrm{d}\tau\right)\Big[y_0\tilde{v}\mathrm{e}^{2t} + \big(v_x(0) - y_0\tilde{v}\big)\mathrm{e}^{-2t}\Big] \tag{5.30a}$$

$$v_y(t) = \frac{1}{x_0}\exp\left(-6\int_0^t \tilde{h}(\tau)\,\mathrm{d}\tau - 2t\right)\Big[\big(v_y(0) - x_0\tilde{v}\big)x_0\mathrm{e}^{4t} + x_0^2\tilde{v}\Big], \tag{5.30b}$$

with

$$\tilde{h}(t) \coloneqq \frac{y_0^2 \mathrm{e}^{8t} + x_0^2}{y_0^2 \mathrm{e}^{8t} + (x_0^2 - y_0^2 + 1)\mathrm{e}^{4t} - x_0^2} \quad \text{and} \quad \tilde{v} \coloneqq y_0 v_x(0) - x_0 v_y(0).$$

If $x_0 = 0$, (5.29) is solved by

$$v_x(t) = \left(y_0^2 \mathrm{e}^{8t} - (y_0^2 - 1)\mathrm{e}^{4t}\right)^{-\frac{1}{2}} v_x(0), \tag{5.31a}$$

$$v_y(t) = \frac{\mathrm{e}^{2t}}{\left(1 + y_0^2\left(\mathrm{e}^{4t} - 1\right)\right)^{\frac{3}{2}}} v_y(0). \tag{5.31b}$$

In order to compute the Lyapunov exponents, all terms in the solution (5.30) have to be ordered by their growth rate as t tends to infinity. Thus, we recall the following definition:

Definition 5.26. A function $f\colon \mathbb{R} \to \mathbb{R}$ is asymptotically bounded below and above by a function $g\colon \mathbb{R} \to \mathbb{R}$, in symbol $f = \Theta(g)$, if there are constants $c, C > 0$ and $t_0 > 0$ such that $c|g(t)| \leq |f(t)| \leq C|g(t)|$ for all $t \geq t_0$.

For the growth rates of (5.30), it remains to determine the growth rate of the integral over $\tilde{h}$. First consider the case $y_0 \neq 0$. For t large enough, $\tilde{h}$ bounded from above by

$$\tilde{h}(t) \leq \frac{y_0^2 \mathrm{e}^{8t} + x_0^2}{y_0^2 \mathrm{e}^{8t}}.$$

Consequently, we have

$$\int_0^t \tilde{h}(\tau)\,\mathrm{d}\tau \leq \int_0^t 1 + \frac{x_0^2}{y_0^2}\mathrm{e}^{-8\tau}\,\mathrm{d}\tau = t - \frac{x_0^2}{8y_0^2}\mathrm{e}^{-8t} + \frac{x_0^2}{8y_0^2}.$$

On the other hand, $\tilde{h}$ is asymptotically bounded below by

$$\tilde{h}(t) \geq \frac{y_0^2 \mathrm{e}^{8t}}{y_0^2 \mathrm{e}^{8t} + (x_0^2 - y_0^2 + 1)\mathrm{e}^{4t}}.$$

Consequently, we have

$$\begin{aligned}\int_0^t \tilde{h}(\tau)\,\mathrm{d}\tau &\geq \int_0^t \left(1+\frac{x_0^2-y_0^2+1}{y_0^2}\mathrm{e}^{-4\tau}\right)^{-1}\mathrm{d}\tau \\ &= \frac{1}{4}\left[\log\left(\mathrm{e}^{4\tau}+\frac{x_0^2-y_0^2+1}{y_0^2}\right)\right]_{\tau=0}^{t} \\ &= \frac{1}{4}\left[\log\left(\mathrm{e}^{4t}+\frac{x_0^2-y_0^2+1}{y_0^2}\right)\right]-\frac{1}{4}\left[\log\left(1+\frac{x_0^2-y_0^2+1}{y_0^2}\right)\right].\end{aligned}$$

Hence, $\exp\left(-6\int_0^t \tilde{h}(\tau)\,\mathrm{d}\tau\right)=\Theta\big(\mathrm{e}^{-6t}\big)$. A direct consequence is that

$$\begin{aligned} v_x(t) &= \Theta\big(\mathrm{e}^{-4t}\big), && \text{if } \tilde{v}=y_0v_x(0)-x_0v_y(0)\neq 0,\\ v_y(t) &= \Theta\big(\mathrm{e}^{-4t}\big), && \text{if } v_y(0)-x_0\tilde{v}\neq 0.\end{aligned}$$

For $v_x(0)^2+v_y(0)^2\neq 0$, either $v_x(t)=\Theta\big(\mathrm{e}^{-4t}\big)$ or $v_y(t)=\Theta\big(\mathrm{e}^{-4t}\big)$. Therefore, the Lyapunov exponents for all reference trajectories with initial values $x_0\neq 0$ and $y_0\neq 0$ are smaller than -4.

It remains to calculate the Lyapunov exponents for the stable and unstable manifolds at $z=0$. First consider the separatrix as reference trajectory, i.e., $y_0=0$ and $x_0\neq 0$. In this case, function $\int_0^t \tilde{h}(\tau)\,\mathrm{d}\tau$ belongs to the class $\Theta(1)$. Since $y_0\tilde{v}=0$, (5.30) yields

$$v_x(t)=\begin{cases}\Theta\big(1\big) & \text{for } v_x(0)=0,\\ \Theta\big(\mathrm{e}^{-2t}\big) & \text{for } v_x(0)\neq 0.\end{cases}$$

Analogously, $v_y(0)-x_0\tilde{v}=v_y(0)(1+x_0^2)$ implies

$$v_y(t)=\begin{cases}\Theta\big(\mathrm{e}^{-2t}\big) & \text{for } v_y(0)=0,\\ \Theta\big(\mathrm{e}^{2t}\big) & \text{for } v_y(0)\neq 0.\end{cases}$$

Denoting by $e_1=(1,0)^\mathsf{T}, e_2=(0,1)^\mathsf{T}$ the canonical basis for $\mathbb{R}^2$, we obtain

$$\lambda(e_1)=-2 \quad \text{and} \quad \lambda(e_2)=2.$$

For $x_0=0$, the Lyapunov exponents can be easily determined by (5.31) to be

$\lambda(e_1) = \lambda(e_2) = -4$. Using the properties of Lyapunov exponents in Proposition 5.24, all exponents $\lambda\big(v(0)\big)$ are smaller than -4.

The bottom line of these rather long calculations is that the separatrix of the Newton flow of $z^2 + 1$ is uniquely determined by the Lyapunov exponents of the desingularized Newton flow. While all Lyapunov exponents for initial values of the reference trajectory off the separatrix are smaller than -4, the exponents for initial value on the separatrix are -2 or 2 (except for $v(0) = 0$).

5.4 A Topological View on Separatrices of Periodic Orbits

In this section, we extend the investigations of Broughan [Bro03a; Bro03b; Bro05]. For this purpose, we denote the set of trajectories with the same stability behavior as *stability region*, e.g., the set containg a center and all periodic orbits around it or the set containg a stable node and all trajectories converging to it are stability regions. In the notation of Broughan, these are called neighborhoods. We try to avoid this term because open sets and balls are often referred to as neighborhoods. Broughan analyzes the stability regions of centers, foci, nodes, and elliptic sectors of holomorphic flows. He was able to show that the boundary components of these stability regions are separatrices in the sense of Definition 4.2. In the following, we restrict ourselves to the case of boundary components of two adjacent centers, i.e. where the stability regions of two centers have non-empty intersection (see Fig. 4.2). We show that the index of trajectories around centers changes by traversing a common separatrix (cf. Figs. 4.2 and 4.3). This section can be found in [HL19]. First, we define the term *transit time* which is needed for the proof of the main result in this section.

Definition 5.27 (Transit Time (cf. Definition 3.2 in [Bro03b]))**.** Let γ be an orbit of the holomorphic flow $z' = f(z)$. For $x, y \in \gamma$ the *transit time* $\tau(x, y)$ is defined by

$$\tau(x, y) \coloneqq \int_x^y \frac{1}{f(z)}\,\mathrm{d}z,$$

where the integration path is given by γ.

The following Theorem 5.28 characterizes separatrices in holomorphic dynamical systems (not only polynomial systems), where two regions with periodic orbits

inside have common boundary. The winding number of a periodic orbit around a center is ± 1 and has the same sign for all periodic orbits around the same center. However, the periodic orbits on the other side of the separatrix (and thus around another center) must have the opposite winding number.

Theorem 5.28. *Let z_0, z_1 be two adjacent centers of the flow (5.1) with a holomorphic function f. Let the stability regions*

$$P_k \coloneqq \{z_k\} \cup \big\{ z^* \in \mathbb{C} \colon \textit{solution of (5.1) with } z(0) = z^* \textit{ is a periodic orbit around } z_k \big\}, \ k \in \{0,1\}$$

have common boundary component $C \subset \partial P_0 \cap \partial P_1$ containing at least two different points (according to Broughan [Bro03b] C is a separatrix). Then it holds $z^* \in C$ iff for all $\varepsilon > 0$ small enough, there exists $z_k^* \in U_\varepsilon(z^*) \cap P_k, \ k \in \{0,1\}$ such that the orbits γ_k of the flow (5.1) with $z(0) = z_k^*$ satisfy $\operatorname{ind}_{\gamma_0}(z_0) \cdot \operatorname{ind}_{\gamma_1}(z_1) = -1$.

Proof. If for all $\varepsilon > 0$ there are $z_k^* \in U_\varepsilon(z^*) \cap P_k, \ k \in \{0,1\}$, then $z^* \in \partial P_0 \cap \partial P_1$ because P_0 and P_1 have empty intersection. According to Broughan [Bro03b], z^* is thus part of a separatrix.

The interesting part of the proof is to show that the index of trajectories changes by traversing the separatrix. Let z^* be part of a boundary component C of $\partial P_0 \cap \partial P_1$. The separatrix C is a trajectory. So for $\varepsilon > 0$ small enough there are two points $x, y \in U_{\varepsilon/2}(z^*) \cap C$ with $x \neq y$. Claim A in the proof of [Bro03b, Theorem 4.1] yields that $\forall \delta > 0 \, \exists \, \varepsilon_\delta > 0$ such that all orbits α_k with

$$x_k' \in \alpha_k \cap U_{\varepsilon_\delta}(x) \cap P_k \neq \emptyset \text{ and } y_k' \in \alpha_k \cap U_{\varepsilon_\delta}(y) \cap P_k \neq \emptyset$$

it holds

$$\big|\tau(x_k', y_k') - \tau(x, y)\big| < \delta \quad \text{for } k \in \{0,1\}.$$

Thus, we have $\big|\tau(x_0', y_0') - \tau(x_1', y_1')\big| < 2\delta$. Since $\delta > 0$ is arbitrary, $\tau(x_0', y_0')$ and $\tau(x_1', y_1')$ must have the same sign. If we take orbits α_k such that x_k' resp. y_k' have minimum distance to x resp. y, then we can make use of the Jordan curve theorem in order to show that the interiors of α_k (which contain z_k) are to the left of α_0 and to the right of α_1 or vice versa. In other words,

$$\operatorname{ind}_{\alpha_0}(z_0) \cdot \operatorname{ind}_{\alpha_1}(z_1) = -1.$$

□

Example 5.29. We consider the function $f(z) = \cosh(z - 1/2)$ again. Figure 4.2 includes the direction field of f. It is easy to see that the index of orbits in the strip $S_k \coloneqq \left\{ z \in \mathbb{C} \colon \operatorname{Im} z \in \big(k\pi, (k+1)\pi\big) \right\}$ is $(-1)^k$. In accordance with Theorem 5.28, the index changes at each separatrix $\operatorname{Im} z = k\pi, k \in \mathbb{Z}$ for $k \in \mathbb{Z}$.

More topological aspects of separatrices emerge in the following section.

5.5 Complex Time

So far, we analyzed dynamical systems $z'(t) = f\big(z(t)\big)$ for a holomorphic function f in some interval $[t_0, t_\mathrm{f}] \ni t$. Both, f and $z(t)$ are complex valued. However, the time t is not a complex variable. Thus, it seems natural to allow the time to be a complex variable in order to have a setting where all variables are defined in the complex plane. The consequences of a complex time point of view of dynamical systems and separatrices are studied in this section. But first, complex time flows are defined. We conclude that real and imaginary time combine lines of constant phase and magnitude in a natural way. The idea of introducing complex time traces back to Lebiedz (personal communication). Moreover, Broughan [Bro03b, p. 12] expects a deeper understanding of separatrices in the light of complex time. The first two subsections of this section are based on [HL19].

For the rest of this section, t is a complex time variable $t = \tau_1 + \mathrm{i}\tau_2$ with $\tau_1, \tau_2 \in \mathbb{R}$. Differential equations $z'(t) \coloneqq \frac{\mathrm{d}z(t)}{\mathrm{d}t} = f\big(z(t)\big)$ are understood in the sense of Definition 2.6. Assuming solutions $z(t)$ being holomorphic functions of complex time, it follows immediately that

$$\frac{\mathrm{d}z(t)}{\mathrm{d}\tau_1} \coloneqq \frac{\mathrm{d}z(\tau_1 + \mathrm{i}\tau_2)}{\mathrm{d}\tau_1} = f\big(z(t)\big) \tag{5.32}$$

$$\frac{\mathrm{d}z(t)}{\mathrm{d}\tau_2} \coloneqq \frac{\mathrm{d}z(\tau_1 + \mathrm{i}\tau_2)}{\mathrm{d}\tau_2} = \mathrm{i} f\big(z(t)\big). \tag{5.33}$$

We refer to (5.32) and (5.33) as *real* and *imaginary time flow* respectively. Since multiplication in $\mathbb{C}$ with $\mathrm{i} = \mathrm{e}^{\mathrm{i}\frac{\pi}{2}}$ corresponds to a rotation by $90°$ in mathematical positive direction in $\mathbb{R}^2$, the real time flow is orthogonal to the imaginary time flow, i.e., $\langle \frac{\mathrm{d}z(t)}{\mathrm{d}\tau_1}, \frac{\mathrm{d}z(t)}{\mathrm{d}\tau_2} \rangle_{\mathbb{R}^2} = 0$. Here, $\langle \cdot, \cdot \rangle_{\mathbb{R}^2}$ denotes the Euclidean inner product in $\mathbb{R}^2$ when the complex values $\frac{\mathrm{d}z(t)}{\mathrm{d}\tau_k}$ are identified in $\mathbb{R}^2$ by their real and imaginary parts.

We call a real time trajectory (5.32) a *positive* (*negative*) *separatrix* if the the positive (negative) maximum interval of existence in τ_1 is finite. Analogously, imaginary time separatrices are defined.

Complex Time Flow of ξ An example for the complex time flow of a holomorphic function is depicted in Fig. 5.7, where the Riemann ξ function is chosen for f. The

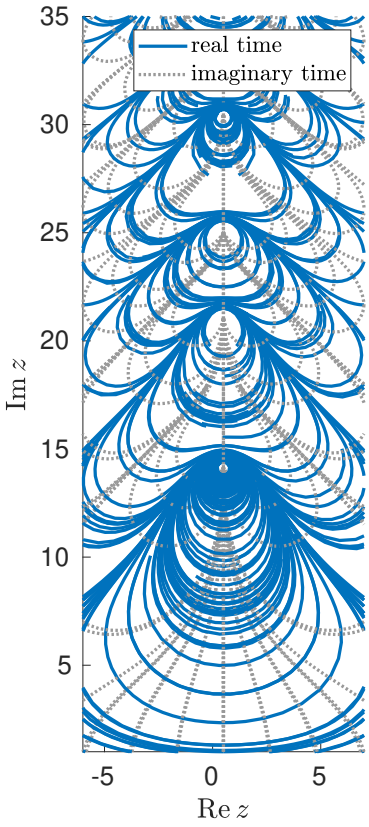

Figure 5.7: Complex time holomorphic flow $z' = f(z) = \xi(z)$. Blue lines are real time trajectories (cf. (5.32), gray lines are imaginary time trajectories (cf. (5.33)).

real time trajectories form the same phase portrait as seen before, e.g., in Fig. 4.1. They are either separatrices or periodic orbits around the zeros of ξ. In contrast, imaginary time trajectories (in gray color) either diverge from or converge to

such a zero of ξ. Forward resp. backward imaginary time separatrices in the sense of phase portrait dividing curves are in between two consecutive real time separatrices for the plotted region.

Broughan shows in [Bro05, Lemma 4.1] that for all $a > 1/2$, (real time) separatrices of the ξ flow do not go to infinity in the strip $[\frac{1}{2}, a] \times \mathbb{R}$, i.e., every separatrix crosses the line $\operatorname{Re} z = a$ for every possible $a > 1/2$. Since Fig. 5.7 suggests that imaginary times separatrices lie in between real time trajectories, every imaginary time separatrix should intersect with the lines $\operatorname{Re} z = a > 1/2$ as well. The following Proposition 5.30 confirms this statement.

Proposition 5.30. *Every separatrix of the imaginary time flow of ξ crosses the line $\operatorname{Re} z = a$ for all $a > 1/2$.*

Proof. Analogous to [Bro05, Proof of Lemma 4.1]. The proof is the same once it is recognized that $|\mathrm{i}\xi(z)| = |\xi(z)|$. □

5.5.1 Complex Time Newton Flow

Considering the Newton flow right-hand side $\frac{f(z)}{f'(z)}$ for the complex time ODE, the corresponding real and imaginary time flows are

$$\frac{\mathrm{d}z(t)}{\mathrm{d}\tau_1} = -\frac{f\big(z(t)\big)}{f'\big(z(t)\big)}, \tag{5.34}$$

$$\frac{\mathrm{d}z(t)}{\mathrm{d}\tau_2} = -\mathrm{i}\frac{f\big(z(t)\big)}{f'\big(z(t)\big)}. \tag{5.35}$$

For constant imaginary time τ_2, the solution of the real time Newton Flow (5.34) satisfies

$$f\big(z(t)\big) = f\big(z(\tau_1 + \mathrm{i}\tau_2)\big) = f\big(z(\mathrm{i}\tau_2)\big)\mathrm{e}^{-\tau_1}.$$

Thus, the real time flow yields lines of constant phase (argument) of f.

In contrast, the solution of the imaginary time Newton flow (5.35) satisfies for fixed real time τ_1

$$f\big(z(t)\big) = f\big(z(\tau_1 + \mathrm{i}\tau_2)\big) = f\big(z(\tau_1)\big)\mathrm{e}^{-\mathrm{i}\tau_2}.$$

Thus, the imaginary time flow yields lines of constant magnitude of f. As seen before, the imaginary time Newton flow is orthogonal to the real time Newton Flow. In this way, complex time in Newton flows unifies lines of constant phase and magnitude of f.

Figure 5.8 shows the real and imaginary time phase portrait for the Newton flow of $\cosh(z-1/2)$. Whenever a real time trajectory crosses an imaginary time trajectory, they intersect orthogonally.

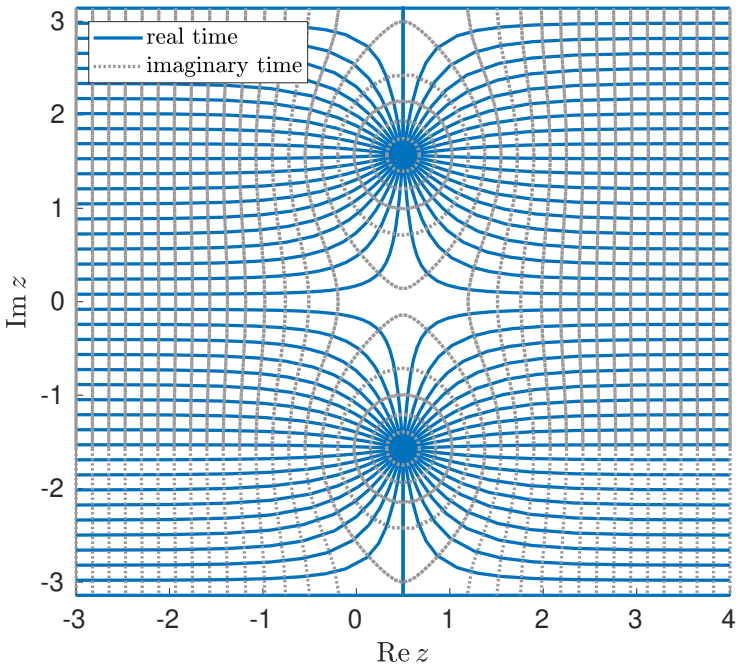

Figure 5.8: Complex time Newton flow trajectories of $\cosh(z-1/2)$ for several initial values $z_0 \in [-3,4] \times [-\pi,\pi]$. Real time trajectories (5.34) are depicted in blue, imaginary time trajectories (5.35) in dotted gray color.

Equilibria of the Complex Time Newton Flow When looking at Proposition 4.10, it is not surprising that the zeros at $z = \frac{1}{2} \pm \mathrm{i}\frac{\pi}{2}$ in Fig. 5.8 are asymptotically stable for the real time Newton flow. The following Theorem 5.31 allows to determine the stability behavior of the imaginary time flow as well.

Theorem 5.31 ([Bro03a, Theorem 2.9]). *Let $f\colon \Omega \to \mathbb{C}$ be a holomorphic function in the open set $\Omega \subset \mathbb{C}$ with a simple zero at z_0. The Taylor series expansion of f about z_0 shows that there is a holomorphic function $h\colon U \to \mathbb{C}$ in a neighborhood U of z_0 satisfying*

$$f(z) = (z - z_0)h(z), \quad h(z) \neq 0 \text{ for all } z \in U.$$

Consider the holomorphic flow of $z' = f(z)$ with $f'(z_0) = h(z_0) = a + \mathrm{i}b \neq 0$ for some $a, b \in \mathbb{R}$. Then, the flow has at z_0:

(a) *a focus if $a \neq 0$ and $b \neq 0$,*

(b) *a node if $b = 0$,*

(c) *a center if $a = 0$.*

That is to say, f has the same type of equilibrium at z_0 as its linearization $(z - z_0)h(z_0)$.

The proof of Proposition 4.10 reveals that for simple zeros z_0 of f, it holds $g'(z_0) = -1$ with $g(z) \coloneqq -\frac{f(z)}{f'(z)}$. If g is replaced by $\mathrm{i}g$ representing the imaginary time Newton flow, one obtains $\mathrm{i}g'(z_0) = -\mathrm{i}$. Consequently, every simple zero of f causes an asymptotically stable node for the real time Newton flow and a center for the imaginary time Newton flow. In this way, the stability of a simple zero changes when real time is replaced by imaginary time and vice versa. Furthermore, Fig. 5.8 also graphically confirms the equilibria at $z = \frac{1}{2} \pm \mathrm{i}\frac{\pi}{2}$ to be indeed centers.

Inverse Images of Circles The solution (5.35) of the imaginary time Newton flow reveals that lines of constant magnitude are actually *circles* of constant magnitude of f: When $f\big(z(t)\big) = f\big(z(\tau_1 + \mathrm{i}\tau_2)\big)$ is plotted for fixed τ_1 in $\mathbb{R}^2$ with its real part on the x-axis and imaginary part on the y-axis one obtains a circle with center at the origin and radius equal to $|f\big(z(\tau_1)\big)|$. In order to calculate the imaginary time Newton flow trajectory $z(\tau_1 + \mathrm{i}\tau_2)$, it is sufficient to pick the circle with radius $|f\big(z(\tau_1)\big)|$ and calculate its inverse image under f. In other words, the imaginary time Newton flow trajectories handled as geometric objects are the inverse images of circles (centered at the origin) under f. The inverse image of a chosen circle under f might have several connected components. Each of these components is a trajectory. In this case, one circle belongs to several imaginary time Newton flow trajectories.

Furthermore, if one is interested how the inverse image of circles under f changes with respect to the radius $r \coloneqq |f\big(z(\tau_1)\big)|$ of the circle, one can observe the following

for holomorphic functions f that only have simple zeros. In the limit $r = 0$, the inverse image under f is exactly the zero set $\mathcal{Z}_f$ of f. As seen before, each of those zeros is a center of the imaginary time Newton flow. Thus, for $r > 0$ small enough, the inverse function of f maps the circle of radius r around 0 to periodic orbits. And the number of these orbits corresponds to the number of zeros in the zero set $\mathcal{Z}_f$.

5.5.2 Topology of Complex Time Flows

The introduction of complex time allows to investigate the topological properties of complex time trajectories and their connection to separatrices. All results of this section are of experimental nature and rely on the previously used example functions cosh and ξ. With a couple of figures, we describe topological phenomena arising in the context of complex time. The content of this subsection and more details can be found in [HL19].

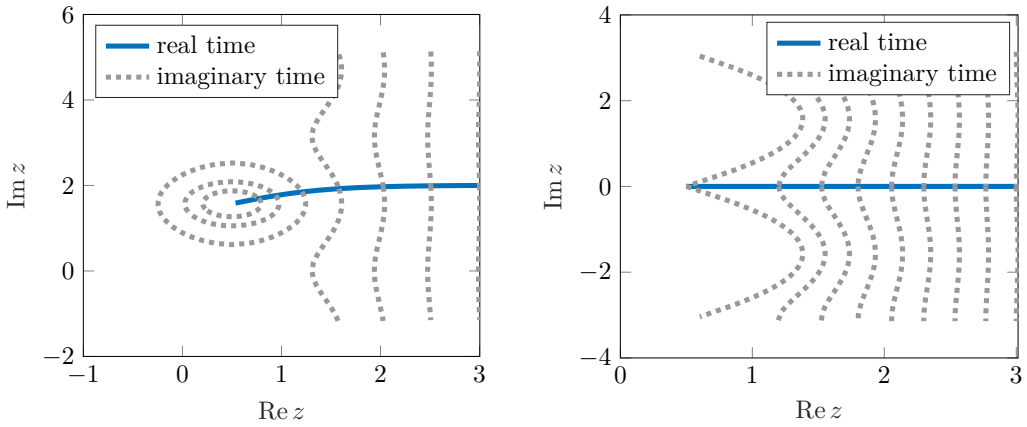

Figure 5.9: Newton flow of cosh in real time (blue trajectories) and imaginary time (gray trajectories). On the left figure, the initial value of the real trajectory is away from all separatrices while on the right figure, it is on a separatrix. See [HL19].

First, take another look at Fig. 5.8 resp. Fig. 5.9 which zooms in two specific real time trajectories. The left figure of Fig. 5.9 shows a real time trajectory (in blue) which is not a separatrix but converges to a zero of $\cosh(z - 1/2)$. If some intermediate values on this real time trajectory (ordered by ascending real time) are used as initial values for the imaginary time Newton flow, some kind of bifurcation occurs.

The first trajectories are non-periodic and have oscillating real part. The oscillation increases until at some (bifurcation) point imaginary time trajectories turn into periodic orbits. In contrast to this, if an initial value for the real time trajectory is on a separatrix (right figure in Fig. 5.9), this bifurcation does not appear. This motivates a topological investigation of separatrices in holomorphic flows.

For another perspective on the complex time flows, consider an open domain $D \subset \mathbb{C}$ and a holomorphic function $h : D \to h(D) \subset \mathbb{C}$. We define the set

$$M_h \coloneqq \Big\{ \big(z, h(z)\big) : z \in D \Big\}.$$

It is well known that the graph of a holomorphic function is a Riemann surface, i.e., a complex manifold of (complex) dimension one; see e.g. [Kod06]. Thus, M_h is a Riemann surface. A *complex manifold* is a generalization of smooth manifolds (cf. Definition 2.29), where essentially $\mathbb{R}$ is substituted by $\mathbb{C}$ and "differentiable" by "holomorphic". For more information about complex manifolds, see [Kod06].

Consider the ODE

$$z'(t) = f\big(z(t)\big), \quad t \in D \subset \mathbb{C},\ f\colon \mathbb{C} \to \mathbb{C} \text{ holomorphic.} \tag{5.36}$$

If $z\colon D \subset \mathbb{C} \to \mathbb{C}$ solves this ODE (for an arbitrarily chosen initial value $z(0) = z_0$) then

$$M_z \coloneqq \Big\{ \big(t, z(t)\big) : t \in D \Big\}$$

is a Riemann surface.

Figure 5.10 shows the Riemann surface of $f(z) = \cosh(z - 1/2)$. It is evident that the Riemann surface for an initial value on the separatrix differs from the Riemann surface off the separatrix (see Fig. 5.9). The theory of Riemann surfaces combines complex analysis with topology and algebra. For example, every connected, compact Riemann surface can be transformed biholomorphically into a smooth algebraic curve defined over the complex numbers (cf. [Kod06; Lam09]). The study of such Riemann surfaces is subject to current research in order to better understand the connections to separatrices.

Finally, we investigate the topology of complex time solutions by considering closed "time" curves and their images under the solution map of a holomorphic ODE. In mathematical symbols, let $\gamma\colon [0,1] \to D \subset \mathbb{C}$ be a closed curve which we call *time curve*. Further let the solution of (5.36) be given by the function $z\colon D \to \mathbb{C}$. Figure 5.11 illustrates the images $z(t)$ of four rectangle time curves. As initial

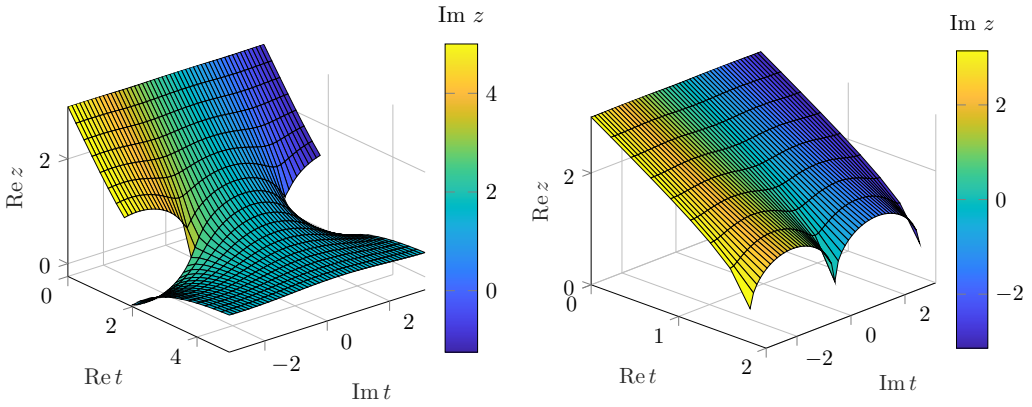

Figure 5.10: Riemann surfaces $\big(t, z(t)\big) \in \mathbb{C}^2$, where z is solution of the complex time differential equation $z' = \cosh(z - 1/2)$. In the left figure, the initial value $z(0)$ is away from all separatrices, while in the right figure $z(0) = 3$ is on a separatrix. In both figures, we first numerically compute a real time trajectory using a time discretization. Then, we use each point of this real time trajectory as initial value of an imaginary time trajectory. See [HL19].

value, we choose $z(0) = z_0 = 3 + \mathrm{i}$. The rectangles start at $t_0 = 0$, continue on the real time until $t_1 = \tau_1$, move along the imaginary time axis until $t_2 = \tau_1 + \mathrm{i}\tau_2$, then move back the real time until $t_3 = 0 + \mathrm{i}\tau_2$ and finally end at the initial time $t_4 = t_0 = 0$. The four rectangles only differ in the choices of $\tau_1, \tau_2 \in \mathbb{R}$. The yellow rectangle image crosses neither the real time separatrices at $\mathrm{Im} z = k\pi, k \in \mathbb{Z}$ nor the imaginary time separatrices at $\mathrm{Im} z = \big(k + \frac{1}{2}\big)\pi, k \in \mathbb{Z}$. While the purple rectangle image crosses an imaginary time separatrix, the green rectangle image crosses a real time separatrix. Only the wine-red rectangle image crosses both a real and imaginary time separatrix. It is evident that only this wine-red rectangle has a non-closed image curve. Numerical examples show that the image of a time rectangle is non-closed for the complex time flow of cosh if and only if the real and imaginary time separatrices are each crossed $n_\mathrm{r} = (2k_\mathrm{r} - 1)$ resp. $n_\mathrm{i} = (2k_\mathrm{i} - 1)$ times for positive integers $k_\mathrm{r}, k_\mathrm{i} \in \mathbb{N}$. Here, n_r and n_i are odd numbers because the mathematical direction of the (real and imaginary time) flow changes in each strip $\mathrm{Im} z \in [k\pi, (k+1)\pi)$ resp. $\mathrm{Im} z \in \Big[\big(k + \frac{1}{2}\big)\pi, \big(k + \frac{3}{2}\big)\pi\Big)$ as we have already seen in Section 5.4 (cf. Fig. 4.2). Thus, once more the separatrices have direct impact on the topology of complex time ODE solutions. A more detailed mathematical analysis of these phenomena may require a deeper knowledge in algebraic geometry and

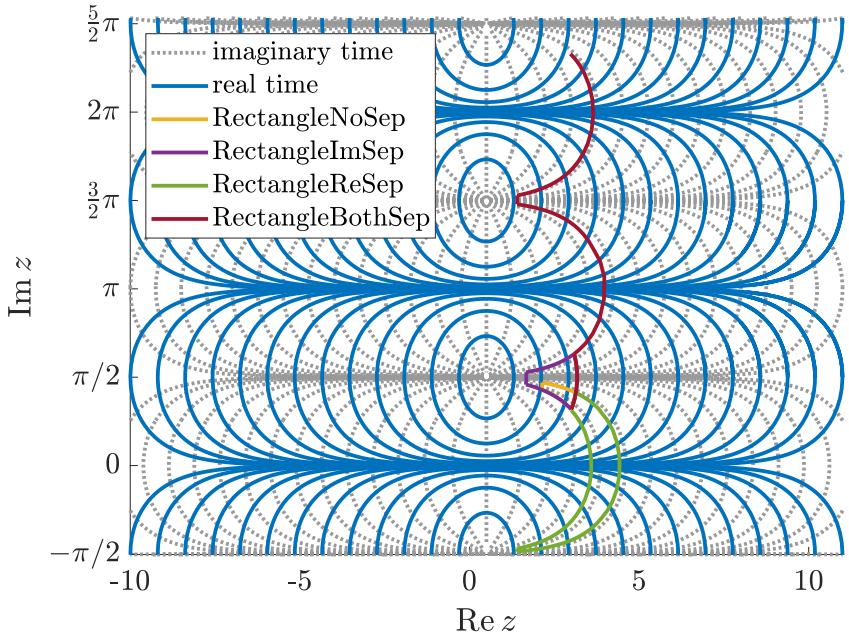

Figure 5.11: Complex time flow of $z' = \cosh(z - 1/2)$. Four different colored rectangles in the complex domain are taken as "time-input" for the solution mapping $z(t)$. Depending on whether they cross the real and imaginary time separatrix they yield closed curves on the solution manifold or not. NoSep: No separatrix is crossed, ImSep: imaginary time separatrix is crossed, ReSep: real time separatrix is crossed, BothSep: both real and imaginary time separatrices are crossed. See [HL19].

topology.

5.5.3 Curvature-Based Approach for the Characterization of Separatrices

The complex time flows in Figs. 5.7 and 5.8 reveal geometric characteristics of separatrices. In this section, we exploit these geometric properties to create an approximation method for the calculation of separatrices. The results in this section are of experimental nature. We present a method that does not calculate the separatrix exactly and for which an analysis is generally hard. Nevertheless, the results examine the impact of separatrices on the curvature of complex time

trajectories.

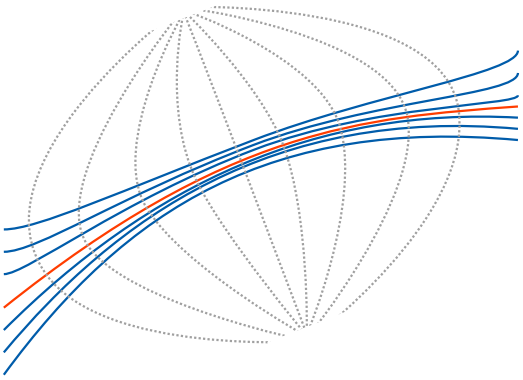

Figure 5.12: Sketch of bundling real time trajectories (blue curves) near separatrix (red curve). Imaginary time flow is depicted in gray dotted lines. Curvature of imaginary time trajectories increases near the (real time) separatrix.

The motivation for the following approximation method is as follows. In the phase plot that shows the real time holomorphic flow of a function f, a bundling of trajectories in the neighborhood of separatrices is observed. However, this bundling is generally a local phenomenon. In contrast to SIMs, separatrices generally do not attract trajectories in the long run. Figure 5.12 sketches such a bundling of solution curves. When following the path of two trajectories that is close to a separatrix, the distance between them generally grows exponentially (cf. Gronwall's inequality Eq. (5.22)). Since imaginary time trajectories cross real time trajectories always orthogonally, it might be expected that the curvature of imaginary time trajectories is maximum at the real time separatrix and vice versa (because of symmetry). This idea is summarized in the following Algorithm 2.

Algorithm 2 Curvature-Based Separatrix Approximation Method

Input Holomorphic dynamical system $z'(t) = f\big(z(t)\big), t \in D \subset \mathbb{C}$.

1: Choose an initial value $z_0 \in \mathbb{C}$.
2: Compute the imaginary time trajectory $z(\mathrm{i}\tau_2)$ through $z(0) = z_0$.
3: Determine τ_2^* such that the curvature of $z(\mathrm{i}\tau_2)$ is maximum at τ_2^*.
4: **return** Approximation $z(\mathrm{i}\tau_2^*)$ ▷ expected to be near a (real time) separatrix.

It remains to derive a formula for the curvature of an imaginary time trajectory.

Analogously to Proposition 5.1, for the curvature of the imaginary time trajectory, we obtain

$$\kappa\big(z(\mathrm{i}\tau)\big) = \frac{|\mathrm{Re} f'\big(z(\mathrm{i}\tau)\big)|}{|f\big(z(\mathrm{i}\tau)\big)|}. \tag{5.37}$$

Remark 5.32. Although Algorithm 2 uses the complex time setting, it is comparable to the flow curvature method (see Section 2.4.2) where the slow manifold resp. the separatrix is approximated by points of a curves with vanishing curvature (see also Section 5.1.1). In contrast to the FCM, our new ansatz uses the curvature in imaginary time.

The next examples show how surprisingly accurate the presented curvature-based approximation method is. However, we present its limits as well.

Example z^2+1**:** In Section 4.2.3 we have already seen that the real time trajectories are geometrically circles and lines. This statement holds for the imaginary time trajectories as well. To see this, we again calculate the curvature of the trajectory $z(\mathrm{i}\tau) = \tan(\mathrm{i}\tau + c)$ for an arbitrary constant $c = c_1 + \mathrm{i}c_2 \in \mathbb{C}$ which is introduced by the equation $z_0 = z(0) = \tan(c)$. Analogous to the calculations in Section 4.2.3 and applying (5.37), we obtain

$$\kappa\big(z(\mathrm{i}\tau)\big) = |\sin(2c_1)| \quad \text{for all } \tau \in \mathbb{R},$$

i.e., all trajectories have constant curvature. Consequently, Algorithm 2 cannot work in this example. Nevertheless, it holds that on the separatrix the imaginary time trajectories have their maximum curvature. This means that the maximum curvature criterion cannot be a sufficient condition for separatrices. With the help of the following examples, it is analyzed whether this criterion yields a necessary condition or not. In any case we examine how the separatrix is approximated.

Example cosh**:** For $f(z) = \cosh(z - 1/2)$ the numerical results of Algorithm 2 is plotted in Fig. 5.13. The small black circles each highlight the points of maximum curvature along the imaginary time trajectories which are plotted as well. The separatrices at $\mathrm{Im} z = k\pi, k \in \mathbb{Z}$ are well approximated. The only outliers are near the equilibria of $\cosh(z - 1/2)$. The reason for the failure of Algorithm 2 is that the corresponding imaginary trajectories are parts of the line $\mathrm{Re} z = 1/2$. Since this line has no curvature, the situation is comparable to the $z^2 + 1$ example.

Our numerical implementation for the search of the local maximum curvature compares the curvature at two consecutive points on the discretized trajectory and picks the first one if the curvature at it is strictly higher. Thus, the algorithm picks the last points on the trajectory in case of the straight lines.

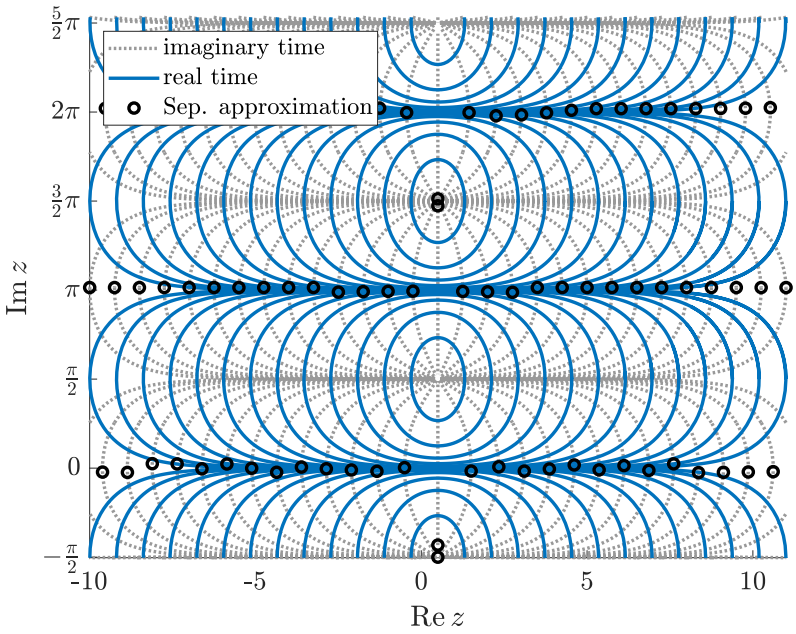

Figure 5.13: Complex time flow of $\cosh(z - 1/2)$. Real time trajectories are plotted with blue color, imaginary time trajectories with gray color. Local maxima of the curvature are plotted with black circles.

Example ξ: Finally, we apply Algorithm 2 to the Riemann ξ function. Due to a missing numerical implementation for the evaluation of the derivative of ξ, we have to approximate the imaginary time curvature

$$\kappa\big(z(\mathrm{i}\tau)\big) = \frac{|\operatorname{Re}\xi'\big(z(\mathrm{i}\tau)\big)|}{|\xi\big(z(\mathrm{i}\tau)\big)|}.$$

We discretize the imaginary time parameter $\tau \in [0, T]$ at $(n+1)$ equidistant points for some $n \in \mathbb{N}$ and $T > 0$. Thus, the imaginary time curve becomes the vector $\mathtt{z=(z_1,\ldots,z_n)}$ with $\mathtt{z}_k = z(\mathrm{i}kh)$ for a fixed step size $h > 0$. The derivative of ξ is approximated by the mean value of the difference quotients to the left and to the

right:

$$\kappa(\mathbf{z}_k) = \kappa\big(z(\mathrm{i}kh)\big) \approx \frac{\big|\mathrm{Re}\big(f(\mathbf{z}_{k+1}) - f(\mathbf{z}_{k-1})\big)\big|}{2h|f(\mathbf{z}_k)|} \quad \text{for } k = 2, \ldots, n-1.$$

The computed approximative values for κ are depicted in Fig. 5.14 with small black circles.

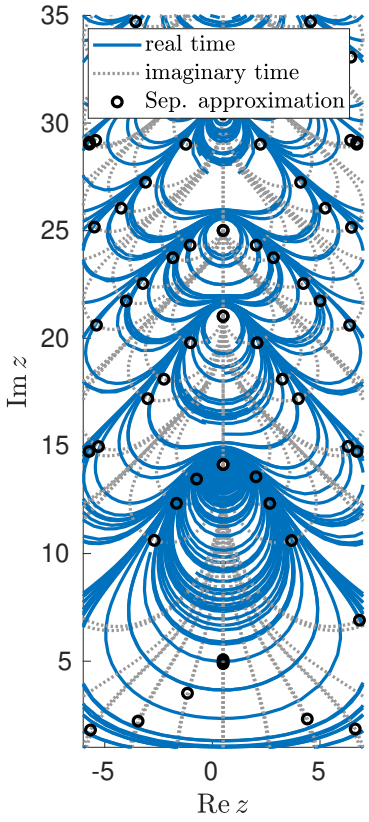

Figure 5.14: Complex time flow of the Riemann ξ function. Real time trajectories are plotted with blue color, imaginary time trajectories with gray color. Discretizing the imaginary time curves, local maxima of the curvature are plotted with black circles.

Although (most of) the black circles seem to be close to separatrices, they do not match the separatrices exactly. Probably, the numerical error for the approximation

of κ does not influence this fact. An analysis for the error is desirable but has not been achieved yet.

In summary, maximizing the curvature of imaginary time trajectories yields approximations for the real time separatrix and vice versa. However, they are not able to characterize the separatrices exactly.

6 Conclusion and Outlook

This chapter briefly summarizes the topics and results of this work. In Section 6.2, we point out open issues and ideas for future work.

6.1 Summary and Conclusion

In the phase space of dynamic systems, two outstanding phase space structures are Slow Invariant Manifolds (SIMs) and separatrices. Both contain essential information on the phase portrait and significantly influence the long-term and stability behavior of trajectories. The aim of this thesis was to study these phase space structures, to identify characteristic geometrical and topological properties, and to generate a deeper understanding of their role for phase portrait.

The first part of this thesis dealt with slow invariant manifolds of slow-fast systems arising, e.g., in chemical reaction mechanisms. The different time scales of partial chemical reactions often led to numerically stiff and high-dimensional differential equations which could only be solved with great numerical effort. However, multiple time scales usually imply the existence of low-dimensional manifolds of the phase portrait if the reactions are modeled by differential equations. Often having the property of fast attraction of nearby trajectories, these slow invariant manifolds can be used to describe the long-term behavior of trajectories. In this work, we studied the applicability of such manifold-based model reduction techniques for optimal control problems where the differential equations come in as infinite dimensional constraints. We introduced the mathematical framework of singularly perturbed systems, SIMs, optimal control problems and their necessary optimality conditions. It was shown that both the SIM approximation methods Zero-Derivative-Principle and Trajectory-Based Optimization Approach, can efficiently be integrated in the optimal control problem such that the resulting new approach simplifies the needed calculations. Two guiding examples showed that both stiffness and the dimension of the problem decreased significantly. We

compared this new approach to already existing and in practice often used direct optimal control methods. The resulting nonlinear program was solved by the interior point solver IPOPT for all implementations.

Besides dissipative multi-scale systems, we considered specific phase space structures of holomorphic flows in the complex plane. In this context, specific trajectories, called separatrices, emerge. They divide the phase portrait into regions that have distinct stability behavior. We studied separatrices for two main reasons. On the one hand, there are common geometric features of separatrices and SIMs. On the other hand, holomorphic flows and separatrices play an important role for the location of zeros of functions, which are central objects of analytic number theory, for instance in the context of the Riemann ξ function. There is some evidence that the behavior of separatrices at infinity influence the location of the roots of ξ. Hence, we studied the phase portrait near infinity and analyzed its characteristics. We introduced holomorphic and Newton flows and argued that a desingularization of the Newton flow makes the global analysis of the phase portrait accessible.

Due to the close connection to SIMs, we applied methods which were developed to approximate and identify SIMs to separatrices as well. For some of the guiding examples, these led to quite accurate approximations despite having some spurious solutions. We proved that critical points at infinity have incoming or outgoing separatrices for polynomial holomorphic dynamical systems. Therefore, the Poincaré sphere and other compactifications of the complex plane are suitable tools to visualize and analyze the global phase portrait. Furthermore, complex time views separatrices from a more general perspective that allowed us to identify some topological properties. For holomorphic dynamical systems having two adjacent centers divided by a separatrix, we were able to characterize the separatrix by different indices of periodic orbits around these centers. Moreover, we showed that Lyapunov exponents are indirectly calculated by the Trajectory-Based Optimization Approach. We demonstrated the benefit of Lyapunov exponents for generating a new tool to distinguish "ordinary" trajectories from separatrices when applied to the desingularized Newton flow.

In summary, it can be argued that the methods, tools and ideas presented in this thesis provide a significantly deeper understanding of separatrices in holomorphic differential equations and a good basis for efficient manifold-based model reduction in optimal control.

6.2 Outlook

This work is only the beginning of making use of manifold-based model reduction techniques in order to solve optimal control problems more efficiently. The presented new approach does not rely on interpolation in an offline computation but can be used online. However, the two low-dimensional examples that were solved, only show a "proof of concept". A mathematically rigorous analysis is still lacking. Furthermore, the computational advantage if applied to high-dimensional problems is not yet clear although expected to be significant.

Many parts of this thesis also serve as reflected survey of the study of separatrices. This opens many fields not yet considered in this work. For instance, we showed that for polynomial holomorphic ODEs critical points at infinity have an incoming or outgoing separatrix. However, the opposite statement is not clear so far: Does every separatrix start at or end in a critical point at infinity? Moreover, we managed to determine the separatrix exactly for a simple example $z' = z^2 + 1$ by the computation of Lyapunov exponents for the desingularized Newton flow. An efficient numerical implementation for the computation of Lyapunov exponents, as well as a general analytic result whether Lyapunov exponents characterize the separatrix is desirable. Furthermore, Section 5.5 might open the field for an algebraic geometrical view.

List of Symbols

Notation	Description
C_0	Symbol for the critical set/manifold.
$C^k(U)$	Space of functions that map from U to $\mathbb{R}$ and its derivatives up to order k exist and are continuous.
$C^k(U,V)$	Space of functions that map from U to V and its derivatives up to order k exist and are continuous.
$C(U)$	Space of continuous functions that map from U to $\mathbb{R}$.
$C(U,V)$	Space of continuous functions that map from U to V.
$D_x f$	Partial derivatives of function f w.r.t. variable x.
ε	Small (time scale separation) parameter $0 < \varepsilon \ll 1$.
h_ε	Regular asymptotic expansion of slow invariant manifold.
J_f	Jacobian matrix of function f.
$\lambda(t)$	Adjoint variable at time t.
$\lambda(v)$	Lyapunov exponent for initial perturbation direction v.
$L^p(\Omega, \mathbb{R}^n)$	Space of all measurable functions that are p-integrable.
$L^\infty(\Omega, \mathbb{R}^n)$	Space of all measurable functions that are essentially bounded.
p	Variable $p = (p_1, p_2)$ often used for compactification of $\mathbb{R}^2$.
S_ε	Symbol for a slow invariant manifold.
$\Theta(f)$	Set of functions asymptotically bounded above and below by function f.
u	Usually the symbol for control variable(s).
$U_r(z)$	Open ball with radius r around z.
$W^{k,p}(\Omega, \mathbb{R}^n)$	Space of all absolutely continuous functions $f : \Omega \to \mathbb{R}^n$ with absolute continuous derivatives up to order $k-1$ and $\|f\|_{k,p} < \infty$.

Notation	Description
x, y	See symbol z.
z	Used for state variables. Often $z = (x, y) \in \mathbb{R}^2$ or $z = x + \mathrm{i}y \in \mathbb{C}$.
$\mathcal{Z}_f$	Zero set of function f containing all roots of f.

Acronyms

BVP	Boundary Value Problem
CIM	Canonical Invariant Manifold
CSP	Computational Singular Perturbation
CSTR	Continuous Stirred Tank Reactor
DAE	Differential-Algebraic Equation
FCM	Flow Curvature Method
FTLE	Finite-Time Lyapunov Exponent
ILDM	Intrinsic Low-Dimensional Manifold
IP	Interior Point
IVP	Initial Value Problem
LICQ	Linear Independence Constraint Qualifications
MEPT	Minimal Entropy Production Trajectory
NLP	Nonlinear Program
OCP	Optimal Control Problem
ODE	Ordinary Differential Equation
PEA	Partial Equillibrium Assumption
QSSA	Quasi-Steady State Approximation
RPV	Reaction Progress Variable
SIM	Slow Invariant Manifold
SQP	Sequential Quadratic Programming
TBOA	Trajectory-Based Optimization Approach
ZDP	Zero-Derivative-Principle

Bibliography

[AD10] J. Albersmeyer and M. Diehl. "The Lifted Newton Method and Its Application in Optimization." In: *SIAM Journal on Optimization* 20.3 (Jan. 2010), pp. 1655–1684.

[Al-+09] A. N. Al-Khateeb et al. "One-dimensional slow invariant manifolds for spatially homogenous reactive systems." In: *Journal of Chemical Physics* 131.2 (2009), p. 024118.

[AMR87] U. M. Ascher, R. M. M. Mattheij, and R. D. Russell. "Numerical solution of boundary value problems for ordinary differential equations." Society for Industrial and Applied Mathematics, 1987.

[And13] J. Andersson. "A general-purpose software framework for dynamic optimization." PhD thesis. Arenberg Doctoral School, KU Leuven, 2013.

[Ari03] J. Arias-de-Reyna. "X-Ray of Riemann zeta-function." 2003. arXiv: `math/0309433 [math.NT]`.

[ASG01] A. C. Antoulas, D. C. Sorensen, and S. Gugercin. "A survey of model reduction methods for large-scale systems." In: *Structured matrices in mathematics, computer science, and engineering. Proceedings of an AMS-IMS-SIAM Joint Summer Research Conference*. Vol. 280. American Mathematical Society, 2001, pp. 193–219.

[Bar17] L. Barreira. "Lyapunov Exponents." Springer International Publishing, 2017.

[BB04] K. A. Broughan and A. R. Barnett. "The holomorphic flow of the Riemann zeta function." In: *Mathematics of Computation* 73.246 (2004), pp. 987–1004.

[Ben+15] E. Benoît et al. "Extending the zero-derivative principle for slow–fast dynamical systems." In: *Zeitschrift für angewandte Mathematik und Physik* 66.5 (2015), pp. 2255–2270.

[Ben91] H. E. Benzinger. "Plane autonomous systems with rational vector fields." In: *Transaction of the American Mathematical Society* 326.2 (1991), pp. 465–483.

[Bie10] L. T. Biegler. "Nonlinear programming: concepts, algorithms, and applications to chemical processes." MOS-SIAM Series on Optimization. Society for Industrial & Applied Mathematics (SIAM), 2010.

[Bod07] M. Bodenstein. "Geschwindigkeit der Bildung des Bromwasserstoffs aus seinen Elementen." In: *Zeitschrift für Physikalische Chemie – Leipzig* 57.1 (1907), pp. 168–192.

[Bod13] M. Bodenstein. "Eine Theorie der photochemischen Reaktionsgeschwindigkeiten." In: *Zeitschrift für Physikalische Chemie – Leipzig* 85.1 (1913), pp. 329–397.

[BP84] H. G. Bock and K. J. Plitt. "A multiple shooting algorithm for direct solution of optimal control problems." In: *Proceedings of the Ninth IFAC World Congress, Budapest*. Proceedings of the Ninth IFAC World Congress, Budapest. 1984.

[Bro03a] K. A. Broughan. "Holomorphic flows on simply connected regions have no limit cycles." In: *Meccanica* 38.6 (2003), pp. 699–709.

[Bro03b] K. A. Broughan. "Structure of sectors of zeros of entire flows." In: *Topology Proceedings* 27.2 (2003), pp. 379–394.

[Bro05] K. A. Broughan. "The holomorphic flow of Riemann's function $\xi(z)$." In: *Nonlinearity* 18.3 (2005), pp. 1269–1294.

[CU13] D. L. Chapman and L. K. Underhill. "The interaction of chlorine and hydrogen. The influence of mass." In: *Journal of the Chemical Society, Transactions* 103 (1913), pp. 496–508.

[Cve07] J. Cvejn. "Optimal Control of a Chemical Reactor." In: *ATP Journal Plus2* 2 (2007), p. 2. URL: `http://www.atpjournal.sk/buxus/docs/casopisy/atp_plus/plus_2007_2/plus63_66.pdf` (visited on 09/25/2017).

[DH08] P. Deuflhard and A. Hohmann. "Numerische Mathematik 1: Eine algorithmisch orientierte Einführung." 4th ed. Walter de Gruyter, 2008.

[Die+02] M. Diehl et al. "An efficient algorithm for nonlinear model predictive control of large-scale systems. Part I: description of the method." In: *Automatisierungstechnik* 50.12 (2002), pp. 557–567.

[DS99] M. J. Davis and R. T. Skodje. "Geometric investigation of low-dimensional manifolds in systems approaching equilibrium." In: *Journal of Chemical Physics* 111.3 (1999), pp. 859–874.

[Edw01] H. M. Edwards. "Riemann's zeta function." Dover Publications Inc., 2001. 330 pp.

[Fen71] N. Fenichel. "Persistence and smoothness of invariant manifolds for flows." In: *Indiana University Mathematics Journal* 21.3 (1971), pp. 193–226.

[Fen74] N. Fenichel. "Asymptotic stability with rate conditions." In: *Indiana University Mathematics Journal* 23.12 (1974), pp. 1109–1137.

[Fen77] N. Fenichel. "Asymptotic stability with rate conditions II." In: *Indiana University Mathematics Journal* 26.1 (1977), pp. 81–93.

[Fen79] N. Fenichel. "Geometric singular perturbation theory for ordinary differential equations." In: *Journal of Differential Equations* 31.1 (1979), pp. 53–98.

[Gea+05] C. W. Gear et al. "Projecting to a slow manifold: singularly perturbed systems and legacy codes." In: *SIAM Journal on Applied Dynamical Systems* 4.3 (2005), pp. 711–732.

[Ger12] M. Gerdts. "Optimal control of ODEs and DAEs." De Gruyter, 2012.

[Gin04] H. Gingold. "Approximation of unbounded functions via compactification." In: *Journal of Approximation Theory* 131.2 (2004), pp. 284–305.

[Gin13] J.-M. Ginoux. "The slow invariant manifold of the Lorenz-Krishnamurthy model." In: *Qualitative Theory of Dynamical Systems* 13.1 (2013), pp. 19–37.

[GR06] J.-M. Ginoux and B. Rossetto. "Differential geometry and mechanics: applications to chaotic dynamical systems." In: *International Journal of Bifurcation and Chaos* 16.04 (2006), pp. 887–910.

[GR08] J.-M. Ginoux and B. Rossetto. "Slow invariant manifolds as curvature of the flow of dynamical systems." In: *International Journal of Bifurcation and Chaos* 18.11 (2008), pp. 3409–3430.

[GS03] X. Gourdon and P. Sebah. "Numerical evaluation of the Riemann Zeta-function." 2003. URL: `http://numbers.computation.free.fr/Constants/Miscellaneous/zetaevaluations.pdf`.

[GS13] H. Gingold and D. Solomon. "More compactification for differential systems." In: *Advances in Pure Mathematics* 03.01 (2013), pp. 190–203.

[Had93] J. Hadamard. "Étude sur les propriétés des fonctions entières et en particulier d'une fonction considérée par Riemann." In: *Journal de mathématiques pures et appliquées* 9.4 (1893), pp. 171–216.

[Hei+17] M. Heitel et al. "Considering Slow Manifold Based Model Reduction for Multiscale Chemical Optimal Control Problems." In: *arXiv e-prints* (2017). arXiv: `1712.01058 [math.OC]`.

[Hei17] P. F. Heiter. "Curvature Based Criteria for Slow Invariant Manifold Computation: From Differential Geometry to Numerical Software Implementations for Model Reduction in Hydrocarbon Combustion." PhD thesis. Ulm University, 2017.

[Hei20] M. Heitel. "Manifold-Based model reduction of optimal control problems." 2020. URL: `https://github.com/mheitel/MR_OCP`.

[Hes64] M. R. Hestenes. "Variational theory and optimal control theory." In: *Computing Methods in Optimization Problems*. Elsevier, 1964, pp. 1–22.

[Hil76] E. Hille. "Ordinary differential equations in the complex domain." A Wiley-Interscience publication. New York: Wiley, 1976.

[HL18] P. Heiter and D. Lebiedz. "Towards differential geometric characterization of slow invariant manifolds in extended phase space: sectional curvature and flow invariance." In: *SIAM Journal on Applied Dynamical Systems* 17.1 (2018), pp. 732–753.

[HL19] M. Heitel and D. Lebiedz. "On Analytical and Topological Properties of Separatrices in 1-D Holomorphic Dynamical Systems and Complex-Time Newton Flows." In: *arXiv e-prints* (2019). arXiv: `1911.10963 [math.DS]`.

[Hul12] K. Hulek. "Elementare Algebraische Geometrie." Vieweg+Teubner Verlag, 2012.

[Ily07] Y. Ilyashenko. "Lectures on analytic differential equations." Vol. 86. American Mathematical Society, 2007.

[JJT80] H. T. Jongen, P. Jonker, and F. Twilt. "The continuous Newton-method for meromorphic functions." In: *Geometrical Approaches to Differential Equations*. Springer, 1980, pp. 181–239.

[JJT88] H. T. Jongen, P. Jonker, and F. Twilt. "The continuous, desingularized Newton method for meromorphic functions." In: *Acta Applicandae Mathematicae* 13.1-2 (1988), pp. 81–121.

[Kod06] K. Kodaira. "Complex manifolds and deformation of complex structures." Springer, 2006.

[Kue15] C. Kuehn. "Multiple time scale dynamics." Vol. 191. Springer International Publishing, 2015.

[Lam09] K. Lamotke. "Riemannsche Flächen." 2nd ed. Springer Berlin Heidelberg, 2009.

[Lam85] S. H. Lam. "Singular perturbation for stiff equations using numerical methods." In: *Recent Advances in the Aerospace Sciences*. Ed. by C. Casci and C. Bruno. Plenum Press, 1985, pp. 3–20.

[Leb04] D. Lebiedz. "Computing minimal entropy production trajectories: An approach to model reduction in chemical kinetics." In: *Journal of Chemical Physics* 120.15 (2004), pp. 6890–6897.

[Leb10] D. Lebiedz. "Entropy-related extremum principles for model reduction of dynamical systems." In: *Entropy* 12.4 (2010), pp. 706–719.

[LG88] S. H. Lam and D. A. Goussis. "Understanding complex chemical kinetics with computational singular perturbation." In: *22nd Symposium on Combustion*. Vol. 22. 1. The Combustion Institute. Elsevier BV, 1988, pp. 931–941.

[LG94] S. H. Lam and D. A. Goussis. "The CSP method for simplifying kinetics." In: *International Journal of Chemical Kinetics* 26.4 (1994), pp. 461–486.

[LRK06] D. Lebiedz, V. Reinhardt, and J. Kammerer. "Novel trajectory based concepts for model and complexity reduction in (bio)chemical kinetics." In: *Model reduction and coarse-graining approaches for multi-scale phenomena*. Springer, 2006, pp. 343–364.

[LRS10] D. Lebiedz, V. Reinhardt, and J. Siehr. "Minimal curvature trajectories: Riemannian geometry concepts for slow manifold computation in chemical kinetics." In: *Journal of Computational Physics* 229.18 (2010), pp. 6512–6533.

[LSU11] D. Lebiedz, J. Siehr, and J. Unger. "A variational principle for computing slow invariant manifolds in dissipative dynamical systems." In: *SIAM Journal on Scientific Computing* 33.2 (2011), pp. 703–720.

[LU16] D. Lebiedz and J. Unger. "On unifying concepts for trajectory-based slow invariant attracting manifold computation in kinetic multiscale models." In: *Mathematical and Computer Modelling of Dynamical Systems* 22.2 (2016), pp. 87–112.

[Lya92] A. M. Lyapunov. "The general problem of the stability of motion." In: *International Journal of Control* 55.3 (Mar. 1992), pp. 531–534.

[May18] A. Mayer. "Die Berechnung von invarianten Mannigfaltigkeiten in holomorphen Flüssen mittels SIM-Methoden." Bachelorarbeit. Cand. thesis. Ulm University, June 27, 2018.

[Mea+16] K. D. Mease et al. "Characterizing two-timescale nonlinear dynamics using finite-time Lyapunov exponents and subspaces." In: *Communications in Nonlinear Science and Numerical Simulation* 36 (2016), pp. 148–174.

[Mei07] J. D. Meiss. "Differential dynamical systems." Society for Industrial and Applied Mathematics, 2007.

[MM13] L. Michaelis and M. L. Menten. "Die Kinetik der Invertinwirkung." In: *Biochemische Zeitschrift* 49 (1913), pp. 333–369.

[MP92] U. Maas and S. B. Pope. "Simplifying chemical kinetics: intrinsic low-dimensional manifolds in composition space." In: *Combustion and Flame* 88 (1992), pp. 239–264.

[Mur93] J. D. Murray. "Mathematical Biology I: An Introduction." Ed. by S. S. Antman et al. Springer, 1993.

[Neu+14] J. W. Neuberger et al. "Newton flow of the Riemann zeta function: separatrices control the appearance of zeros." In: *New Journal of Physics* 16.10 (2014), p. 103023.

[Neu+15] J. W. Neuberger et al. "The Riemann hypothesis illuminated by the Newton flow of ζ." In: *Physica Scripta* 90.10 (2015), p. 108015.

[NW06] J. Nocedal and S. J. Wright. "Numerical Optimization." 2nd ed. Springer Series in Operations Research and Financial Engineering. Springer, New York, 2006.

[Odl19] A. Odlyzko. "Tables of zeros of the Riemann zeta function." 2019. URL: `http://www.dtc.umn.edu/~odlyzko/zeta_tables` (visited on 10/15/2019).

[Per00] L. Perko. "Differential equations and dynamical systems." Springer, 2000.

[Pon+62] L. S. Pontryagin et al. "The mathematical theory of optimal processes." Interscience Publishers, New York, 1962.

[Pow+15] J. M. Powers et al. "Slow attractive canoncial invariant manifolds for reactive systems." In: *Journal of Mathematical Chemistry* 53 (2015), pp. 737–766.

[PW10] J. Prüss and M. Wilke. "Gewöhnliche Differentialgleichungen und dynamische Systeme." Springer, 2010.

[Reh13] M. Rehberg. "A numerical approach to model reduction for optimal control of multiscale ode." PhD thesis. Ulm University, 2013.

[Rie59] B. Riemann. "Über die Anzahl der Primzahlen unter einer gegebenen Grösse." In: *Monatsberichte der Königlichen Preußischen Akademie der Wissenschaften zu Berlin* (1859), pp. 136–144.

[Roe03] R. K. W. Roeder. "On Poincaré's fourth and fifth example of limit cycles at infinity." In: *Journal of Mathematics* 33.1 (2003), pp. 353–378.

[RWL08] V. Reinhardt, M. Winckler, and D. Lebiedz. "Approximation of slow attracting manifolds in chemical kinetics by trajectory-based optimization approaches." In: *Journal of Physical Chemistry A* 112.8 (2008), pp. 1712–1718.

[Sch+18] W. P. Schleich et al. "Equivalent formulations of the Riemann hypothesis based on lines of constant phase." In: *Physica Scripta* 93.6 (2018), p. 065201.

[Tes04] G. Teschl. "Ordinary differential equations and dynamical systems." 1st ed. Vol. 140. American Mathematical Society, 2004.

[Tik52] A. N. Tikhonov. "Systems of differential equations containing small parameters in the derivatives." In: *Matematicheskii sbornik* 73.3 (1952), pp. 575–586.

[Tit86] E. C. Titchmarsh. "The theory of the Riemann zeta-function." 2nd ed. Oxford University Press, 1986.

[WB06] A. Wächter and L. T. Biegler. "On the implementation of an interior-point filter line-search algorithm for large-scale nonlinear programming." In: *Mathematical Programming* 106.1 (2006), pp. 25–57.

[WF18] S. Wagner and F. Finckh. "Separatrizen des Newtonflusses sind die Ränder der Attraktionsbereiche." Student project at Ulm University. July 14, 2018.

[Zag+09] A. Zagaris et al. "Analysis of the accuracy and convergence of equation-free projection to a slow manifold." In: *ESAIM: Mathematical Modelling and Numerical Analysis* 43.4 (2009), pp. 757–784.

Notes on Copyrights

The contents and figures in Sections 3.3 and 3.4 are part of an article which is published on arXiv:

> M. Heitel et al. "Considering Slow Manifold Based Model Reduction for Multiscale Chemical Optimal Control Problems." In: *arXiv e-prints* (2017). arXiv: 1712.01058 [math.OC]

The contents and figures in Chapter 5, in particular Sections 5.2 and 5.4 and partly Sections 4.2.1 and 5.5, are part of an article which is published on arXiv:

> M. Heitel and D. Lebiedz. "On Analytical and Topological Properties of Separatrices in 1-D Holomorphic Dynamical Systems and Complex-Time Newton Flows." In: *arXiv e-prints* (2019). arXiv: 1911.10963 [math.DS]